




2022

PERIPHERALLY RESTRICTED DELIVERY SYSTEM PROVIDES INSIGHTS ON THE ROLE OF CNS IN PRECIPITATING OPIOID- INDUCED CONSTIPATION

Dengpan Liang
University of the Pacific

Follow this and additional works at: https://scholarlycommons.pacific.edu/uop_etds

 Part of the [Chemicals and Drugs Commons](#), [Medicinal and Pharmaceutical Chemistry Commons](#), and
the [Other Public Health Commons](#)

Recommended Citation

Liang, Dengpan. (2022). *PERIPHERALLY RESTRICTED DELIVERY SYSTEM PROVIDES INSIGHTS ON THE
ROLE OF CNS IN PRECIPITATING OPIOID-INDUCED CONSTIPATION*. University of the Pacific, Dissertation.
https://scholarlycommons.pacific.edu/uop_etds/3819

This Dissertation is brought to you for free and open access by the University Libraries at Scholarly Commons. It
has been accepted for inclusion in University of the Pacific Theses and Dissertations by an authorized
administrator of Scholarly Commons. For more information, please contact mgebney@pacific.edu.

PERIPHERALLY RESTRICTED DELIVERY SYSTEM PROVIDES INSIGHTS ON THE
ROLE OF CNS IN PRECIPITATING OPIOID-INDUCED CONSTIPATION

By

Dengpan Liang

A Dissertation Submitted to the

Graduate School

In Partial Fulfillment of the

Requirements for the Degree of

DOCTOR OF PHILOSOPHY

Thomas J. Long School of Pharmacy
Pharmaceutical and Chemical Sciences

University of the Pacific
Stockton, California

2022

PERIPHERALLY RESTRICTED DELIVERY SYSTEM PROVIDES INSIGHTS ON THE
ROLE OF CNS IN PRECIPITATING OPIOID-INDUCED CONSTIPATION

By

Dengpan Liang

APPROVED BY:

Thesis Advisor: Mamoun M. Alhamadsheh, Ph.D.

Committee Member: Miki S. Park, Ph.D.

Committee Member: Qinliang Zhao, Ph.D.

Committee Member: Wade Russu, Ph.D.

Committee Member: Jesika Faridi, Ph.D.

Department Chair: William K. Chan, Pharm.D., Ph.D.

PERIPHERALLY RESTRICTED DELIVERY SYSTEM PROVIDES INSIGHTS ON THE
ROLE OF CNS IN PRECIPITATING OPIOID-INDUCED CONSTIPATION

Copyright 2022

By

Dengpan Liang

DEDICATION

To my loving and supportive parents, Liguang and Qiuling, and to my many beloved friends and family.

ACKNOWLEDGEMENTS

First and foremost, I would like to thank my advisor Dr. Mamoun M. Alhamadsheh. There is no word to express my gratitude for his constant guidance and support. Dr. Alhamadsheh has been more than a research advisor to me, and I am proud to call him a friend as well as a teacher. His advice and guidance on several academic, professional, personal, and career choices have given me a much wider perspective on life. I have always enjoyed working in his lab and hope I can follow what I have learned from him in coming years. I would like to thank Dr. Li for bringing the CPU-Pacific joint culture program and the support all along the way. I would like to acknowledge and thank Dr. Miki S. Park, Dr. Qinliang Zhao, Dr. Russu, and Dr. Faridi for having served on my thesis committee. I would like to thank Dr. Miki Park and Dr. Felmlee for her kindness, support, and guidance through the many projects we have worked on together. I would also like to thank Dr. William Chan and Dr. Hyun Joo for the help and guidance. I would like to thank Dr. Uchizono for the guidance of statistics. I would like to thank my partner Tuhin and Fang who work shoulder to shoulder with me. I would like to thank my colleagues Dr. Mark Miller, Dr. Wabel Albusairi, Dr. Arindom, Raghavendra, Toufiq, Guangming, Hala, Arjun, Rasha, Abdulmalek, and Josh for their contribution towards my research and for their friendship.

I am grateful to all my friends, Ruiqi, Chao, Yuntao, Yingbo, Yifan, Shen, Jingda, Xuequn, Zhixin, Hao, You, Michael, Mallika, Zizhao and Zhaoxu for their encouragement

and support and for being a part of me like a family during my stay in Stockton. I would thank Dr. Al's family for their support. Last and but not least, I would like to thank my family for their unconditional love and support.

This is only one-third of the work during my Ph.D. More accomplishments can be found in Tuhin's dissertation, future publications from our lab papers and published paper in Fang Liu, Toufiq Ul Amin, Dengpan Liang, Miki S. Park, and Mamoun M. Alhamadsheh. "Enhancing the Pharmacokinetic Profile of Interleukin 2 through Site-Specific Conjugation to a Selective Small-Molecule Transthyretin Ligand." *Journal of Medicinal Chemistry* 64, no. 19 (2021): 14876-14886; Arindom Pal, Wabel Albusairi, Fang Liu, Md Tariqul Haque Tuhin, Mark Miller, Dengpan Liang, Hyun Joo et al. "Hydrophilic small molecules that harness transthyretin to enhance the safety and efficacy of targeted chemotherapeutic agents." *Molecular Pharmaceutics* 16, no. 7 (2019): 3237-3252; Mark Miller, Arindom Pal, Wabel Albusairi, Hyun Joo, Beverly Pappas, Md Tariqul Haque Tuhin, Dengpan Liang et al. "Enthalpy-driven stabilization of transthyretin by AG10 mimics a naturally occurring genetic variant that protects from transthyretin amyloidosis." *Journal of Medicinal Chemistry* 61, no. 17 (2018): 7862-7876; "Peripherally restricted transthyretin-based delivery system for probes and therapeutics avoiding opioid-related side effects." *Nature Communications*, 13(1), pp.1-15 (2022). Tuhin, M.T.H.*, Dengpan Liang* (*co-first-author), Liu, F.*, Aldawod, H., Amin, T. U., Ho, J. S., ... & Alhamadsheh, M. M..(Tuhin et al., 2022)

PERIPHERALLY RESTRICTED DELIVERY SYSTEM PROVIDES INSIGHTS ON THE ROLE OF CNS IN PRECIPITATING OPIOID-INDUCED CONSTIPATION

Abstract

By Dengpan Liang

University of the Pacific
2022

A serious opioid crisis is affecting public health and economics, eroding people's quality of life. 80% of patients who receive opioids suffer from adverse effects such as Opioid-induced constipation (OIC)(Kumar, Barker, & Emmanuel, 2014). However, there is no efficient medicine for these adverse effects. Notably, mainstream theory supports that analgesia effects are mainly controlled by CNS while OIC is predominately controlled by peripheral (Gao et al., 2021; Manara, Bianchi, Ferretti, & Tavani, 1986; Mori et al., 2013; Moss, 2019; Reimer et al., 2009; Stein, 2018; Thomas et al., 2008). In addition, the sites of action of opioid was based on the assumption that mu-opioid receptor antagonists (PAMORAs), did not cross the blood-brain barrier (BBB). Unfortunately, the BBB crossing of PAMORAs mislead the understanding of the role of the central nervous system (CNS) and gastrointestinal tract playing in the adverse effects such as opioid-induced constipation (OIC). Here, we developed a novel technology platform to prevent drugs from crossing the BBB. By applying this technology, naloxone- and oxycodone conjugates demonstrated superior potency, peripheral selectivity, pharmacokinetics, and effectiveness in rats compared to

currently clinically used PAMORAs. By the help of these probes, it is revealed for the first time to that the mu-opioid receptors in the CNS played more important role in OIC than the peripheral receptors, which overturned the old theory. And the new theory points the way to better future PAMORAs drug design.

TABLE OF CONTENTS

Table of Contents	9
List of Tables.....	12
List of Figures	13
List of Abbreviations.....	16
Chapter 1: General Introduction	17
Transthyretin	17
Structure of TTR	17
TTR Acts As Carrier Protein.....	18
AG10 Conjugation Increase Selectivity.....	18
Compound 1, An AG10 Analogue Does Not Cross BBB.....	19
Chapter 2: Blood-Brain Barrier and Opioid	21
2.1 Physiology of Blood-Brain Barrier	21
2.2 Approach To Prevent Crossing The Blood-Brain Barrier	21
2.3 Opioids, Central And Peripheral Effects.....	22
Chapter 3: Design the Truly Peripheral Opioid Antagonists	24
3.1 Hypothesis.....	24
3.2 Molecular Designs	25
Chapter 4: Synthesis of AG10-L1-Nal and AG10-L2-Nal	29
Chapter 5: Evaluation the In Vitro Activity	46
5.1. Evalutation of the binding to TTR	46

	10
5.1.1 Method:.....	46
5.1.2 Results:.....	48
5.2. Evaluation of the binding to opioid receptors.....	50
5.2.1 Method: Human Mu-opioid Receptor Binding (agonist radioligand) Assay.....	50
5.2.2 Method: Human Delta And Rat Kappa-opioid Receptor (agonist radioligand) Binding Assays.	51
5.2.3 Results: AG10-Naloxone Conjugates Displays High Affinity to Mu-opioid Receptor.....	52
5.2.4 Results: Exhibited High Affinity To Delta- And Kappa- Opioid Receptors.....	54
5.3. AG10-L2-Nal displayed competitive antagonistic activity in mu-opioid receptor functional assays.	56
5.3.1 Method: Functional activity assays.....	56
5.3.2 Result: AG10-L2-Nal Displays Competitive Agonism Activity To Mu-opioid Receptor.	57
Chapter 6: Evaluation the BBB Penetration and Pharmacokinetics.....	61
6.1 Serum Stability.....	61
6.2 Method for Evaluating BBB Penetration.....	63
6.3 Method For LCMS.....	64
6.4 Results of BBB Penetration	68
6.5 Method For Pharmacokinetics Study.....	70
6.6 Results For Pharmacokinetics Study	71
Chapter 7: Evaluation the In Vivo Efficacy of AG10-L2-Nal	74

	11
7.1 Evaluation of The Hot Plate Latency	74
7.2 Evaluation of Opioid-induced Constipation	78
Chapter 8: Exploring the Mists Behind the Low Efficiency	82
8.1 TTR Did Not Limit The Binding of AG10-L2-Nal To Opioid Receptor	82
8.2 AG10-L2-Nal Did Not Act As A Partial Agonist in Vivo	84
8.3 AG10-L2-Nal Provides New Insights Mu-opioid Receptors In The CNS Play Important Role In OIC.....	86
8.4 Proof From The Opposite Direction – Peripheral Concentrated Opioid Agonist.....	89
8.5 Confirmed From The Opposite Direction –Peripherally Restricted Opioid Agonist Probe.....	91
Chapter 9: Discussion.....	103
References	108

LIST OF TABLES

Table

1. Mass spectrometer conditions for multiple reaction monitoring (MRM) of the tested compounds.68
2. Pharmacokinetic parameters of naloxone, naloxegol and AG10-L2-Nal determined from the plasma concentrations after intravenous dosing.72
3. Pharmacokinetic parameters of naloxone, naloxegol and AG10-L2-Nal determined from the plasma concentrations after subcutaneous dosing.73
4. Pharmacokinetic parameters of oxycodone and AG10-L2-Oxy determined from the plasma concentrations after the subcutaneous dosing.98

LIST OF FIGURES

Figures

1	Crystal structure of TTR with monomers colored individually.....	18
2	Tri-functional molecule targeting the PSMA expressed cancer cell while reducing the passive diffusion to normal cell(Pal et al., 2019).	19
3	Brain uptake compound 1 in brain tissue and CSF. Brain or CSF to plasma ratio of compound 1.....	20
4	Concept of the AG10-based approach to limit BBB penetration of therapeutic molecules.	25
5	Chemical structures of compounds used in our studies.....	27
6	Modeled complexes of AG10-L1-Nal and AG10-L2-Nal to both TTR and mu- opioid receptors.	28
7	Synthesis of naloxone derivative 7.....	29
8	¹ H NMR spectrum of compound 6.....	31
9	¹³ C NMR spectrum of compound 6.....	31
10	¹ H NMR spectrum of compound 7.....	33
11	¹³ C NMR spectrum of compound 7.....	33
12	Synthesis of compound 11.....	34
13	¹ H NMR spectrum of compound 8.....	35
14	¹³ C NMR spectrum of compound 8.....	36
15	¹ H NMR spectrum of compound 9.....	37
16	¹³ C NMR spectrum of compound 9.....	38
17	¹ H NMR spectrum of compound 11.	39

18	¹³ C NMR spectrum of compound 11.	40
19	Supplementary Scheme 3.	40
20	¹ H NMR spectrum of AG10-L1-Nal.	42
21	¹³ C NMR spectrum of AG10-L1-Nal.	42
22	HPLC traces of AG10-L1-Nal.....	43
23	¹ H NMR spectrum of AG10-L2-Nal.	44
24	¹³ C NMR spectrum of AG10-L2-Nal.	45
25	HPLC traces of AG10-L1-Nal.....	45
26	Chemical structure of FPE probe	46
27	Chemical structure of Fluorescence Polarization Probe.....	48
28	Binding affinity of test compounds (0.01 μM to 20 μM) to TTR in buffer using fluorescence polarization assay.	49
29	FPE assay to evaluate the binding affinity and selectivity of the compounds to TTR.....	49
30	mu-opioid receptor binding assays	54
31	delta-opioid receptor (agonist radioligand) binding assays of (a) AG10-L2-Nal and (b) AG10-L2-Oxy.	55
32	kappa-opioid receptor (agonist radioligand) binding assays of (a) AG10-L2-Nal and (b) AG10-L2-Oxy.	56
33	Antagonist functional assay of AG10-L2-Nal and naloxegol.....	58
34	Competitive antagonism of morphine by AG10-L2-Nal at the human mu-opioid receptor.	60
35	Serum stability of AG10-L2-Nal in mouse, rat, and human serum.	62

36	LC-MS/MS calibration curves used to quantitate naloxone, naloxegol, and AG10-L2-Nal in rat plasma, brain, and CSF.	67
37	(a) Brain to plasma ratios and (b) CSF to plasma ratios of AG10-L2-Nal, naloxegol, and naloxone.	70
38	a Pharmacokinetics profile of AG10-L2-Nal, naloxegol, and naloxone.	72
39	Hot plate study of opioid antagonists in male Sprague-Dawley rats.....	76
40	GI transit study of opioid antagonists.....	80
41	Hot plate and gastrointestinal (GI) transit efficacy studies of AG10-L2-Nal (in the presence and absence of AG10) against morphine.....	83
42	Evaluating the potential partial agonistic behavior of AG10-L2-Nal	85
43	Evaluating the contribution of mu-opioid receptors in the CNS to analgesia and OIC.	89
44	Gastrointestinal (GI) transit assay of loperamide and Fentanyl.	91
45	Synthesis of AG10-L2-Oxy (4).	92
46	¹ H NMR Spectrum for AG10-L2-Oxy (4).....	95
47	¹³ C NMR Spectrum for AG10-L2-Oxy (4).	95
48	HPLC traces of AG10-L2-Oxy (4).	96
49	LC-MS/MS calibration curves used to quantitate oxycodone and AG10-L2-Oxy in rat plasma, brain, and CSF.....	98
50	Pharmacokinetic and pharmacodynamic evaluation of AG10-Oxycodone conjugate (AG10-L2-Oxy).	101

LIST OF ABBREVIATIONS

TTR	Transthyretin
T4	Thyroxine
FPE	Fluorescence Probe Exclusion
FP	Fluorescence Polarization
BBB	Blood-Brain Barrier
CNS	Central Nervous System
AUC	Area Under the Curve
IV	Intravenous
ICV	Intracerebroventricular
SC	Subcutaneous
MNTX	Methylnaltrexone
PAMORA	Peripherally acting mu-opioid receptor antagonist
DMSO	Dimethyl sulfoxide
DMF	Dimethylformamide
PEG	Polyethylene glycol

CHAPTER 1: GENERAL INTRODUCTION

Transthyretin

Transthyretin (TTR, also named as pre-albumin) is a protein that is synthesized by liver and circulates in blood and cerebrospinal fluid (CSF) It acts as a primary carrier of retinol (vitamin A) and a backup carrier of thyroxine (T_4) (<1% bound) through binding to holo-retinol-binding protein (RBP)(Blake, Geisow, Oatley, Rerat, & Rerat, 1978; Monaco, Rizzi, & Coda, 1995).

The normal range of TTR concentration in blood is between 3.5 to 7 μM while in CSF the concentration is around 500 nM(Stabilini, Vergani, Agostoni, & Agostoni, 1968).

Structure of TTR

Human TTR is a 55 kDa homotetrameric protein with four identical monomers. Each TTR monomer consists of 127 amino acid residues, which forms an extensive β -sheet structure (Figure 1) (Foss, Wiseman, & Kelly, 2005; Richardson & Cody, 2009). The four identical subunits (or monomers) of TTR form an internal channel at the weaker dimer-dimer interface where two T_4 molecules can bind to the resulting tetramer(Cody & Wojtczak, 2009). In addition to the thyroid hormones (T_4) and its metabolites, other pharmacologic agents and natural products, such as plant flavonoids, and nonsteroidal analgesic drugs can also bind in the T_4 for binding sites of TTR(Cody & Wojtczak, 2009).

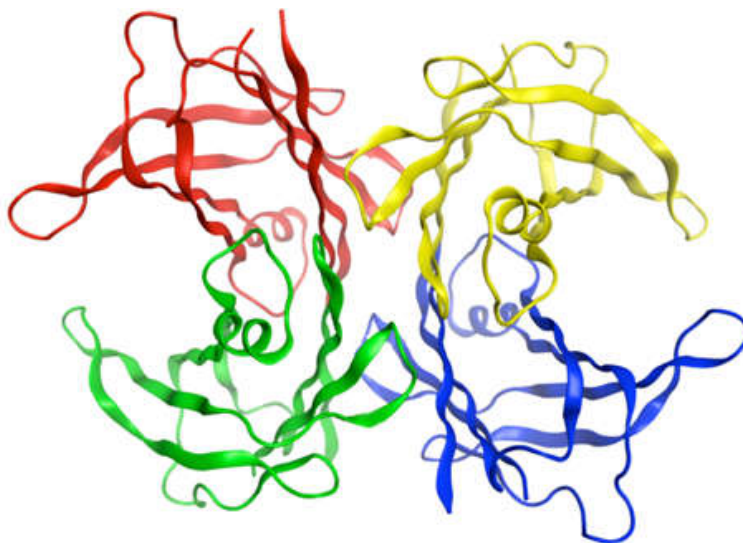


Figure 1. Crystal structure of TTR with monomers colored individually(Penchala et al., 2013).

TTR Acts As Carrier Protein

Recently, our group discovered a TTR binder AG10, which can reversibly binds to TTR T4 pockets(Miller et al., 2018; Penchala et al., 2013). Based on AG10, we designed ligands for half-life Extension (TLHE) for peptide and protein(Liu, Ul Amin, Liang, Park, & Alhamadsheh, 2021; Pal et al., 2019; Penchala et al., 2015). In this biomimetic system, AG10 were used as a ligand to harness TTR, and the peptide or protein was conjugated to AG10 through a linker. The TTR carries the conjugates circulating in the blood. The reversible binding of the conjugate can be released from TTR and bind to the target due to the higher affinity to the target. This successful technology increases the half-life by around 5 fold without compromising the binding affinity(Pal et al., 2019; Penchala et al., 2015).

AG10 Conjugation Increase Selectivity

Interestingly, the AG10 conjugation platform not only increases the half-life but also

increases the selectivity of the conjugates. In the previous study of our group, a tri-functional molecule including target ligand, payload, and AG10 (Figure 2), decreased the undesired passive diffusion to the normal cells while maintaining the IC_{50} on the target cancer cell and thus increased the selectivity by around 1000 fold(Pal et al., 2019). The high selectivity and the unique biodistribution of the AG10 conjugation platform will have a potential application.

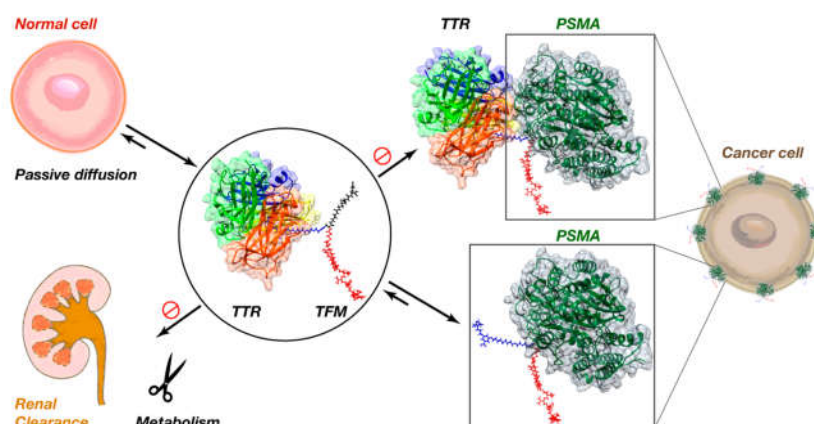


Figure 2. Tri-functional molecule targeting the PSMA expressed cancer cell while reducing the passive diffusion to normal cell(Pal et al., 2019).

Compound 1, An AG10 Analogue Does Not Cross BBB

There is something even more interesting. When we analyzed the pharmacokinetics profile of the linker compound **1**, we found that compound **1** does not penetrate the rat brain. Compound **1** was intravenously (IV) administrated through the cannula in the jugular vein. 30 minutes later, blood, brain tissue, and CSF were collected and the concentration of

compound **1** was quantified by LC-MS. The concentration of the rat plasma is 1.85 ± 0.34 μM , and the brain to plasma ratio for **1** (1.2%) and the CSF to plasma ratio (1.3%) (Figure 3) were less than 2%, which is defined as the threshold not considering to cross the BBB(Shaffer, 2010). Because during the brain and CSF collection, there is some unavoidable contamination.

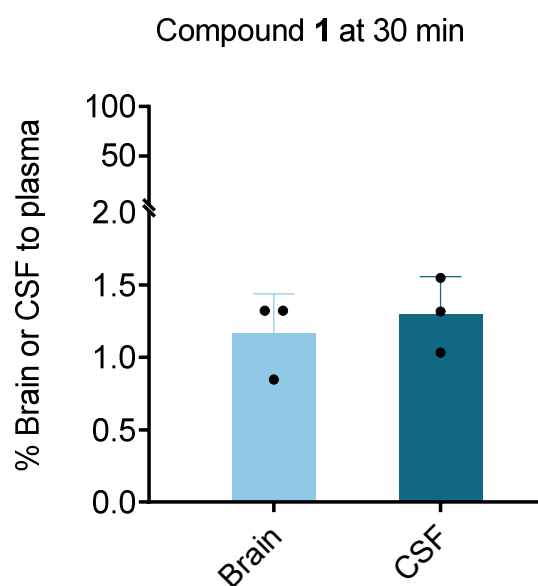


Figure 3. Brain uptake compound **1** in brain tissue and CSF. Brain or CSF to plasma ratio of compound **1**. 30 minutes after 50 $\mu\text{mol/kg}$ of compound **1** was injected into rats, plasma, brain, and CSF were collected and concentration of the compound **1** was quantified by LC-MS. The Bar graphs represent the respective mean (\pm s.d.) ($n = 3$ for each group) (Helped by Fang)

CHAPTER 2: BLOOD-BRAIN BARRIER AND OPIOID

2.1 Physiology of Blood-Brain Barrier

The blood-brain barrier (BBB) is formed by endothelial cells of the capillary wall, astrocyte end-feet of capillaries, and pericytes embedded in the basement membrane of capillaries. At the interface between the blood and the brain, endothelial cells are connected by tight junctions consisting of smaller subunits of transmembrane proteins such as occludins, junction adhesion molecules such as JAM-A and claudins (Daneman & Prat, 2015). The tight junction reduces the paracellular flux of hydrophilic molecules. In contrast, small hydrophobic molecules can cross the membrane along the concentration gradient (Ballabh, Braun, & Nedergaard, 2004). Nutrients such as glucose and amino acid cross the barrier via the transporters.

2.2 Approach To Prevent Crossing The Blood-Brain Barrier

Even though there are several therapeutics and for delivering drugs across the BBB, there are limited approach and limited investigation on prevent the drug crossing the BBB (Banks, 2016). On the other hand, separating the central and peripheral effects is needed to reduce the undesired the central side effects. It showed the potential of the linker, compound **1**, had a potential to prevent the drug conjugates from penetrating the brain.

Many PAMORAs are based on the structure of morphinan where the additional polarity is introduced by forming a quaternary salt at the morphinan nitrogen (e.g., methylnaltrexone, which is a quaternary derivative of naltrexone). However, the

introduction of the quaternary ammonium group in opioid antagonists often leads to a 10 to 100-fold reduction in potency. For example, methylnaltrexone (MNTX) exhibits only 1% to 3% of the affinity for the mu-opioid receptors as naltrexone itself (Greenwood-Van Meerveld & Standifer, 2008). The issues presented by quaternary opiates' metabolic instability can be solved by employing opiate derivatives in which the required hydrophilicity is added to opioids by adding a short polyethylene glycol (PEG). For example, naloxegol is a naloxone derivative in which the tertiary amino group is preserved, and a short PEG is added to the morphinan ring at the 6-position (Floettmann, Bui, Sostek, Payza, & Eldon, 2017).

2.3 Opioids, Central And Peripheral Effects

Opioid agonists, such as morphine, oxycodone, and heroin, bind to the opioid receptor, triggering the G-protein, subsequently promoting the K^+ channel and inhibiting the Ca^{2+} channel, reducing the signal transmission through the neuron, finally producing the morphine-like effects (Sobczak, Salaga, Storr, & Fichna, 2014). The central effects include analgesia, sedation, nausea, and respiratory depression, while the peripheral effects are mainly opioid-induced constipation (OIC) (Stein et al., 2009). Mainstream theory supports that analgesia effects is mainly controlled by CNS while OIC is predominately controlled by peripheral (Gao et al., 2021; Manara et al., 1986; Mori et al., 2013; Moss, 2019; Reimer et al., 2009; Stein, 2018; Thomas et al., 2008). For example, morphine by systemic administration distributes into gastrointestinal tract (GI tract) causing OIC, into brain causing analgesia effects, respiratory depression, and others CNS effects. Opioid-induced constipation (OIC) is the most prevalent adverse effect of opioid use, impacting 80% of patients using opioids

for cancer pain or chronic non-cancer pain. OIC can be difficult to treat and, in contrast to other side effects, tolerance to OIC does not develop (Kumar et al., 2014; Moss & Rosow, 2008; Nalamachu et al., 2015). Although laxatives are the first-line treatment for treating OIC, they do not attack the underlying mechanism of OIC, and so most patients will not have their constipation adequately cured with laxative. Surveys showed that 25-50% of patients skipped, decreased, or discontinued their opioid medication because of OIC, even preferring accepting pain instead of constipation (Bell et al., 2009; Chamberlain, Rhiner, Slatkin, Stambler, & Israel, 2020).

CHAPTER 3: DESIGN THE TRULY PERIPHERAL OPIOID ANTAGONISTS

3.1 Hypothesis

The reverse binding to TTR and the higher binding affinity to opioid receptors allow the AG10-conjugates' release from TTR and selectively bind to the opioid receptors. Because there is no bulky group like covalent conjugates, the intrinsic activity of the AG10-conjugates would be unaffected. The TTR carrying will increase the circulation half-life of the conjugates. And the hydrophilicity of the compound **1** and the TTR protection will prevent the molecules going into brain. Based on the mainstream theory, this potent molecules by systemic administration will be restricted to peripheral, reversing the OIC by GI tract, while do not affect the analgesia effects by CNS (Figure 4). This should be potential for truly peripheral restricted opioid conjugates for therapeutics and allow the investigation about the site of action of opioids.

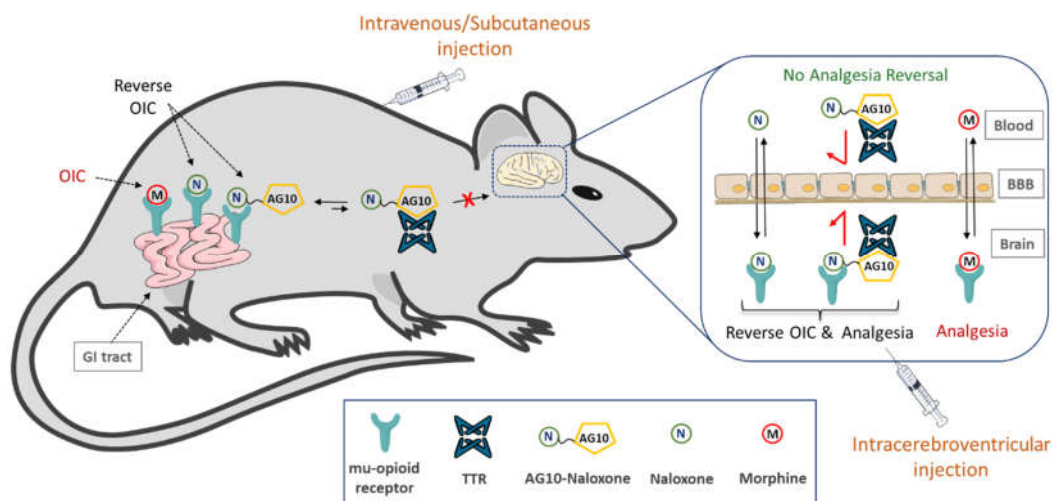


Figure 4. Concept of the AG10-based approach to limit BBB penetration of therapeutic molecules. Lipophilic mu-opioid receptor antagonists (e.g., naloxone) are hypothesized to reverse opioid-induced constipation (OIC) caused by the interaction of morphine (opioid agonist) with mu-opioid receptors in the gastrointestinal (GI) tract. However, these antagonists can also cross the blood-brain barrier (BBB) and displace morphine from the mu-opioid receptors in the brain, which results in reversing the intended analgesic effect of morphine. By conjugating naloxone to the hydrophilic derivative of AG10, we generated an AG10-Naloxone conjugate that has limited penetration across the BBB. The high peripheral selectivity of the AG10-Naloxone conjugate to the mu-opioid receptors in the GI tract is attributed to the high polarity of the AG10 ligand and reversible binding to the abundant plasma protein, transthyretin (TTR). Increasing the hydrophilicity of molecules is typically associated with fast renal excretion and shorter in vivo half-life. Unlike other approaches, the binding of our hydrophilic AG10 conjugates to TTR in plasma (TTR half-life is ~2 days) results in an extended circulation half-life. Because of their high selectivity to the peripheral tissues, the AG10-Naloxone conjugate should reverse the action of opioid agonists (e.g., morphine) in the GI tract without compromising the analgesic effect of opioid agonists in the brain or precipitating opioid-related withdrawal symptoms. In addition, direct intracerebroventricular administration of the AG10-Naloxone conjugate in the brain will allow for evaluating the role of mu-opioid receptors in the brain in causing analgesia and constipation, without any effect on mu-opioid receptors in the periphery.

3.2 Molecular Designs

The undesired adverse effect of morphine is notorious. Thus, naloxone would be an ideal candidate and was chosen to address these issues for the following considerations.

First, naloxone has a strong affinity for the mu-opioid receptor ($K_i = 0.29$ nM), which is the main opioid receptor involved with OIC. Because of its lipophilicity, naloxone can pass the blood-brain barrier more readily, resulting in higher concentrations in the brain. This property would be perfect for determine whether or not our strategy is successful in restricting lipophilic molecule penetration of the BBB. Naloxone has a well-established structure-activity relationship (SAR). The binding affinity of agonists and antagonists like morphine and naloxone was not significantly affected when the morphinan structure was modified at the 6-position. Naloxegol (naloxone with the hydrophilic polyethylene glycol side chain at 6-position) is an example of naloxegol (Figure 5). Naloxegol's ability to bind to the mu-opioid receptors remained strong, despite this change. Besides, modeling indicated that the length of the linker would also influence the binding affinity (Figure 6). Thus, two naloxone conjugates with different length of linker were designed for the further study. The details of synthesis will be described in the next chapter.

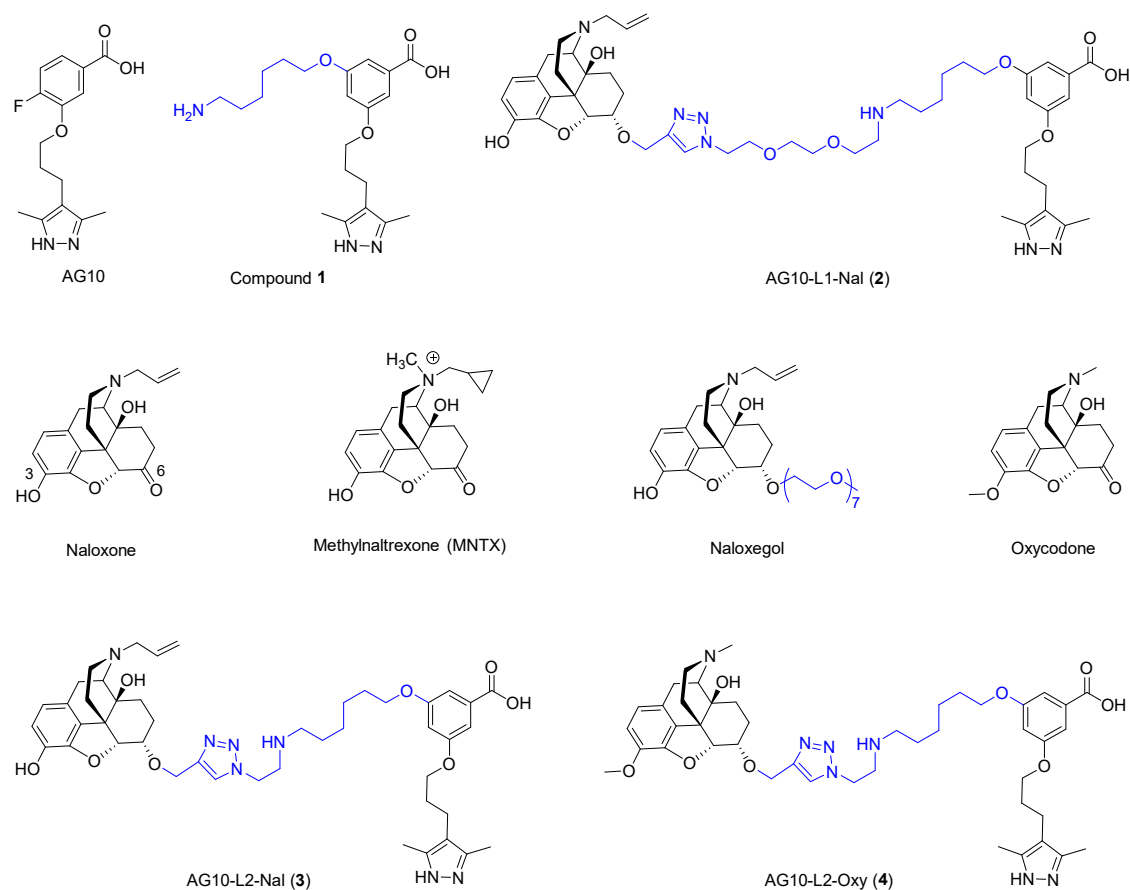


Figure 5. Chemical structures of compounds used in our studies.

AG10 and compound 1 are selective TTR ligands. Naloxone is an opioid antagonist that crosses the blood-brain barrier (BBB). MNTX and naloxegol are PAMORAs approved to treat OIC. AG10-L1-Nal and AG10-L2-Nal are conjugates of AG10 and naloxone using linkers (L1 and L2) of different lengths. Oxycodone is an analgesic opioid agonist. AG10-L2-Oxy is a conjugate of AG10 and oxycodone. (Data generated with Tuhin)

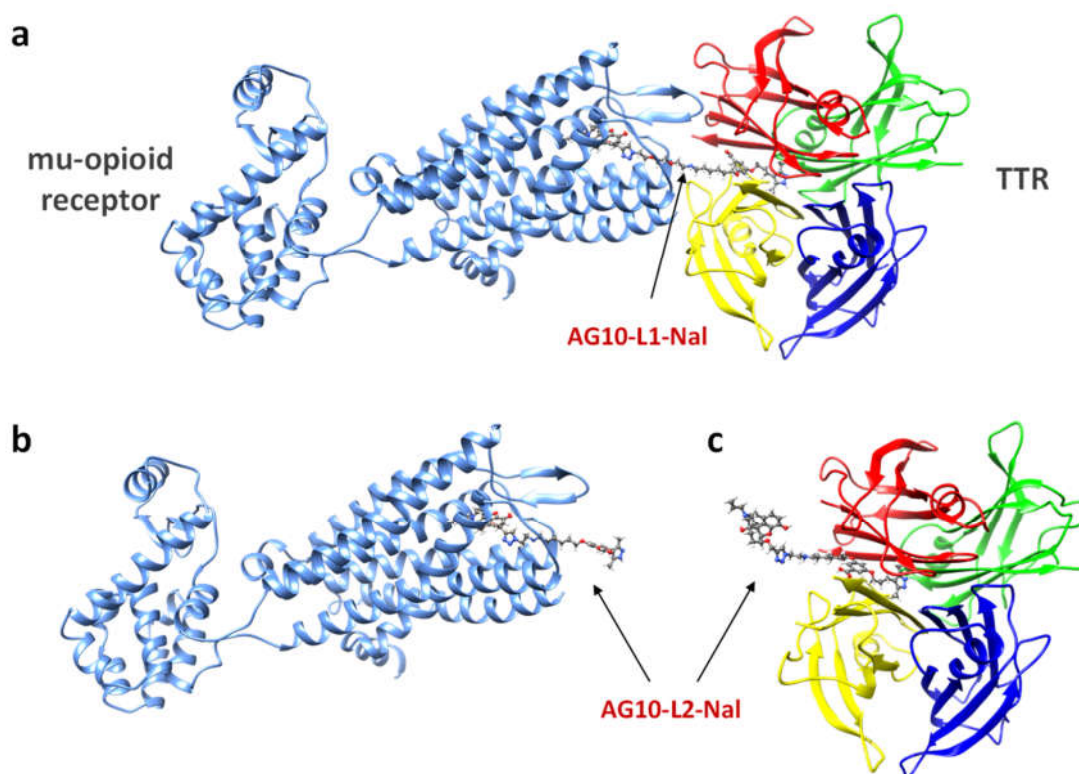


Figure 6. Modeled complexes of AG10-L1-Nal and AG10-L2-Nal to both TTR and mu-opioid receptors. **a** The linker length for AG10-L1-Nal (~ 20 Å) is long enough to allow AG10-L1-Nal to bind to both the mu-opioid receptor and transthyretin (TTR) simultaneously. The AG10-L2-Nal linker is shorter which allows AG10-L2-Nal to bind to either **b** the mu-opioid receptor (pdb id: 4DKL)(Manglik et al., 2012) or **c** TTR (pdb id: 4HIQ)(Penchala et al., 2013) but not both proteins at the same time. Because of the higher affinity of AG10-L2-Nal to the mu-opioid receptor ($K_i = 1.3$ nM) over TTR ($K_d = 333$ nM), AG10-L2-Nal will preferentially bind to the mu-opioid receptor over TTR. (Data helped by Dr. Hyun Joo)

CHAPTER 4: SYNTHESIS OF AG10-L1-NAL AND AG10-L2-NAL

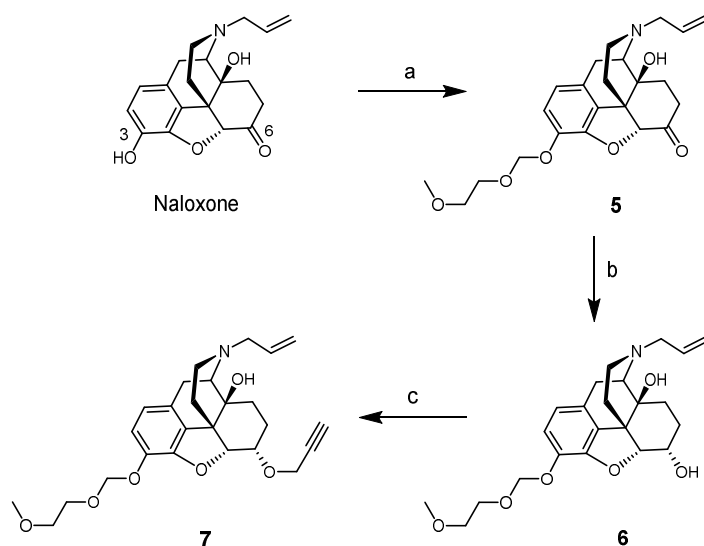
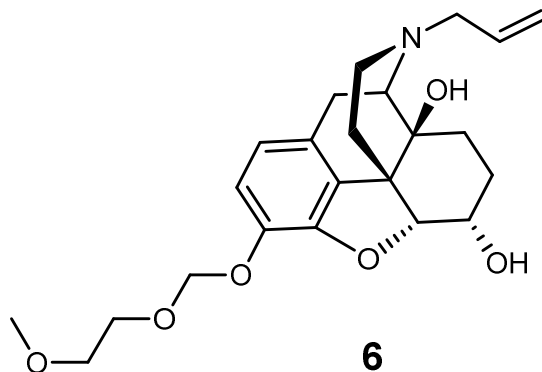


Figure 7. Synthesis of naloxone derivative 7.

(a) diisopropylethylamine, 2-methoxyethoxymethyl chloride, CH_2Cl_2 , room temperature, overnight; (b) sodium triethylborohydride, THF, 0°C , 3.5 hours; (c) sodium hydride, DMF, propargyl bromide, 4 hours. (Data generated with Tuhin)



(4*R*,4*aS*,7*S*,7*aR*,12*bS*)-3-allyl-9-((2-methoxyethoxy)methoxy)-1,2,3,4,5,6,7,7*a*-octahydro-4*aH*-4,12-methanobenzofuro[3,2-*e*]isoquinoline-4*a*,7-diol (α -6-OH-3-MEM-O-Naloxol) (6).

Compound **5** was synthesized as reported (Patent US 8,563,726 B2). **5** (3-MEM-O-naloxone base) (100 mg, 0.24 mmol, 1 equiv) under nitrogen atmosphere at 0°C in anhydrous tetrahydrofuran (6 mL), 1M solution of sodium triethylborohydride (0.36 mL, 0.36 mmol, 1.5 equiv) slowly was added to the solution. The solution was stirred for 5 hours in a nitrogen environment before being brought to room temperature. The surplus sodium triethylborohydride was then destroyed by slowly adding acetic acid (0.5 mL). Under reduced pressure, the solvent was withdrawn, and the residual residue was dissolved in CH₂Cl₂ (30 mL). 0.1 N HCl/NaCl water solution (3x30 mL) was used to extract the CH₂Cl₂ phase, and the combined aqueous extracts were washed with CH₂Cl₂ (1x30 mL). To bring the pH of the aqueous solution to 8, sodium carbonate was added. The organic extracts were mixed, dried over anhydrous Na₂SO₄, filtered, and the solvent was withdrawn under reduced pressure, and the resultant residue was dried overnight in vacuum to get compound **6** (89 mg, 0.21 mmol, 89% isolated yield) ESI-MS: Exact mass calcd for C₂₃H₃₁NO₆ [M+H]⁺ 418.2, [M+Na]⁺ 440.2; found: 417.8, 440.3. NMR data showed that the more than 99% of the product was α-6-OH-3-MEM-O-naloxol, no β epimer was detected.

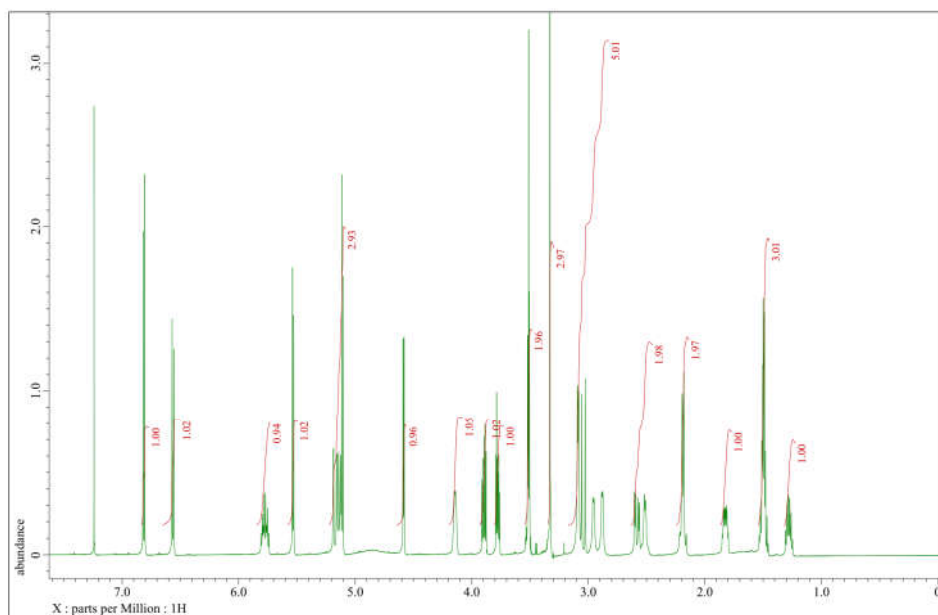


Figure 8. ^1H NMR spectrum of compound 6.

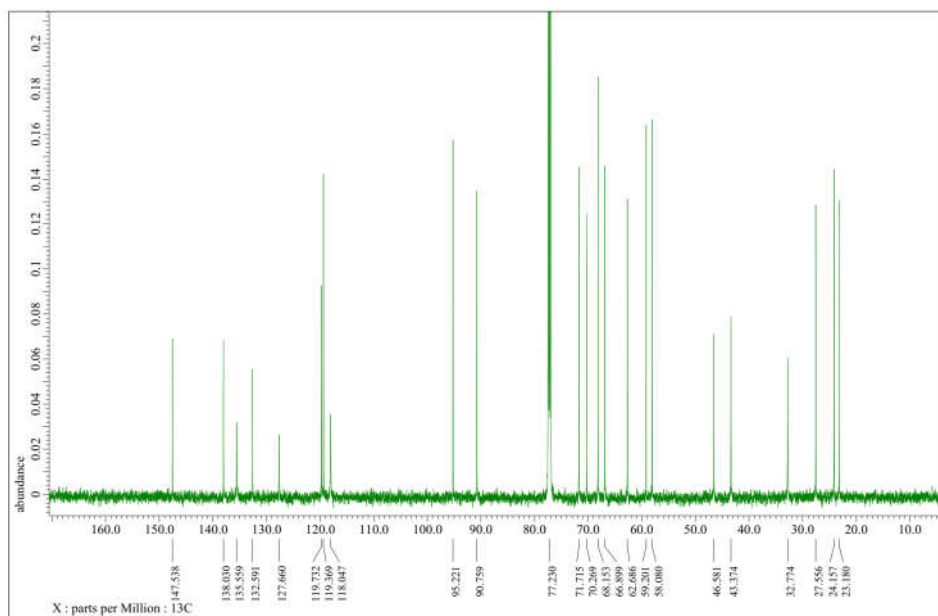
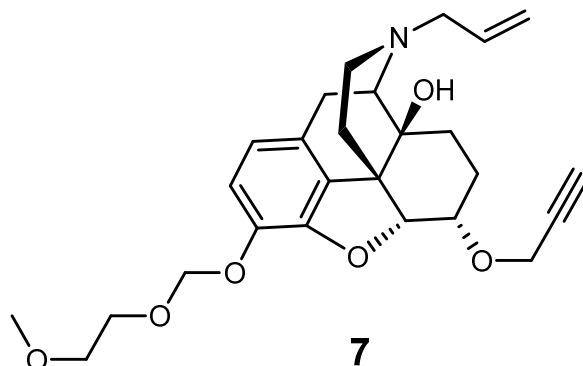


Figure 9. ^{13}C NMR spectrum of compound 6.



(4R,4aS,7S,7aR,12bS)-3-allyl-9-((2-methoxyethoxy)methoxy)-7-(prop-2-yn-1-yloxy)-1,2,3,4,5,6,7,7a-octahydro-4aH-4,12-methanobenzofuro[3,2-e]isoquinolin-4a-ol (**7**).

Slowly added sodium hydride (60 percent in oil) (12.79 mg, 0.32 mmol, 1.5 equiv) to a solution of -6-OH-3-MEM-O-Naloxol (**6**) (89 mg, 0.21 mmol, 1 equiv) in anhydrous dimethylformamide (2 mL) under an inert atmosphere at 0 °C (via an ice bath). For one hour, the solution was stirred in a nitrogen atmosphere. The solution was then treated with propargyl bromide (80 percent w/v) (47.54 L, 0.32 mmol, 1.5 equiv). To quench the reaction, 0.5 mL deionized water was added to the reaction mixture after 4 hours. The solution was then treated with 50 mL ethyl acetate before being extracted with brine (4x25 mL), and the combined aqueous extracts were washed with ethyl acetate again (1x25 mL). The ethyl acetate fractions were combined, dried over anhydrous Na₂SO₄, filtered, and the solvent was removed under reduced pressure. Flash column chromatography (silica gel, 0-100 percent ethyl acetate/hexane) was used to isolate compound **7** (73 mg, 0.16 mmol, 75 percent isolated yield) as a brownish viscous liquid. ESI-MS: Exact mass calcd for C₂₆H₃₃NO₆ [M+H]⁺ 456.2, [M+Na]⁺ 478.2; found: 456.6, 478.6.

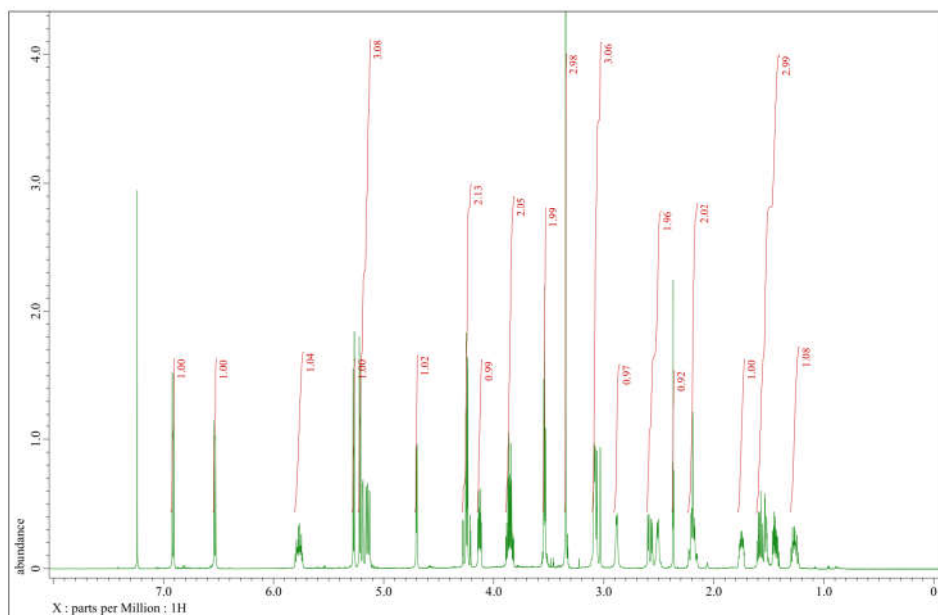


Figure 10. ^1H NMR spectrum of compound 7.

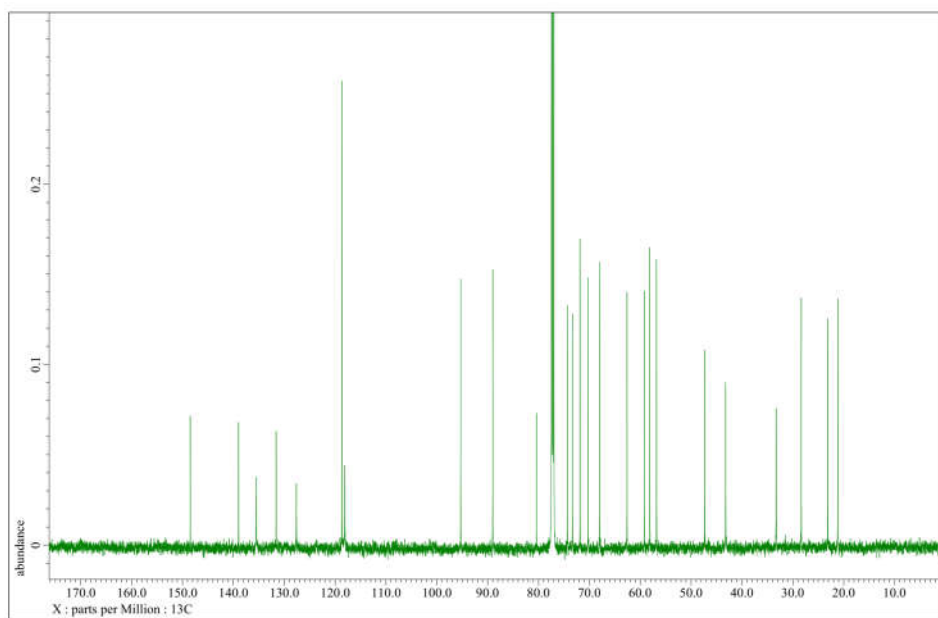


Figure 11 ^{13}C NMR spectrum of compound 7.

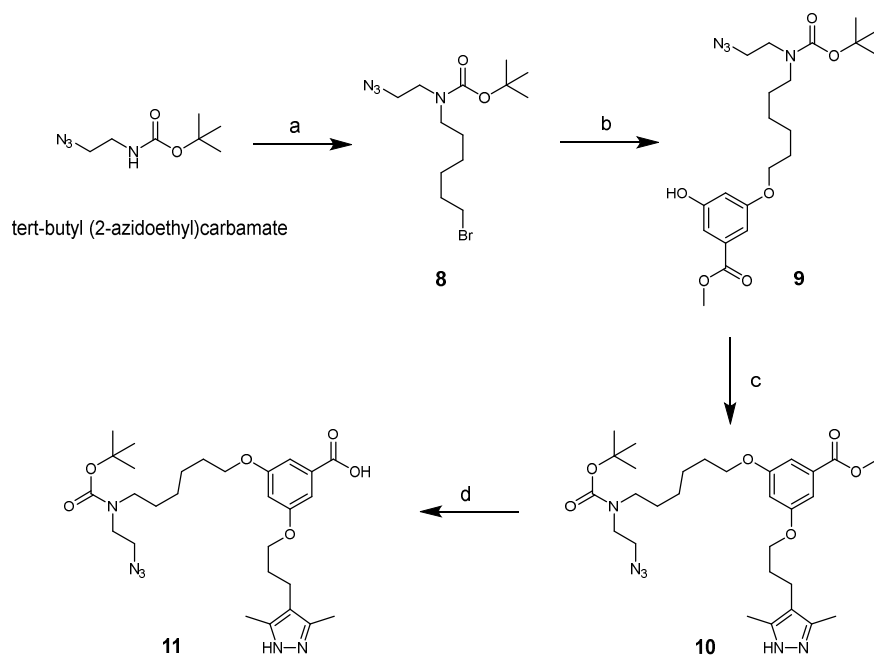
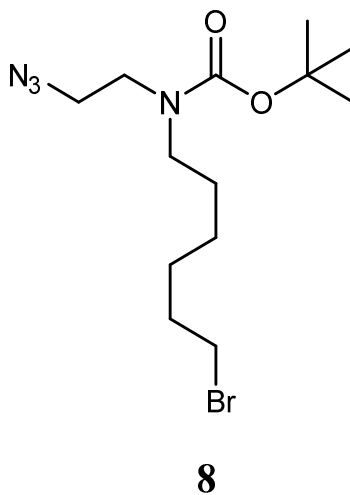


Figure 12. Synthesis of compound 11.

(a) sodium hydride, 1,6-dibromohexane, DMF, room temperature, 2 hours; (b) methyl 3,5-dihydroxybenzoate, K_2CO_3 , DMF, room temperature, 16 hours; (c) triphenylphosphine, 3-(3,5-dimethyl-1H-pyrazol-4-yl)propan-1-ol, diisopropyl azodicarboxylate, THF, ultrasonication, 15 minutes; (d) $LiOH \cdot H_2O$, H_2O/THF (1:1), room temperature, 14 hours. (Data generated with Tuhin)



tert-butyl (2-azidoethyl)(6-bromohexyl)carbamate (**8**)

Under an inert environment, sodium hydride (60 percent in oil) was added to a solution of tert-butyl (2-azidoethyl)carbamate (6000 mg, 32.24 mmol, 1 equiv) (2579 mg, 64.48 mmol, 2 equiv). A nitrogen atmosphere was used for stirring the solution for one hour. The solution was then mixed completely at once with 1,6-dibromohexane (density = 1.58 g/mL) (24.68 mL, 161.1 mmol, 5 equiv). After two hours, 5 mL deionized water was gently added to the reaction mixture while stirring to quench it. The solution was then added 400 mL ethyl acetate and extracted with brine (3x150 mL), and the combined aqueous extracts were rinsed with ethyl acetate again (1x150 mL). Drying the mixed ethyl acetate fractions over anhydrous Na₂SO₄, filtering, and removing the solvent at reduced pressure. To obtain compound **8**, the residue was purified by flash column chromatography (silica gel, 0-100 percent ethyl acetate/hexane) (3890 mg, 11.14 mmol, 35 percent isolated yield). ESI-MS: exact mass calcd for C₁₃H₂₅BrN₄O₆ [M+Na]⁺ 371.1; found: 371.1.

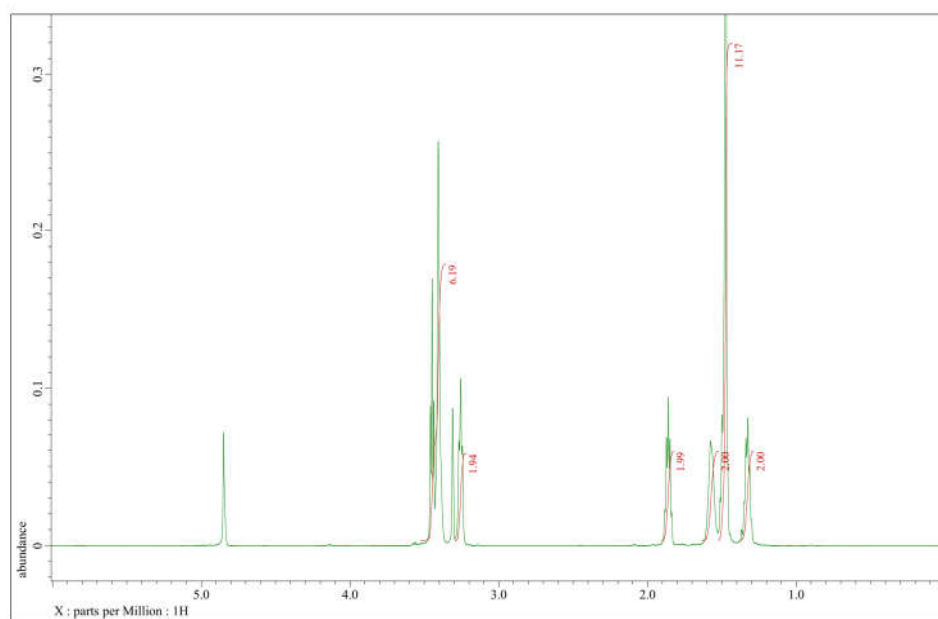


Figure 13. ¹H NMR spectrum of compound 8.

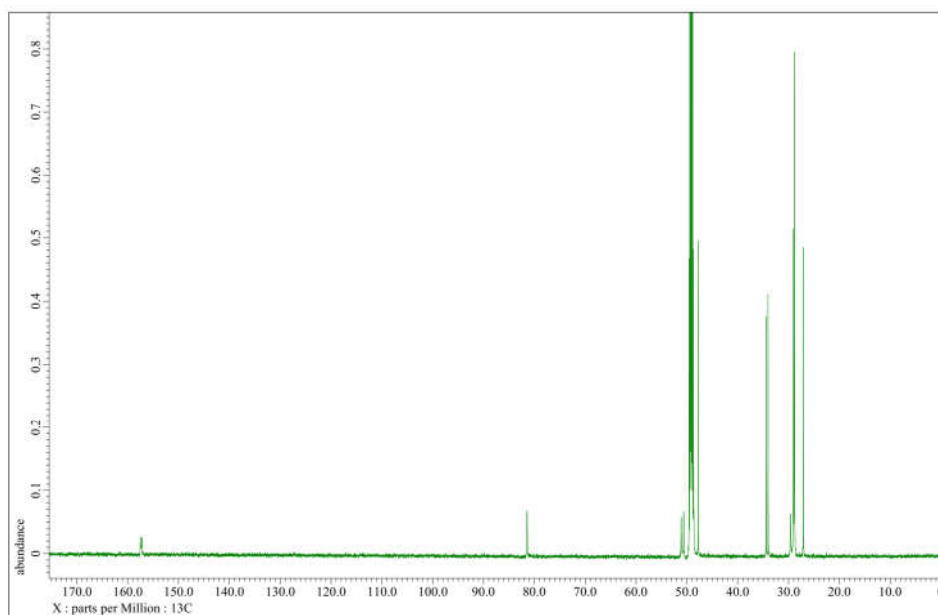
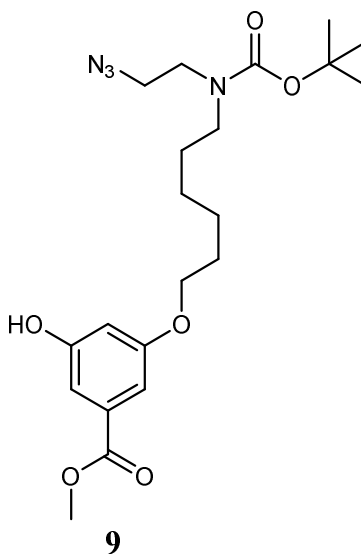


Figure 14. ^{13}C NMR spectrum of compound 8.



Methyl 3-(((6-((2-azidoethyl)(tert-butoxycarbonyl)amino)hexyl)oxy)-5-hydroxybenzoate (9).

K_2CO_3 (3890 mg, 11.14 mmol, 1 equiv) was added to a solution of 8 (3890 mg, 11.14 mmol, 1 equiv) and methyl 3,5-dihydroxybenzoate (5620 mg, 33.42 mmol, 3 equiv) in anhydrous dimethylformamide (30 mL) (2309 mg, 16.71 mmol, 1.5 equiv). At room

temperature, the suspension was agitated for 16 hours. Water was used to quench the suspension, which was then diluted with 300 mL ethyl acetate and washed with brine (3x150 mL). The ethyl acetate fraction was concentrated in vacuum after being dried over anhydrous sodium sulfate. The solution was concentrated under decreased pressure, and the residue was purified by flash column chromatography (silica gel, 0-20% ethyl acetate/hexane) to get 9 (2.86 g, 59 percent yield); ESI-MS: exact mass calcd for $C_{21}H_{32}N_4O_6$ $[M+Na]^+$ 459.2; found: 459.5.

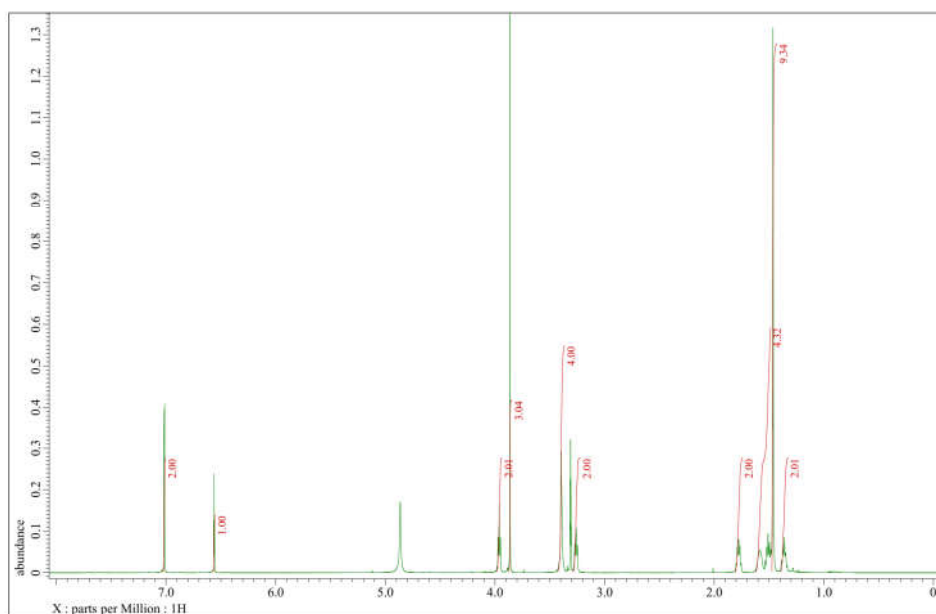


Figure 15. 1H NMR spectrum of compound 9.

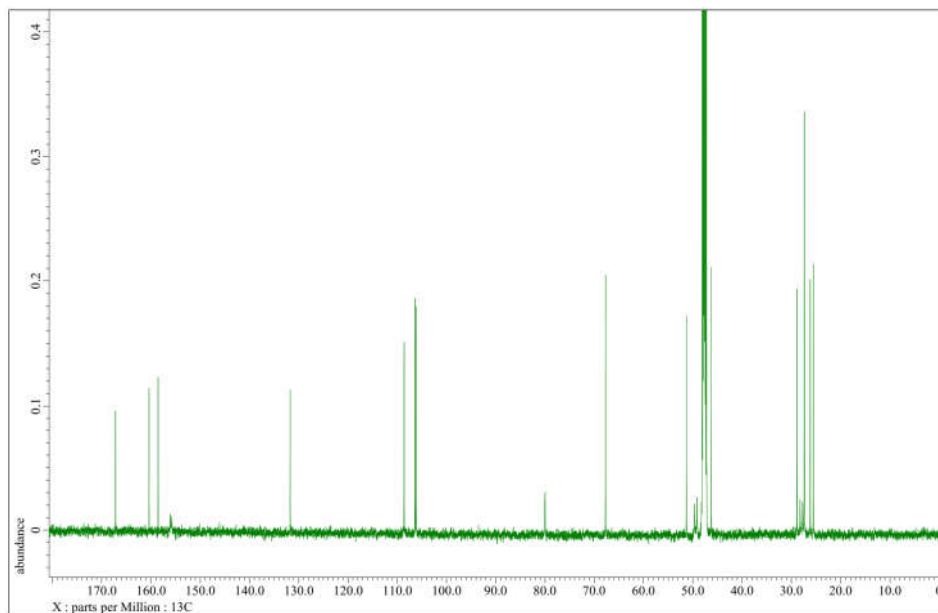
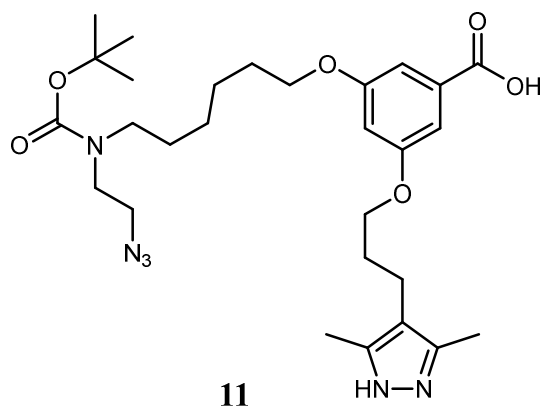


Figure 16. ^{13}C NMR spectrum of compound 9.



3-((6-((2-azidoethyl)(tert-butoxycarbonyl)amino)hexyl)oxy)-5-(3-(3,5-dimethyl-1H-pyrazol-4-yl)propoxy)benzoic acid (**11**).

Compound **9** (1000 mg, 2.29 mmol, 1 equiv), 3-(3,5-dimethyl-1H-pyrazol-4-yl)propan-1-ol (371 mg, 2.41 mmol, 1.05 equiv), and triphenylphosphine (750 mg, 2.86 mmol, 1.25 equiv) were mixed and sonicated for 2 minutes at 42 KHz (Müller et al., 2017). Then, diisopropyl azodicarboxylate (616 L, 2.86 mmol, 1.25 equiv) was added dropwise over

a 2-minute period and sonicated for 15 minutes. Under decreasing pressure, the solution was concentrated. To obtain intermediate **10**, the residue was purified by flash column chromatography (silica gel, 0-10 percent MeOH/CH₂Cl₂) (941 mg, 72 percent yield).

LiOH.H₂O was added to a solution of **10** (1915 mg, 3.33 mmol, 1 equiv) in a combination of THF (8 mL) and water (8 mL) (280 mg, 6.67 mmol, 2 equiv). After 14 hours of heating at 50 °C, the reaction mixture was concentrated under decreased pressure. The aqueous solution was adjusted to a pH of 4 with acetic acid, and the solution was concentrated under decreased pressure. Ten percent methanol in ethyl acetate was used to remove the residue. Under reduced pressure, the mixed organic extracts were condensed to produce **11** (1.09 g, 59% yield); ESI-MS: exact mass calcd for C₂₈H₄₂N₆O₆ [M+H]⁺ 559.3; found: 559.5.

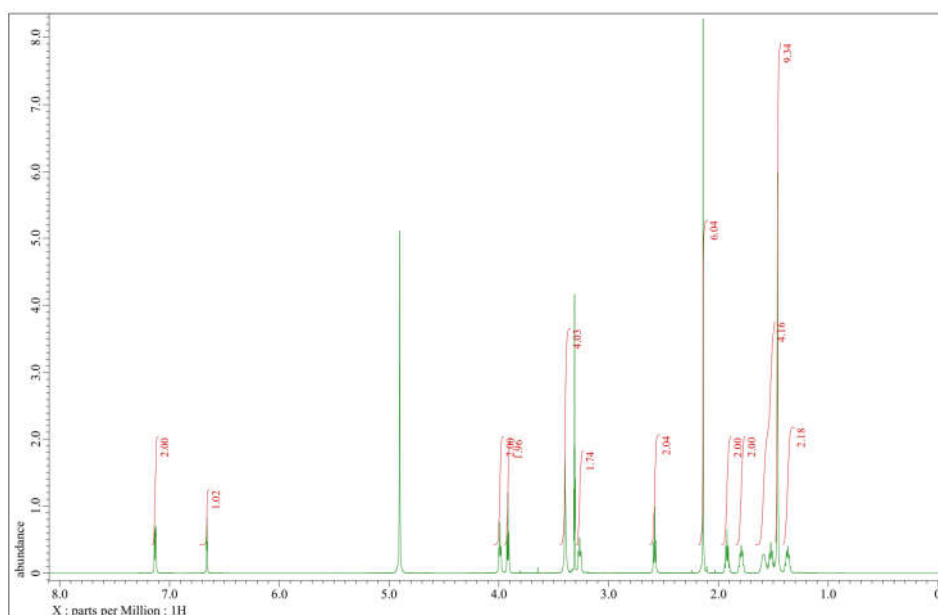


Figure 17. ¹H NMR spectrum of compound 11.

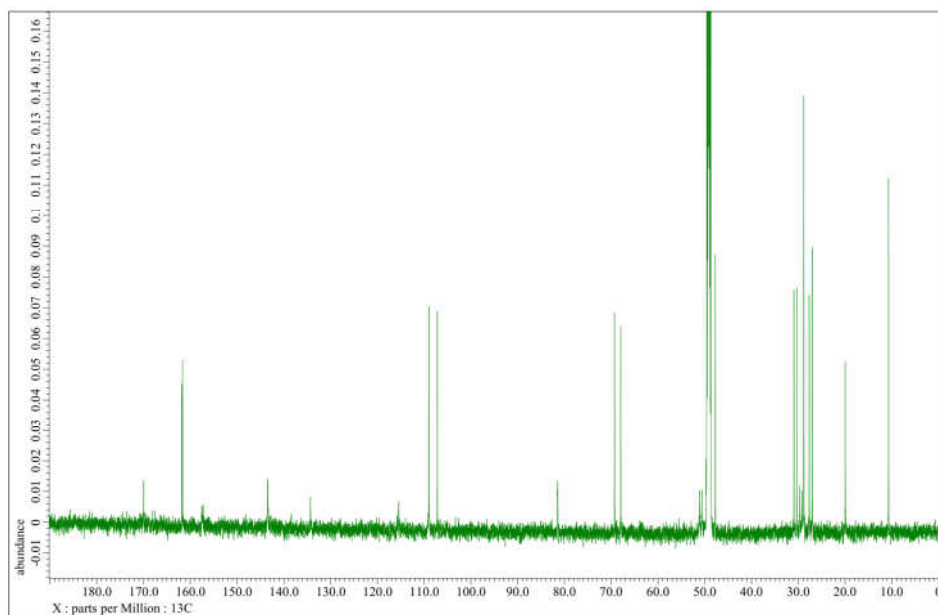


Figure 18. ^{13}C NMR spectrum of compound 11.

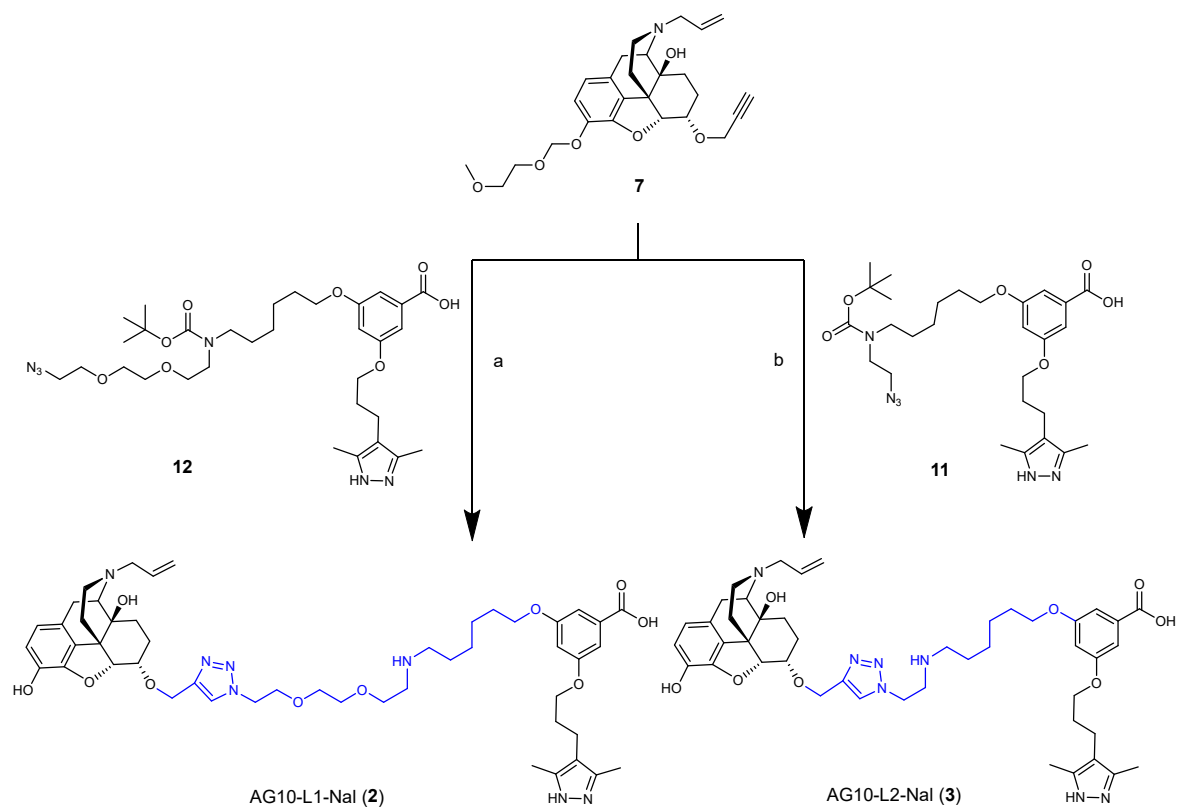
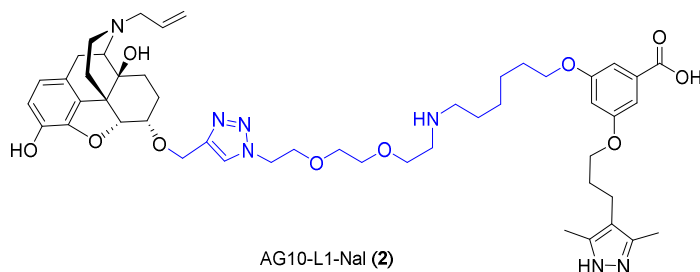


Figure 19. Supplementary Scheme 3.

Synthesis of AG10-L1-Nal (2) and AG10-L2-Nal (3). (a) (i) Compound 11, CuSO_4 , sodium ascorbate, $\text{THF}/\text{H}_2\text{O}$ (4:1), room temperature, overnight; (ii) $\text{CH}_2\text{Cl}_2/\text{TFA}$ (4:1), room

(Figure 19 Continued)

temperature, 2 hours; (b) (i) Compound 11, CuSO₄, sodium ascorbate, THF/H₂O (4:1), room temperature, overnight; (ii) CH₂Cl₂/TFA (4:1), room temperature, 2 hours. (Data generated with Tuhin)



3-((6-((2-(2-(2-(4-(((4R,7S,7aR,12bS)-3-allyl-4a,9-dihydroxy-2,3,4,4a,5,6,7,7a-octahydro-1H-4,12-methanobenzofuro[3,2-e]isoquinolin-7-yl)oxy)methyl)-1H-1,2,3-triazol-1-yl)ethoxy)ethoxy)ethyl)amino)hexyl)oxy)-5-(3-(3,5-dimethyl-1H-pyrazol-4-yl)propoxy)benzoic acid (AG10-L1-Nal) (2).

Compound **7** (21 mg, 0.0461 mmol, 1 equiv), **12** (29.8 mg, 0.0461 mmol, 1 equiv, synthesized as reported earlier(Pal et al., 2019)), CuSO₄·5H₂O (2.9 mg, 0.0115 mmol, 0.25 equiv), and sodium ascorbate (4.6 mg, 0.0231 mmol, 0.5 equiv) were used to perform the click (CuAAC) coupling in 3 mL mixture of THF/H₂O at room temperature, the reaction mixture was stirred overnight. Under vacuum pressure, the solution was concentrated. Hexane:ethyl acetate was used to remove the residue. The combined organic extracts were condensed at reduced pressure to provide an intermediate that could be directly employed in the following phase. Then, to a solution of the intermediate, a combination of TFA and CH₂Cl₂, (1:4 ratio) (1 mL) was added, and the reaction mixture was agitated for 2 hours at room temperature. The solution was concentrated under decreased pressure and purified using preparative HPLC to obtain AG10-L1-Nal (2) (18 mg, 43% yield in two processes) (98 percent purity by HPLC); *t_R* (C4 column) = 10.0 minutes; *t_R* (C18 column) = 19.2 minutes; HRMS (DART) *m/z*: calcd for C₄₉H₆₈N₇O₁₀ [M+H]⁺ 914.5022; found: 914.5039.

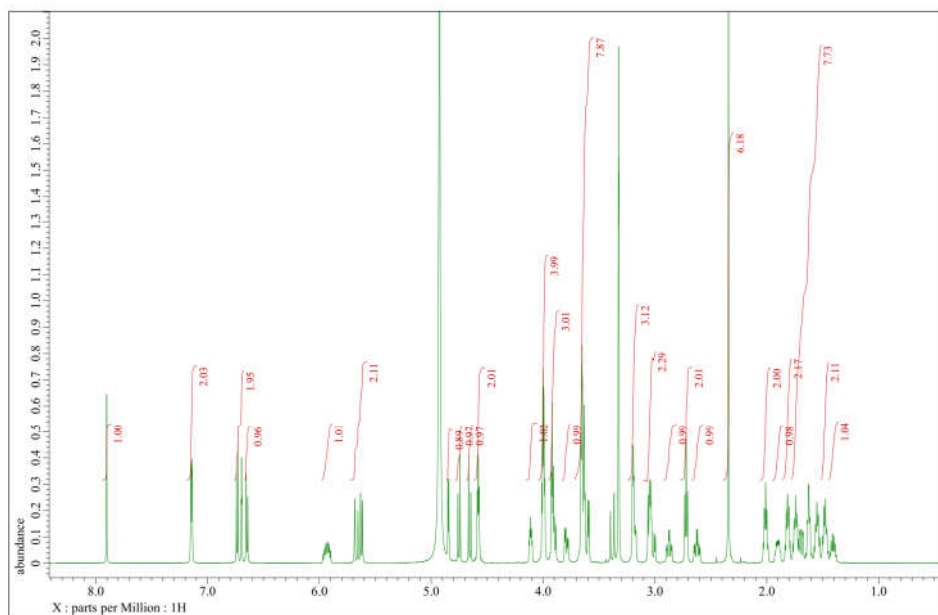


Figure 20. ¹H NMR spectrum of AG10-L1-Nal.

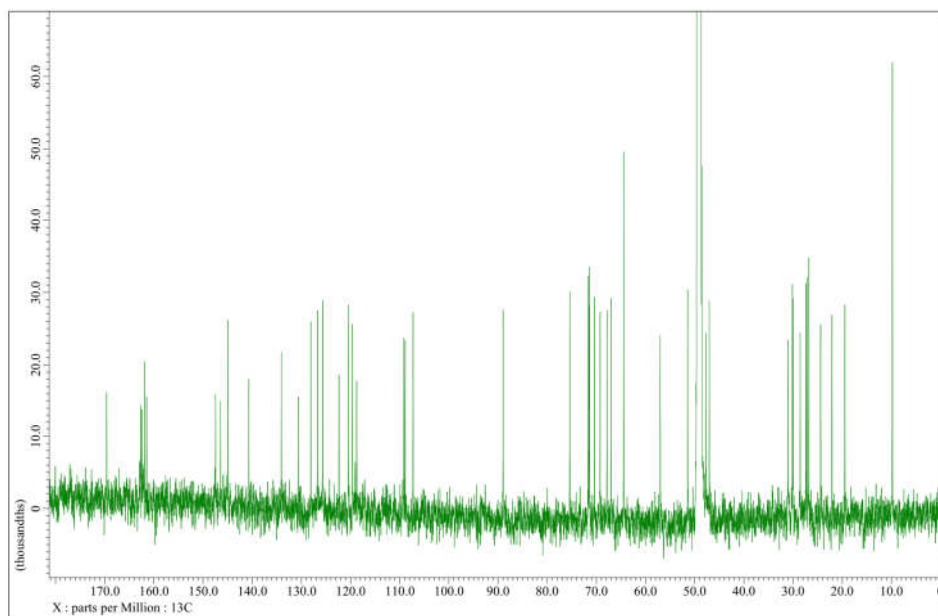


Figure 21 ¹³C NMR spectrum of AG10-L1-Nal.

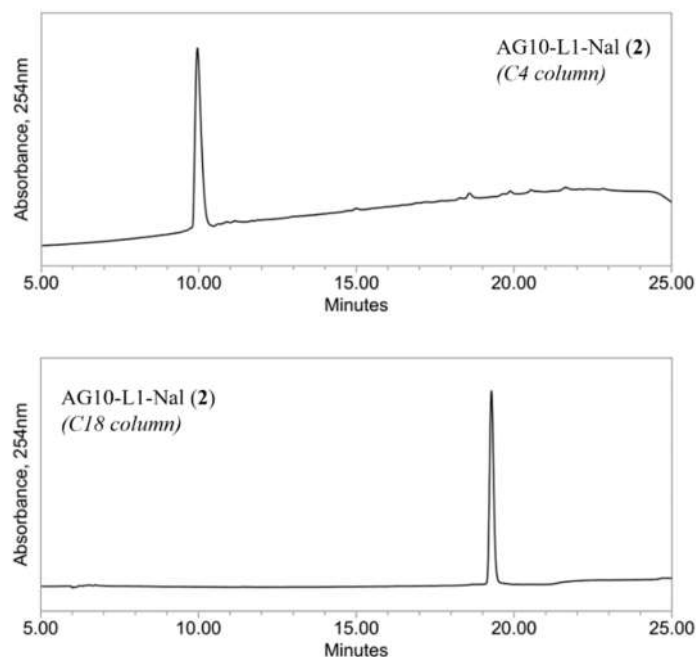
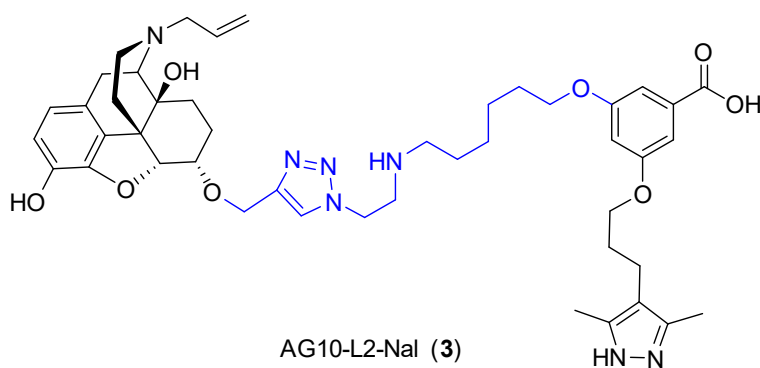


Figure 22 HPLC traces of AG10-L1-Nal



3-(((6-((2-(4-(((4R,7S,7aR,12bS)-3-allyl-4a,9-dihydroxy-2,3,4,4a,5,6,7,7a-octahydro-1H-4,12-methanobenzofuro[3,2-e]isoquinolin-7-yl)oxy)methyl)-1H-1,2,3-triazol-1-yl)ethyl)amino)hexyl)oxy)-5-(3-(3,5-dimethyl-1H-pyrazol-4-yl)propoxy)benzoic acid (AG10-L2-Nal) (3).

Compound **7** (260 mg, 0.571 mmol, 1 equiv), Compound **11** (319 mg, 0.571 mmol, 1 equiv), CuSO₄·5H₂O (37 mg, 0.148 mmol, 0.25 equiv), and sodium ascorbate (57 mg, 0.286 mmol, 0.5 equiv) were used to perform the click (CuAAC) coupling in a 5 mL mixture of

THF/H₂O. (4:1). At room temperature, the reaction mixture was stirred overnight.

Under reduced pressure, the solution was concentrated. Hexane:ethyl acetate was used to remove the residue. The combined organic extracts were condensed at reduced pressure to provide an intermediate that could be directly employed in the following phase. Then, to a solution of the intermediate, a combination of TFA and CH₂Cl₂, (1:4 ratio) (1 mL) was added, and the reaction mixture was agitated for 2 hours at room temperature. The solution was concentrated under decreased pressure and purified using preparative-HPLC to give AG10-L2-Nal (3) (216 mg, 46% yield in two processes) (98 percent purity by HPLC); HRMS (DART) *m/z*: calcd for C₄₅H₆₀N₇O₈ [M+H]⁺ 826.4498; found: 826.4490.

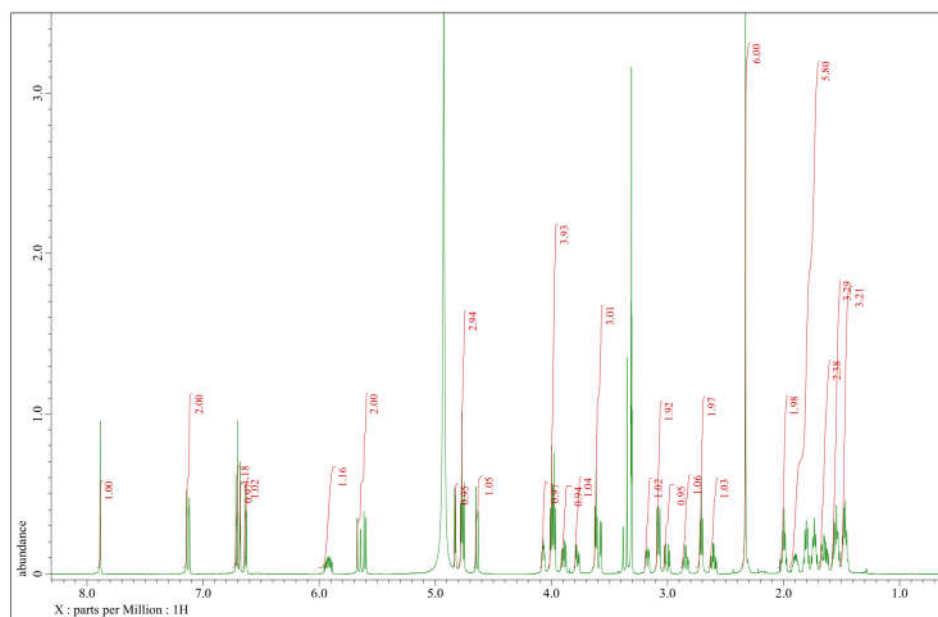


Figure 23 ^1H NMR spectrum of AG10-L2-Nal.

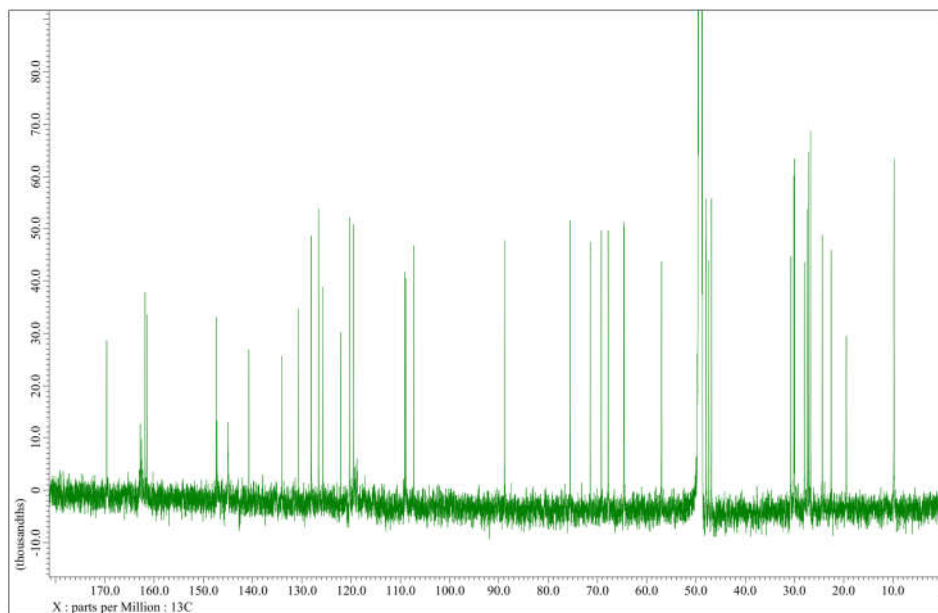


Figure 24 ^{13}C NMR spectrum of AG10-L2-Nal.

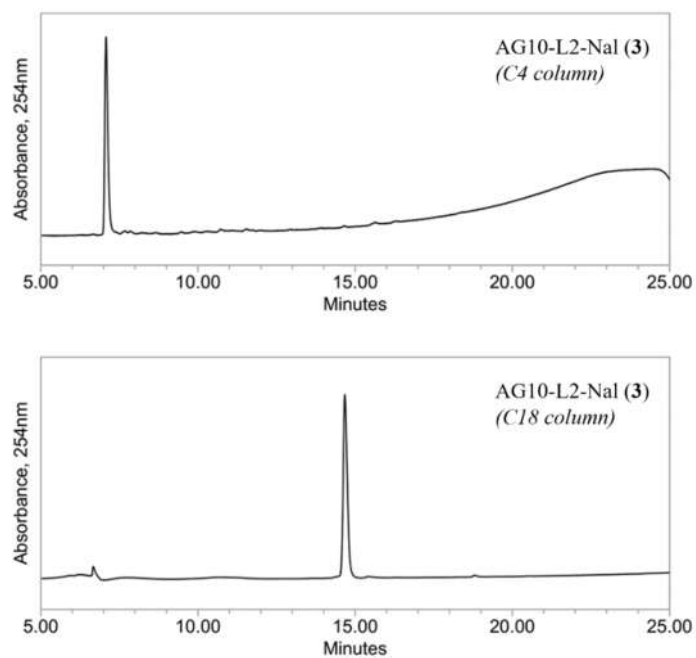


Figure 25 HPLC traces of AG10-L1-Nal.

CHAPTER 5: EVALUATION THE IN VITRO ACTIVITY

5.1. Evalutation of the binding to TTR

In order to evaluate the binding affinity to TTR, we used the fluorescence probe exclusion (FPE) assay as previously reported (Miller et al., 2018; Penchala et al., 2013). In this assay, a probe (Figure 26) was used which has no fluorescence by itself, however, it forms a fluorescent conjugate and emits fluorescence once it covalently binds to lysine 15 (K15) in the T4 binding site of TTR. Stabilizers that bind to the T4 site of TTR will decrease FPE probe binding as observed by lower fluorescence. The lower fluorescence observed indicates a higher binding affinity of the stabilizer.

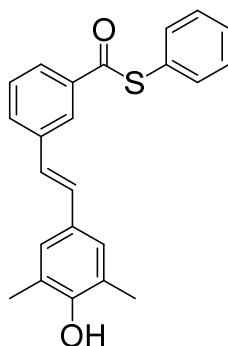


Figure 26 Chemical structure of FPE probe.

5.1.1 Method

The binding affinity and selectivity of ligands compound **1**, AG10-L1-Nal, AG10-L2-Nal, and AG10-L2-Oxy to TTR in human serum were assessed by their ability to compete with the binding of a fluorescent probe exclusion (FPE probe) binding to TTR in human

serum, as previously described(Choi, Connelly, Reixach, Wilson, & Kelly, 2010; Choi & Kelly, 2011). AG10 and tafamidis were utilized as the controls samples. An aliquot (98 μ L) of human serum was mixed with 1 μ L of test compounds (1.0 mM stock solution in DMSO; 10 μ M final concentration in serum) and 1 μ L of FPE probe (0.36 mM stock solution in DMSO; 3.6 μ M final concentration in serum). The fluorescence signal (λ_{ex} = 328 nm and λ_{em} = 384 nm) were monitored every 15 minutes for 6 hours at 25 °C using a SpectraMax M5 microplate reader.

The binding affinity of compound **1**, AG10-L1-Nal, AG10-L2-Nal, and AG10-L2-Oxy to TTR in buffer was evaluated using a previously described Fluorescence Polarization (FP) assay(Alhamadsheh et al., 2011). In a 384-well plate, serial dilutions of compound **1**, AG10-L1-Nal, AG10-L2-Nal, and AG10-L2-Oxy (0.010 μ M to 20 μ M) were added to a solution of FP-probe (50 nM) (Figure 27) and TTR (300 nM) in assay buffer (PBS pH 7.4, 0.01% Triton-X100, 1% DMSO in 25 μ L final volumes). At room temperature, the samples were allowed to equilibrate for 20 minutes via agitation on a plate shaker. Fluorescence polarization measurements were performed using a SpectraMax M5 Microplate Reader (λ_{ex} = 485 nm and λ_{em} = 525 nm; λ_{cutoff} = 515 nm), The data were fitted to the following equation to obtain the IC₅₀ values.

$$y = \frac{A - D}{\left(1 + \left(\frac{X}{C}\right)\right)^B + D}$$

where A=maximum FP signal, B = slope, C = apparent binding constant (K_{app}), and D = minimum FP signal. The binding constant (K_d) values were determined from the IC₅₀

values using the Cheng–Prusoff equation. All reported data represent the mean \pm s.d. ($n = 3$).

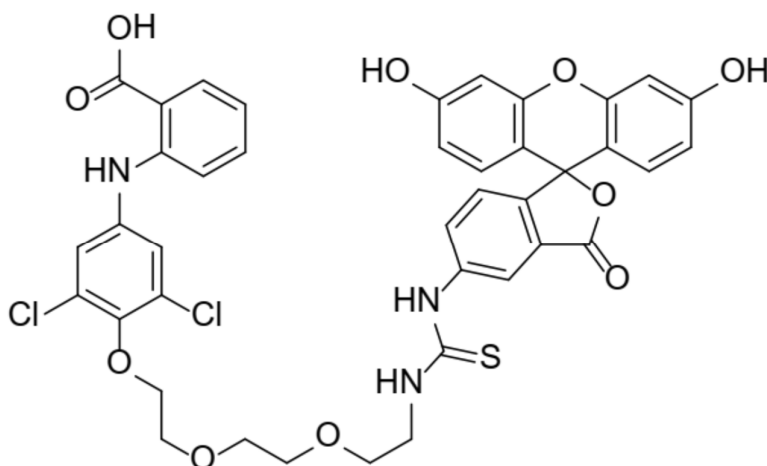


Figure 27 Chemical structure of Fluorescence Polarization Probe.

5.1.2 Results

AG10-L1-Nal's affinity for TTR in buffer was determined using the fluorescence polarization (FP) binding assay (Alhamadsheh et al., 2011) ($K_d = 485.3$ nM; Figure 28). This binding affinity is less than the that of **1** ($K_d = 68.5$ nM; Figure 28). This decrease in TTR binding affinity, however, may be beneficial in allowing AG10-L1-Nal to preferentially engage with target mu-opioid receptors. To be effective in vivo, AG10-Naloxone conjugates must be able to bind to TTR selectively in the presence of over 4,000 other human blood proteins. Using a well-established TTR serum fluorescence probe exclusion (FPE) selectivity assay (Choi et al., 2010; Choi & Kelly, 2011), the selectivity of AG10-L1-Nal binding to TTR was determined. The observations indicated that AG10-L1-Nal retained a very high affinity for TTR in human serum ($71.5 \pm 1.8\%$ TTR occupancy) (Figure 29). Notably, AG10-L1-Nal outperformed the TTR stabilizer tafamidis (an authorized treatment

for TTR amyloidosis; $48.9 \pm 2.1\%$ TTR occupancy)(Bulawa et al., 2012).

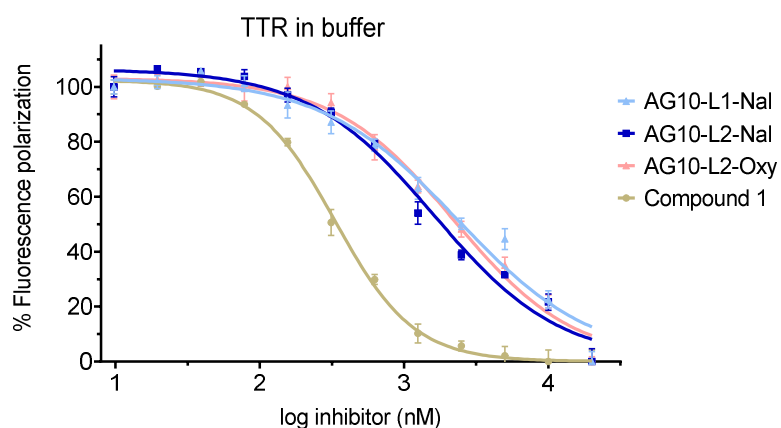


Figure 28. Binding affinity of test compounds (0.01 μM to 20 μM) to TTR in buffer using fluorescence polarization assay.

The binding constant (K_d) values were calculated using the Cheng–Prusoff equation from IC_{50} values. Data represent the mean \pm s.d. ($n = 3$). (Data generated with Tuhin)

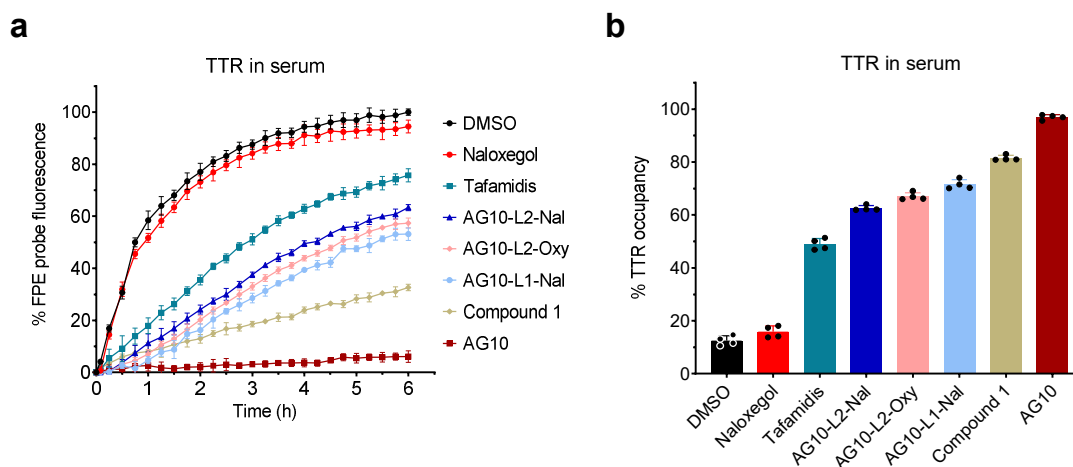


Figure 29 FPE assay to evaluate the binding affinity and selectivity of the compounds to TTR
a The change in fluorescence generated by covalent FPE probe modification of TTR in human serum (TTR concentration, $\sim 5 \mu\text{M}$) was observed for 6 hours in the presence of FPE probe alone (black circles) or probe with TTR ligands (colors; $10 \mu\text{M}$). The lower the binding affinity and fluorescence of the FPE probe, the higher the ligand's binding selectivity for TTR. b Bar graph representation of the percentage of TTR in human serum occupied by test substances in the presence of the FPE probe after 3 hours of incubation relative to the probe alone. Error bars indicate mean \pm s.d. ($n = 4$). (Data generated with Tuhin)

5.2. Evaluation of the binding to opioid receptors

In vitro mu-, kappa-, and delta-opioid receptor binding assays were performed by Eurofins Cerep in their France site. Naloxone, naloxegol, AG10-L1-Nal, AG10-L2-Nal, oxycodone, and AG10-L2-Oxy were tested for mu-opioid receptor binding. AG10-L2-Nal and AG10-L2-Oxy were also tested for kappa- and delta-opioid receptor binding.

5.2.1 Method: Human Mu-opioid Receptor Binding (agonist radioligand) Assay

Human mu-opioid receptor (h-MOR) expression exhibited a high affinity recognition of the mu-opiate specific ligand [³H]-DAMGO (D-ala2, N-methyl-phe4, glyo15) enkephalin. This binding can be displaced by compounds with high affinity for mu-opioid receptors. In this assay [³H]-DAMGO was employed as the ligand in this test at a concentration of 0.5 nM with a K_d value of 0.35 nM. DAMGO was used as the control inhibitor. Naloxone, AG10-L1-Nal, and AG10-L2-Nal were tested at concentrations of 0.01, 0.1, 1, 10, and 100 nM. The concentrations of naloxegol tested were 0.1, 1, 10, 100, and 1000 nM. The concentrations of oxycodone tested were 0.01, 0.1, 1, 10, 100, and 500 nM. And for AG10-L2-Oxy, concentrations of 0.1, 1, 10, 100, 500, and 1000 nM were tested. The experiment required 120 minutes of incubation at room temperature. AG10-L1-Nal and AG10-L2-Nal were also examined for mu-opioid receptor binding in the presence of TTR (1 μ M).

The percentage inhibition of control specific binding obtained in the presence of the test drugs is reported.

$$100 - \left(\frac{\text{measured specific binding}}{\text{control specific binding}} \times 100 \right)$$

The IC₅₀ values and Hill coefficients (nH) were determined by non-linear regression analysis of the competition curves generated with mean replicate values using Hill equation curve fitting.

$$Y = D + \left[\frac{A - D}{1 + \left(\frac{C}{C_{50}} \right)^{nH}} \right]$$

where Y = specific binding, A = left asymptote of the curve, D = right asymptote of the curve, C = compound concentration, $C_{50} = IC_{50}$, and nH = slope factor. This analysis was carried out using software developed at Cerep (Hill software) and validated against data collected using the commercial software SigmaPlot® 4.0 for Windows® (SPSS Inc., 1997). The Cheng-Prusoff equation was used to obtain the inhibition constants (K_i).

$$K_i = \frac{IC_{50}}{(1 + \frac{L}{K_d})}$$

where L = concentration of radioligand in the assay and K_d = affinity of the radioligand for the receptor. A scatchard plot is used to determine the K_d .

Results indicating an inhibition more than 50% are regarded as substantial effects of the test substances. 50% is the most frequently used cut-off value for further study (determination of IC_{50} values from concentration-response curves).

5.2.2 Method: Human Delta And Rat Kappa-opioid Receptor (agonist radioligand)

Binding Assays

For the delta-opioid receptor (human) binding assay, [3H]-DADLE was employed as a ligand at 0.5 nM concentration with a K_d value of 0.6 nM. DPDPE was used as the control inhibitor. AG10-L2-Nal was tested at doses of 0.1, 1, 10, 50, and 100 nM in duplicate. The concentrations of AG10-L2-Oxy tested were 1, 10, 100, 1000, and 2000 nM. The assay required 60 minutes of incubation at room temperature. For the kappa opioid receptor (rat) binding assay, [3H] U 69593 was employed as a ligand at 1 nM concentration with a K_d value of 2 nM. In this example, U 50488 hydrochloride was used as a control inhibitor. AG10-L2-Nal was tested at doses of 0.1, 1, 10, 50, and 100 nM in duplicate. The assay required

60 minutes of incubation at room temperature. IC_{50} and K_d values were determined using the same procedure as for the mu-opioid receptor binding assay.

5.2.3 Results: AG10-Naloxone Conjugates Displays High Affinity to Mu-opioid

Receptor

AG10-L1-Nal's binding affinity ($K_i = 0.81$ nM) was 3-fold lower than naloxone ($K_i = 0.29$ nM) and 3.5-fold higher than naloxegol ($K_i = 2.9$ nM) (Figure 30). To make it like it would be in real life, binding affinity of AG10-L1-Nal to the mu-opioid receptors was tested in the presence of extra TTR (1 μ M). Interestingly, when TTR was present, there was a 9-fold drop in the affinity of AG10-L1-Nal to the mu-opioid receptors, which is why the binding affinity of AG10-L1-Nal dropped to 7.4 nM. Because of this, a modeling study was conducted to figure out why AG10-L1-Nal's ability to bind to TTR and the mu-opioid receptor had less power. Linker between AG10 and naloxone is long enough (~ 20 Å) to make a three-way complex with both TTR and mu-opioid receptors, it was shown in (Figure 6). We think this ternary complex may have caused some steric hindrance from TTR that made it more difficult for AG10-L1-Nal to bind to the mu-opioid receptor. The shorter linker of AG10-L2-Nal only allowed it to bind to either the TTR or the mu-opioid receptor at one time, prohibiting it from binding to both at the same time (Figure 6). The mu-opioid receptor binding affinities of AG10-L2-Nal in the absence and presence of TTR were determined to test our hypothesis. In the absence of TTR, the binding affinity of AG10-L2-Nal ($K_i = 0.35$ nM) was similar to that of naloxone ($K_i = 0.29$ nM) and was 8.3-fold stronger than that of naloxegol ($K_i = 2.9$ nM). However, in the presence of excess TTR (1 μ M), the

binding affinity of AG10-L2-Nal ($K_i = 1.3$ nM) was 5.7-fold and 2.2-fold higher, respectively than that of AG10-L1-Nal and naloxegol (Figure 30). This was also 17-fold better than that of MNTX ($K_i = 22.1$ nM)(Floettmann et al., 2017). As a result, it was obvious that the linker system plays a key role in the mu-opioid receptor's preferred binding over TTR. Thus, AG10-L2-Nal was selected as our lead molecule for biological testing due to its optimal binding affinity.

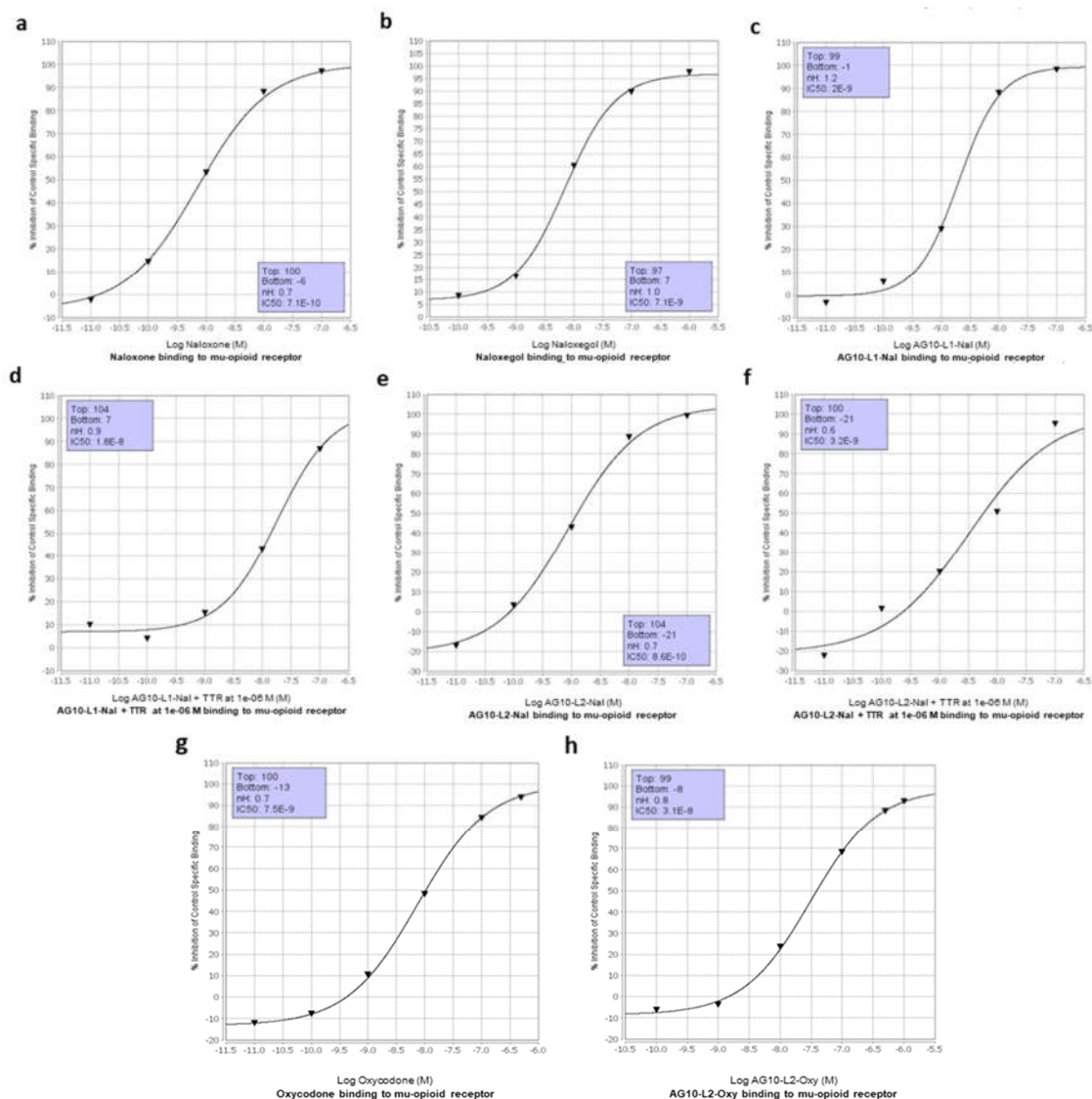


Figure 30 mu-opioid receptor binding assays.

Naloxone, naloxegol, AG10-L1-Nal, AG10-L2-Nal, oxycodone, and AG10-L2-Oxy (a-h). The inhibitory binding constant (K_i) values were calculated using the Cheng–Prusoff equation from IC_{50} values. (Data generated by Eurofins Cerep, France)

5.2.4 Results: Exhibited High Affinity To Delta- And Kappa- Opioid Receptors.

To ensure that the modification of naloxone's structure with the AG10-linker had no substantial effect on its binding to other opioid receptors, the binding of AG10-L2-Nal to delta- and kappa-opioid receptors was examined. Both naloxegol and MNTX were shown

to be ineffective at binding to the delta and kappa opioid receptors, whereas AG10-L2-Nal maintained excellent binding affinity to both receptors (Figure 31 and Figure 32). The affinity of AG10-L2-Nal for delta-opioid receptors ($K_i = 5.5$ nM and 0.12 nM, respectively) is similar to that of naloxone ($K_i = 12.6$ nM and 2 nM for the delta- and kappa-opioid receptor, respectively). This is significantly higher than that of naloxegol ($K_i = 203$ nM and 8.7 nM for the delta- and kappa-opioid receptors, respectively) and MNTX ($K_i = 1,900$ nM and 10.9 nM for delta- and kappa-opioid receptors, respectively)(Floettmann et al., 2017).

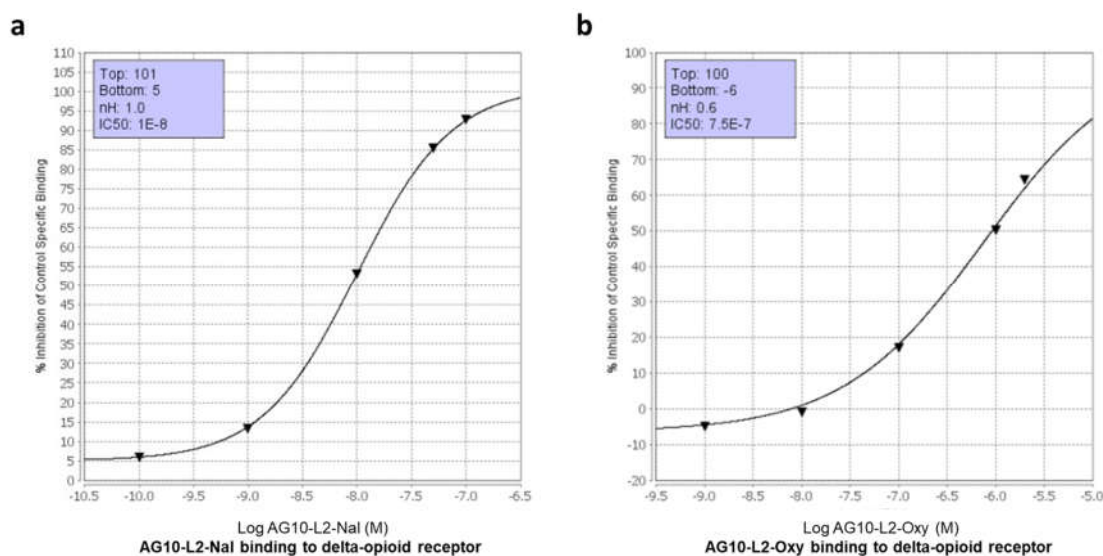


Figure 31 delta-opioid receptor (agonist radioligand) binding assays of (a) AG10-L2-Nal and (b) AG10-L2-Oxy.

The inhibitory binding constant (K_i) values were calculated using the Cheng–Prusoff equation from the IC_{50} values. Source data are provided as a Source Data file (Data generated by Eurofins Cerep, France)

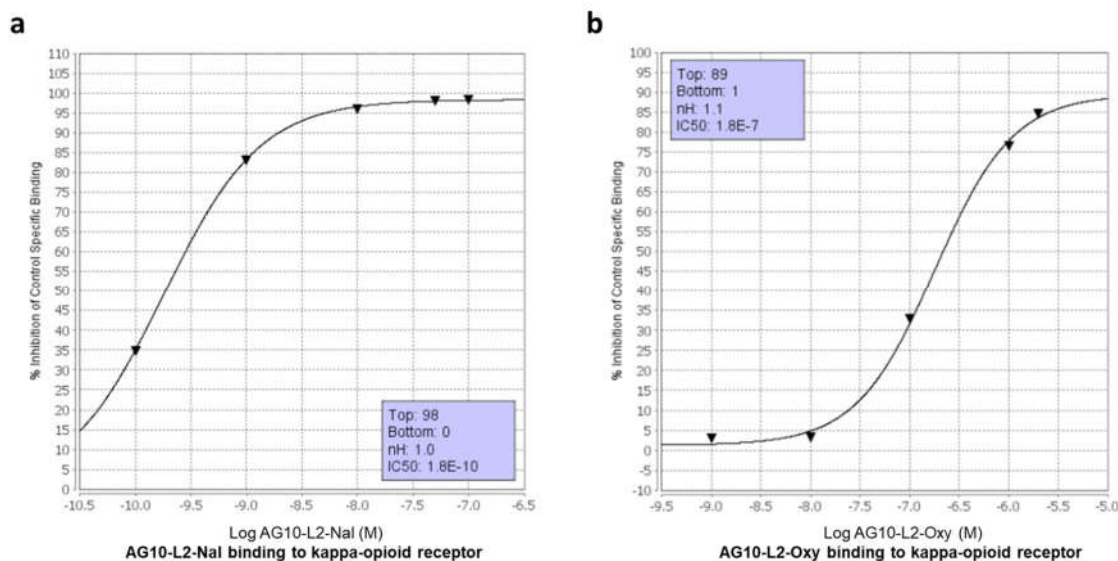


Figure 32 kappa-opioid receptor (agonist radioligand) binding assays of (a) AG10-L2-Nal and (b) AG10-L2-Oxy.

The inhibitory binding constant (K_i) values were calculated using the Cheng–Prusoff equation from the IC_{50} values. Source data are provided as a Source Data file. (Data generated by Eurofins Cerep, France)

5.3. AG10-L2-Nal displayed competitive antagonistic activity in mu-opioid receptor functional assays.

To confirm the activities of the naloxone, conjugates were not influenced by AG10, functional assay was conducted to evaluate the agonism.

5.3.1 Method: Functional activity assays

Compounds were tested for human mu-opioid agonist activity in [35 S]GTP γ S functional binding assay using CHO-K1 cells which stably express human recombinant opiate receptor. The experiments were performed at Eurofins, Panlabs (Taiwan Province, China). The experimental procedure was performed as reported (Alt et al., 1998). The test compounds or vehicle were pre-incubated with the membranes (0.016 mg/mL) and 3 μ M GDP in modified HEPES pH 7.4 buffer at 25°C for 20 minutes. Later, SPA beads were added for additional 60 minutes at 30°C. And 0.3 nM [35 S]GTP γ S was added to initiate the reaction and incubated

for an additional 30 minutes. Reaction was terminated by filtration. DAMGO was used as an agonist reference to define the E_{\max} and naltrexone was used as an antagonist reference.

For agonism assay, the test compounds were 20 μ M AG10-L2-Nal or naloxegol, and activity was measured by more than 50 percent increase of [35 S]GTP γ S binding response relative to DAMGO (reference agonist). For antagonism assay, AG10-L2-Nal and naloxegol were tested in series dilution from 10 μ M to 0.01 nM. The activity was measured by the compound inhibition of DAMGO induced [35 S]GTP γ S binding response. Naltrexone was used as a reference antagonist.

For the [35 S]GTP γ S competitive functional assay, morphine was tested (in the absence and presence of 0.4 μ M AG10-L2-Nal) at concentrations ranging from 200 μ M to 0.01 μ M. The experiments were conducted at 10 concentrations (each concentration was tested in duplicate experiments).

5.3.2 Result: AG10-L2-Nal Displays Competitive Agonism Activity To Mu-opioid

Receptor

In the [35 S]GTP γ S functional binding assay, using membranes of CHO-K1 cells stably expressing human mu-opioid receptors, AG10-L2-Nal (20 μ M) exhibited 2% agonism (mean value of 4 experiments) relative to DAMGO (EC_{50} = 13.2 nM). Naloxegol displayed 6% agonism at 20 μ M. Parallel testing of AG10-L2-Nal, naloxegol, and the potent opioid antagonist naltrexone in the mu-opioid receptor functional assay demonstrated that AG10-L2-Nal potency (IC_{50} = 7.5 nM) is similar to that of naltrexone (IC_{50} = 10.9 nM) and 10-fold more potent than naloxegol (IC_{50} = 72 nM) (Figure 33). These values correspond to equilibrium dissociation constant (K_B) of 0.81 nM for AG10-L2-Nal and 7.7 nM for naloxegol. The K_B value for naloxegol is similar to the reported literature value (K_B = 11 nM)(Floettmann et al., 2017). Importantly, our functional assay data fit well with the

competitive binding assay data, discussed above, where the binding affinity of AG10-L2-Nal ($K_i = 0.35 \text{ nM}$) is 8-fold higher than that of naloxegol ($K_i = 2.9 \text{ nM}$).

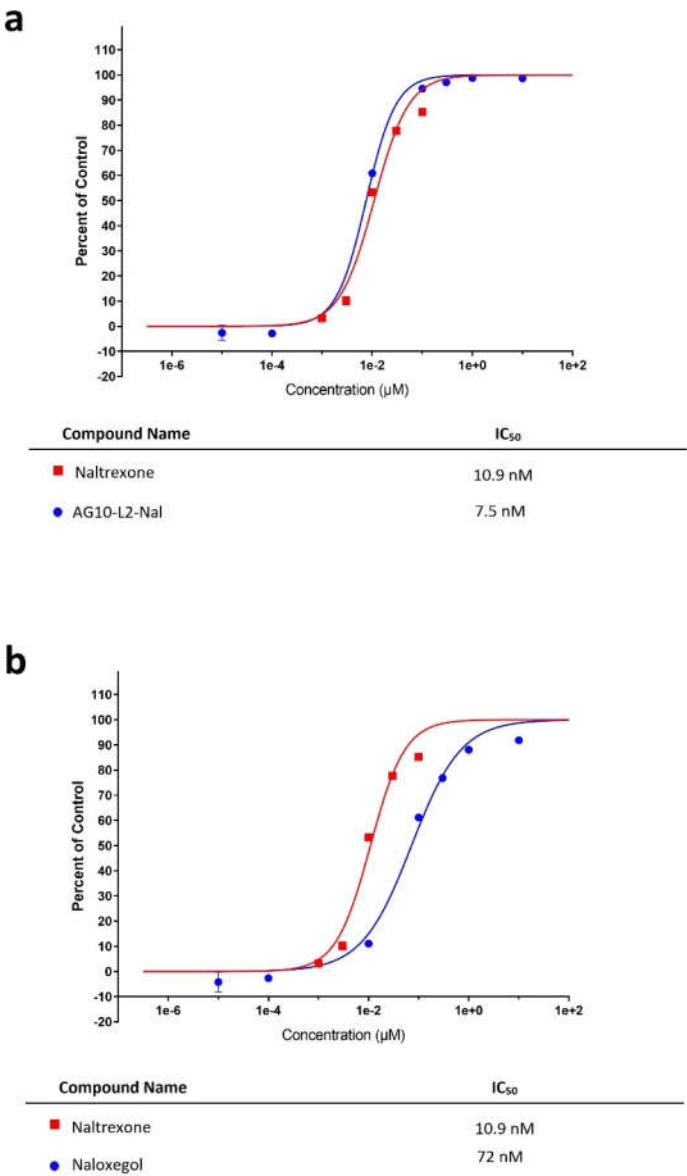
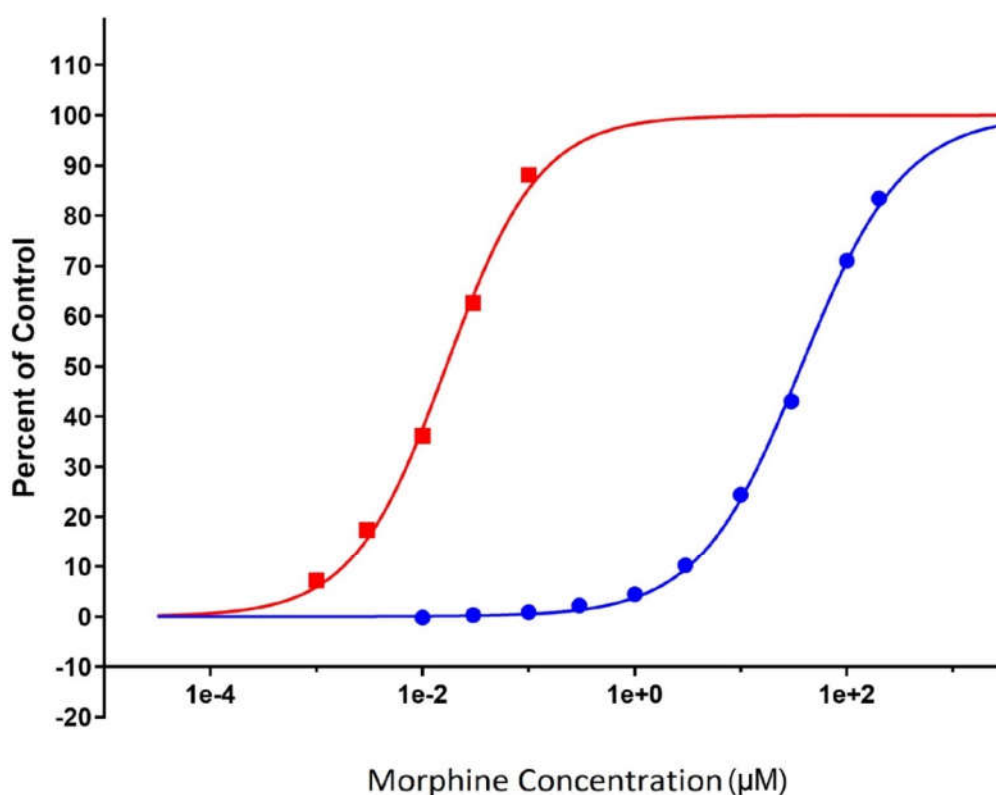


Figure 33 Antagonist functional assay of AG10-L2-Nal and naloxegol. Human mu-opioid receptor guanosine 5-O-(3-[³⁵S]thio)triphosphate ([³⁵S]GTPγS) antagonist functional binding assays of **(a)** AG10-L2-Nal, and **(b)** naloxegol. Antagonistic functional binding activity of human mu-opioid receptors expressed in the membranes of CHO-K1 cells from Chinese hamster ovary was used in these assays. 8 testing concentrations are shown. Error bars indicate mean ± s.d. (Each data point represents mean value of duplicate

(Figure 33 Continued)

experiments relative to inhibition of DAMGO-induced bound [35 S]GTP γ S). The potent mu-opioid receptor antagonist, naltrexone, was used as a reference compound in both the assays. (Data generated by Eurofins Panlabs Inc, Taiwan Province, China)

In Schild-type experiments, AG10-L2-Nal elicited parallel rightward shifts in the morphine dose response curve without any accompanying reduction in the maximal response (E_{\max}) produced by morphine (Figure 34). The EC_{50} of morphine ($EC_{50} = 0.039 \mu\text{M}$) was increased by 950-fold in the presence of AG10-L2-Nal (the EC_{50} of morphine + 0.4 μM AG10-L2-Nal = 37.2 μM). These results demonstrate that AG10-L2-Nal is a potent competitive antagonist of morphine at the human mu-opioid receptor.



Compound Name	EC ₅₀
■ Morphine	0.039 μM
● Morphine + 0.4 μM AG10-L2-Nal	37.2 μM

Figure 34 Competitive antagonism of morphine by AG10-L2-Nal at the human mu-opioid receptor.

The effect of 0.4 μM AG10-L2-Nal on morphine agonist concentration-response curve, as measured by guanosine 5-O-(3-[³⁵S]thio)triphosphate ([³⁵S]GTPγS binding) are shown. Agonistic functional binding activity of human mu-opioid receptors expressed in the membranes of CHO-K1 cells from Chinese hamster ovary was used in these assays. 10 testing concentrations are shown. Error bars indicate mean ± s.d. (Each data point represents mean value of duplicate experiments). In the Schild-type experiments, 0.4 μM AG10-L2-Nal elicited parallel rightward shifts in the morphine concentration-response curve with no reduction in the maximal response (E_{\max}). (Data generated by Eurofins Panlabs Inc, Taiwan Province, China)

CHAPTER 6: EVALUATION THE BBB PENETRATION AND PHARMACOKINETICS

6.1 Serum Stability

Before BBB penetration study, stability of the compound need to be evaluated to whether there is fragment or metabolite forming. If so, these fragments or metabolites also need to be quantified in the BBB penetration study.

6.1.1 Method For Serum Stability

Samples of AG10-L2-Nal, 100 μ M, were incubated at 37°C in serum from humans, mice, and rats. Solvent B (95 percent methanol, 0.1% trifluoroacetic acid in water) was added to each sample and centrifuged for five minutes at 15,000 rpm. The supernatant was stored at -20°C for 5 minutes before being centrifuged at 15000 rpm for another 5 minutes. The supernatant was analyzed by WatersTM XBridge C18 column (4.6x250mm, μ 5m) on Waters HPLC system linked to Waters 2998 photodiode array detector operating between the UV ranges of 200-400nm. With a gradient method of rising from 0% to 100% solvent B in 20 minutes, HPLC analysis was conducted. A mixture of acetonitrile-water (5:95 v/v) and 0.1 percent trifluoroacetic acid in solvent A and solvent B flowed through the mobile phase at a rate of 0.5 mL/minute. Experiment was conducted triplicated in parallel.

6.1.2 Result: AG10-L2-Nal is Stable in Serum

AG10-L2-Nal's stability in mouse, rat, and human serum was investigated by HPLC (Figure 35). When incubated at 37 °C for at least 48 hours, data revealed that AG10-L2-Nal was stable in all three sera (with 100 percent of the antibody still present). This suggests

that no fragment or metabolite of AG10-L2-Nal need to be analyzed in the BBB penetration study. Only the AG10-L2-Nal compound itself needs to be evaluated. Furthermore, if no AG10-L2-Nal can be detected in the brain tissue or CSF, this compound will not penetrate the BBB as any forms.

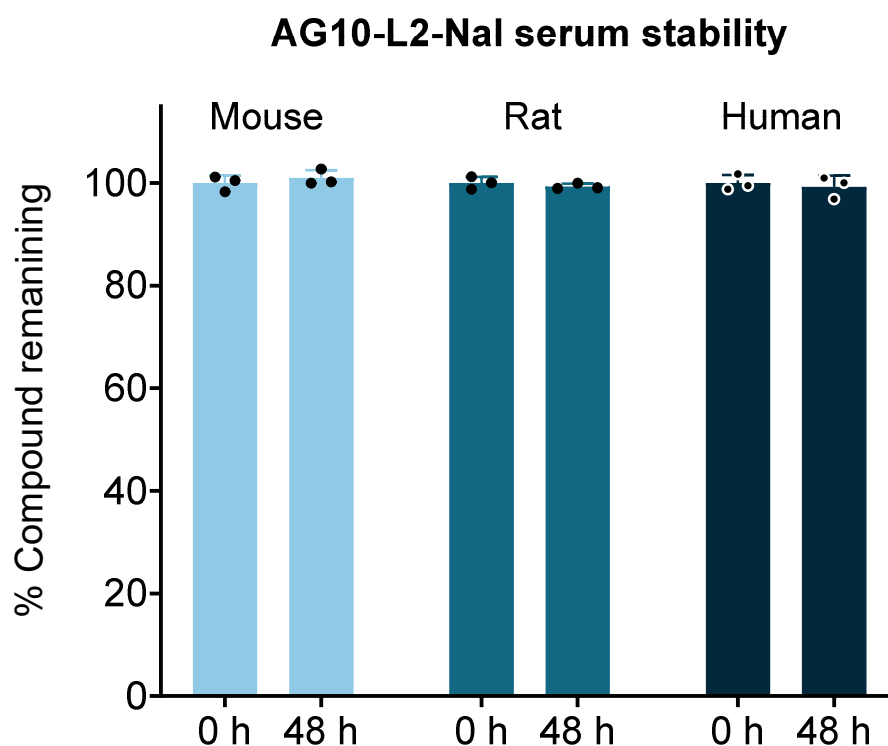


Figure 35 Serum stability of AG10-L2-Nal in mouse, rat, and human serum.

AG10-L2-Nal (100 μ M) was incubated in serum at 37 $^{\circ}$ C, and the respective amount remained in corresponding media was analyzed at 0 and 48 hours by HPLC. Bar graphs represent the mean of % compound remaining \pm s.d. ($n = 3$). (Data generated with Tuhin)

6.2 Method for Evaluating BBB Penetration

20 μ L of samples were injected for LC-MS/MS analysis. Agilent 1200 HPLC coupled with a triple quadrupole mass spectrometer (AB SCIEX API 3000™) was used to quantitate the analytes in the plasma, brain, and CSF samples. The mobile phase was composed of solvent A consisting of methanol-water (5:95, v/v) containing 0.1% formic acid and solvent B consisting of methanol-water (95:5, v/v) containing 0.1% formic acid, at a flow rate of 0.5 mL/minute, and the injection volume was 20 μ L. LC-MS/MS analysis was performed on a Waters™ XBridge C18 (4.6x150 mm, 5 μ m) using gradient methods for all the compounds. The turbo spray ion source was set in the positive ionization mode. Fragmentation pattern and peak areas were used to identify and quantitate the test compounds, respectively.

6.2.1 Animal Used For The Experiment

Jugular vein Male Sprague-Dawley rats that were about 6 to 8 weeks old were used in a variety of animal studies. Charles River Laboratories Inc., Hollister, CA, USA, provided the rats, which weighed between 226 and 250 grams each. The Charles River Institutional Animal Care and Use Committee (IACUC) made sure that pre- and post-operative care was done the right way. In standard polycarbonate disposable rat cages, each rat was kept in a separate cage with a bed of wood shavings. At 18-26°C, 50-70% relative humidity, light hours: 7:00 am-7:00 pm. Five days for acclimatization after animal arrive. National Institutes of Health (NIH) rules were followed to take care for animals at University of the Pacific. The IACUC at the university also approved them. 19R02 and 21R03 were used in this study.

6.2.2 Procedure of Brain Uptake Study

For this study jugular vein cannulated male Sprague Dawley rats were used. Animals were randomized in different treatment groups ($n = 3$ each group). 200 μL 50 $\mu\text{mol/kg}$ of compound **1** or 4.84 $\mu\text{mol/kg}$ dose of naloxone, naloxegol, or AG10-L2-Nal were dosed by IV administration. 200 μL sterile saline was given to flush the jugular vein cannula. The dosing solution (vehicle) formulation were: 10% DMSO, 20% PEG400 and 70% sterile deionized water. The rats were anesthetized 30 minutes after the dosing by intraperitoneal injection of 90 mg/kg ketamine and 9 mg/kg xylazine. The CSF samples were collected from the cisterna magna with a 22-gauge needle. Next, brain samples were harvested and subsequently kept frozen in the liquid nitrogen. And then, the blood samples were collected from the aortic exsanguination with a 20-gauge needle.

6.3 Method For LCMS

The blood, brain tissue, and CSF samples were analyzed by LCMS by the methods described as following.

6.3.1 Samples Preparation For LCMS

The brain was immediately frozen by the liquid nitrogen. Plasma samples were obtained by upper layer of centrifugation of blood at 1500 g for 10 minutes at 4 $^{\circ}\text{C}$. All the CSF, brain, and plasma samples were stored in the -80 $^{\circ}\text{C}$ for further analysis. Stock solutions of compound **1** (20 mM), AG10-L2-Nal (**3**) (10 mM), naloxegol (10 mM), naloxone (20 mM) were prepared in DMSO solution. The working solutions were prepared by serial dilution of the DMSO solution mentioned above. The calibration curve standards were prepared by spiking aliquots (1 μL) of each working solution to 49 μL blank rat plasma, artificial CSF (125 mM NaCl, 2.5 mM KCl, 1.26 mM CaCl_2 , and 1.18 mM MgCl_2), or blank

rat brain homogenate. Quality control (QC) samples prepared at low, medium, and high concentrations were extracted at the same time with the animal samples.

Two volumes of homogenizing solution (w:v) were used to homogenize the brain tissue (PBS buffer). When extracting compound **1**, 50 μ L brain homogenate, plasma or CSF sample was added 200 μ L of extraction buffer (methanol-water (95:5, v/v) containing 0.1% formic acid with 15 ng/mL Chloro-AG10 as internal standard). When extracting naloxone, naloxegol, and AG10-L2-Nal, 50 μ L sample was precipitated with 100 μ L of extraction buffer (methanol-water (95:5, v/v) containing 0.1% formic acid with 15 ng/mL naloxone-D5 as internal standard). A mixture of methanol and water (95:5) containing 0.1 percent formic acid was used to extract the double blank samples, which were extracted with the extraction buffer that did not include the internal standard. The CSF, brain homogenate, and plasma samples were vortexed for 30 seconds each before being stored at -20°C for 5 minutes to prevent contamination. In the following step, the samples were centrifuged for 5 minutes at 15000 rpm; the supernatant was collected and held in the -20°C freezer for 5 minutes; and then the samples were centrifuged for another 5 minutes at 15000 rpm. The materials were maintained at -80°C until they could be analyzed further.

6.3.2 LC-MS/MS analysis

For the LC-MS/MS analysis, a total of 20 mL of samples were used. The analytes in the plasma, brain, and CSF samples were quantified using an Agilent 1200 high-performance liquid chromatography system paired with an AB SCIEX API 3000TM triple quadrupole mass spectrometer. In this experiment, the mobile phase solvent A, was composed of methanol-

water (5:95, v/v) and 0.1 percent formic acid, and solvent B, was composed of methanol-water (95:5, v/v) and 0.1 percent formic acid. The flow rate of the mobile phase was 0.5 mL/minute, and the injection volume was 20 μ L. For all of the substances, LC-MS/MS analysis was carried out on a WatersTM XBridge C18 (4.6x150 mm, 5 μ m) using gradient techniques on a WatersTM XBridge C18 (4.6x150 mm, 5 μ m). For compound **1**, gradient method of growing linearly from 0-80 percent solvent B in 0-5 minutes, stayed at 80 percent solvent B for 7 minutes, then dropped down from 80-0 percent solvent B in 1 minute and stayed at 0 percent solvent B for 1 minute. Compound **1** had a retention duration of 9.2 minutes, while chloro-AG10 had a retention period of 11.1 minutes. For for naloxone, naloxone-d5, naloxegol, and AG10-L2-Nal, HPLC gradient begin with 0-100 percent solvent B for 0-5 minutes, then 100 percent solvent B at 5-8.5 minutes, 100 percent solvent B at 8.5-9.5 minutes, and then went back to 0 percent solvent B at 9.5-10.5 minutes. The retention time for naloxone, naloxone-d5, naloxegol, and AG10-L2-Nal are 6.45 minutes, 6.45 minutes, 7.45 minutes, and 7.66 minutes, respectively.

The turbo spray ion source was operated at the positive ionization mode of the turbo spray ion source was used. As indicated previously, the test compounds were identified and quantified using the fragmentation pattern and peak areas, respectively. Chloro-AG10 was employed as an internal standard for the quantitation of compound **1**. The nebulizer gas (NEB), curtain gas (CUR), collision gas (CAD), ion spray voltage (IS), and temperature (TEM) were set as 10, 10, 10, 5000 and 425, respectively.

Naloxone-D5 was employed as an internal standard for naloxone, naloxegol, and

AG10-L2-Nal quantitation. There were 14, 10, 10, 2000, and 425 volts of ion spray voltage and 425 degrees of temperature in the nebulizer gas, curtain gas, collision gas, and CAD source parameters. 10.5 minutes was the total time for this run.

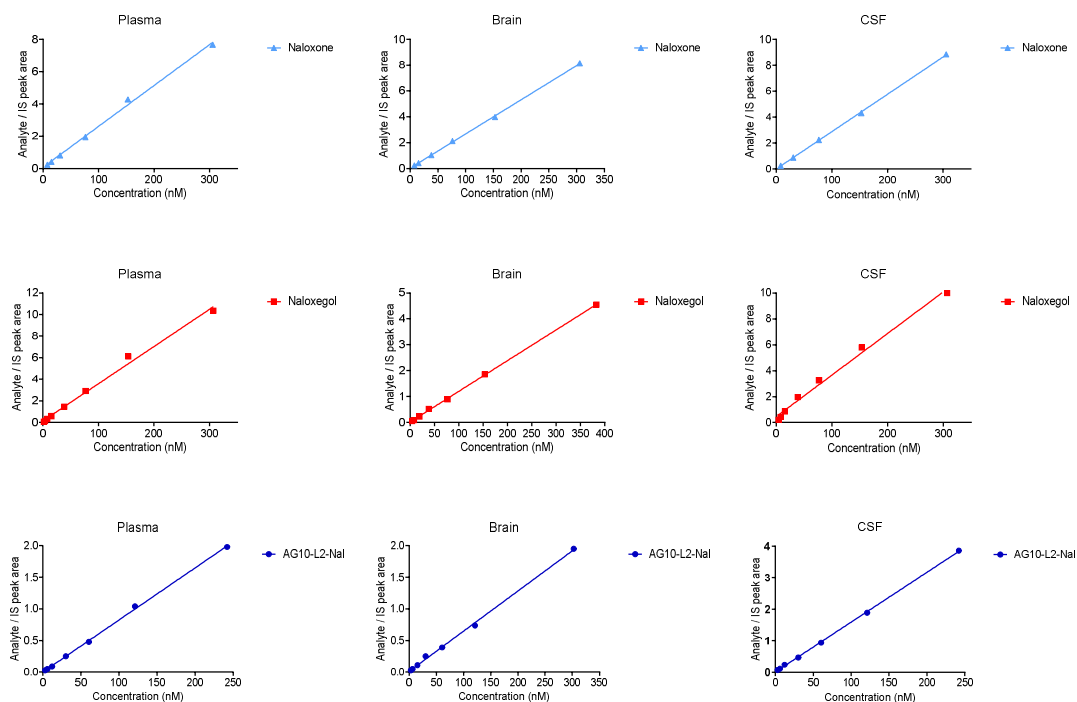


Figure 36 LC-MS/MS calibration curves used to quantitate naloxone, naloxegol, and AG10-L2-Nal in rat plasma, brain, and CSF.

The calibration curves were for the BBB, intravenous, and subcutaneous pharmacokinetic studies. The identities of the compounds were determined using the following Q1/Q3 transition masses for naloxone (328.0/310.0), IS reference naloxone-D5 (333.3/315.0), naloxegol (652.4/634.2), and AG10-L2-Nal (413.9/405). See Supplementary Table 1 for the detailed multiple reaction monitoring (MRM) parameters. Source data are provided as a Source Data file. (Helped by Fang)

Table 1

Mass Spectrometer Conditions For Multiple Reaction Monitoring (MRM) of The Tested Compounds.

Compounds	Q1 Mass (Da)	Q3 Mass (Da)	Declustering potential (volts)	Focusing potential (volts)	Entrance potential (volts)	Collision energy (volts)	Collision cell exit potential (volts)
Compound 1	390.2	372.1	51	170	10	29	24
Chloro-AG10	309.0	109.2	31	270	10	31	8
Naloxone	328.0	310.0	66	220	10	29	8
Naloxone-D5	333.3	315.0	61	160	10	33	18
Naloxegol	652.4	634.2	66	370	10	45	22
AG10-L2-Nal	413.9	405.0	36	50	10	21	20
Oxycodone	316.4	241.1	39	150	10	40	30
Oxycodone D6	322.4	304.5	36	140	10	27	18
AG10-L2-Oxy	814.6	469.1	70	293	11.5	55	30

6.4 Results of BBB Penetration

AG10-L2-Nal was tested for BBB penetration against two FDA-licensed opioid antagonists: naloxone (an opioid antidote that quickly crosses the BBB) and naloxegol (a PAMORA authorized for OIC due to its restricted BBB penetration). Through the use of a jugular vein cannula, test compounds were administered to rats by IV route. 30 minutes after treatment, plasma, brain tissue, and CSF were collected and the concentration of the compounds were measured by LC-MS (Figure 36 and Table 1). The percentage brain to plasma ratio and the percentage CSF to plasma ratio of naloxone were 490 percent and 119 percent (Figure 37), respectively, according to the results of the study. These results are consistent with the literature, which had shown that the concentration of naloxone in the brain and CSF is higher than the concentration in plasma (Ngai, Berkowitz, Yang, Hempstead, &

Spector, 1976). Naloxegol had a brain to plasma ratio of 29% and a CSF to plasma ratio of 15%, respectively. The 15-29% of naloxegol that crosses the BBB is significantly greater than the 2% criteria for designating the chemical as BBB-crossing. While naloxegol levels in the brain and CSF were far lower than those of naloxone, it was remarkable that significant quantities of naloxegol passed the BBB. In comparison to naloxone, the brain-to-plasma and CSF-to-plasma ratios of AG10-L2-Nal (1.4 percent and 1%, respectively; Figure 37) were significantly lower. When AG10-L2-Nal was compared to naloxegol, the brain to plasma ratio decreased by 20 times and the CSF to plasma ratio decreased by a 15 times. This finding reveals unequivocally that AG10-L2-Nal is a highly peripherally selective opioid antagonist.

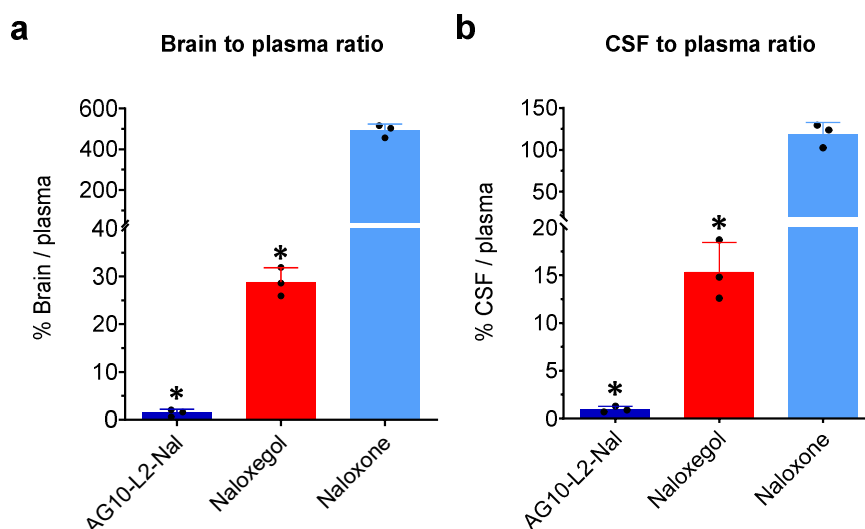


Figure 37 (a) Brain to plasma ratios and (b) CSF to plasma ratios of AG10-L2-Nal, naloxegol, and naloxone.

Male Sprague Dawley rats were dosed intravenously with 4.84 $\mu\text{mol/kg}$ of test compounds (equivalent to 1.6 mg/kg, 3.2 mg/kg, and 4 mg/kg for naloxone, naloxegol, and AG10-L2-Nal, respectively). The plasma, brain tissue, and CSF were collected at 30 minutes after dosing. The ratio of the brain (ng/g) versus plasma concentration (ng/mL) is expressed as the percentage brain to plasma ratio. The ratio of the CSF (ng/mL) versus plasma concentration (ng/mL) is expressed as the percentage CSF to plasma ratio. Bar graphs show the respective mean (\pm s.d.) ($n = 3$ for each group). Statistical differences were determined using one-way ANOVA followed by Tukey's Post Hoc test (* $P < 0.05$ compared to naloxone). For the brain to plasma ratio experiment $F(2,6) = 678.0$, $P < 0.0001$ and for the CSF to plasma ratio experiment $F(2,6) = 174.6$, $P < 0.0001$. (Data generated with Fang and Tuhin)

6.5 Method For Pharmacokinetics Study

In order to study intravenous (IV) pharmacokinetics (PK), jugular vein cannulated male Sprague Dawley rats (225-250 g; 7-8 weeks old) were used from Charles River. For the IV PK study, each animal was administered one intravenous bolus dosage of naloxone, naloxegol, or AG10-L2-Nal (4.84 mol/kg) in 200 μL dosing solution, followed by an injection of 200 μL sterile saline to flush the jugular vein cannula ($n = 3$ rats per group). At

predefined time points (0.033, 0.5, 1, 2, 4, 6, 8, 12, and 24 hours after dosing), 200 μ L blood samples were obtained from each rat via jugular vein cannula in heparinized tubes and replenished with sterile normal saline. Blood samples were prepared in the same manner as described in the brain uptake study.

6.6 Results For Pharmacokinetics Study

The half-life of AG10-L2-Nal in the circulation of rats was lengthened due to TTR. Rats were used to assess the pharmacokinetic characteristics of AG10-L2-Nal, naloxone, and naloxegol. These molecules were initially delivered intravenously as a single dose (4.84 μ mol/kg) (Figure 38 and Table 2). At predefined time periods (varying from 2 minutes to 24 hours), blood samples were taken via the jugular vein cannula, and concentrations of the test substances were measured using established LCMS/MS techniques (Figure 36 and Table 1). AG10-L2-Nal's pharmacokinetic profile was significantly distinct from that of naloxone and naloxegol. At any given time, plasma concentrations of AG10-L2-Nal were greater than those of naloxone and naloxegol. While there was no detectable level of naloxone and naloxegol 4 and 8 hours, respectively, after dose, AG10-L2-Nal was still detectable 24 hours later. The half-life of AG10-L2-Nal (half-life = 5.98 ± 0.81 hours) was 7-fold and 3.5-fold greater than that of naloxone and naloxegol (half-lives = 0.87 ± 0.13 hours and 1.72 ± 0.32 hours, respectively). This was because AG10-L2-Nal clearance (0.29 ± 0.02 L/h/kg) was much lower than that of naloxone and naloxegol (3.39 ± 0.55 L/h/kg and 6.54 ± 0.29 L/h/kg, respectively). Importantly, the AUC (Area Under the Curve) of AG10-L2-Nal was 23-fold and 12-fold higher than naloxegol and naloxone (741.34 ± 33.65 and 1455.11 ± 254.89 nM·h,

respectively). These results significantly support and corroborate our hypothesis that TTR recruitment can definitely lengthen the half-life and improve the pharmacokinetic profile of AG10-L2-Nal in vivo.

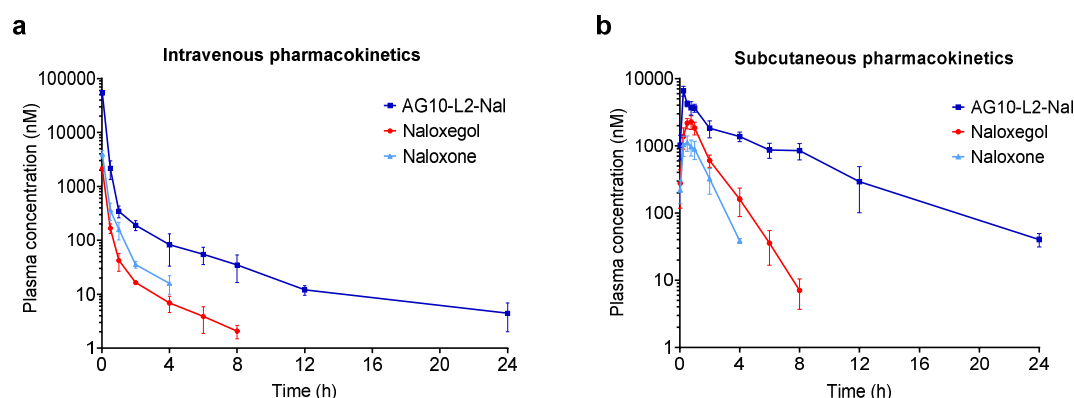


Figure 38 a Pharmacokinetics profile of AG10-L2-Nal, naloxegol, and naloxone. a single intravenous bolus dose of 4.84 $\mu\text{mol/kg}$ (equivalent to 5.2 mg/kg, 10.4 mg/kg, and 13.2 mg/kg for naloxone, naloxegol, and AG10-L2-Nal, respectively) were administered to rats ($n = 3$ for each group). The concentration of the test compounds in plasma was determined at different time points and expressed as means \pm s.d. of three biological replicates. (Data generated with Fang and Tuhin)

Table 2

Pharmacokinetic Parameters of Naloxone, Naloxegol And AG10-L2-Nal Determined From The Plasma Concentrations After Intravenous Dosing.

	k (1/h)	$t_{1/2}$ (h)	AUC _{inf} (nM.h)	CL (L/h/kg)	V _{ss} (L/kg)
Naloxone	0.81 ± 0.13	0.87 ± 0.13	1455.11 ± 257.18	3.39 ± 0.55	1.23 ± 0.42
Naloxegol	$0.41 \pm 0.06^*$	1.72 ± 0.27^a	741.34 ± 33.65^a	$6.54 \pm 0.29^{*a}$	$2.76 \pm 0.39^{*a}$
AG10-L2-Nal	$0.12 \pm 0.02^*$	$5.98 \pm 0.81^*$	$16912.96 \pm 1085.27^*$	$0.29 \pm 0.02^*$	$0.12 \pm 0.02^*$

Statistical differences were determined using one-way ANOVA followed by Tukey's multiple comparison test. For k, $F(2,6) = 50.36$, $P = 0.0002$; for $t_{1/2}$, $F(2,6) = 90.94$, $P < 0.0001$; for AUC_{inf}, $F(2,6) = 603.5$, $P < 0.0001$; for CL, $F(2,6) = 224.4$, $P < 0.0001$; for V_{ss}, $F(2,6) =$

(Table 2 Continued)

48.0, $P < 0.0001$. (* represents $P < 0.05$ compared to naloxone group, a represents $P < 0.05$ of naloxegol compared to AG10-L2-Nal group). All data are presented as mean (\pm s.d.) ($n = 3$ rats per group). (Data generated with Fang and Tuhin)

Table 3

Pharmacokinetic Parameters of Naloxone, Naloxegol And AG10-L2-Nal Determined From The Plasma Concentrations After Subcutaneous Dosing.

	k (1/h)	$t_{1/2}$ (h)	AUC _{inf} (nM*h)	CL/F (L/h/kg)	V _{ss} /F (L/kg)
Naloxone	1.03 \pm 0.1	0.67 \pm 0.07	1761.87 \pm 236.85	9.10 \pm 1.22	8.94 \pm 2.08
Naloxegol	0.79 \pm 0.02 * a	0.88 \pm 0.02 a	3682.32 \pm 565.51 a	4.37 \pm 0.71 * a	5.58 \pm 0.96
AG10-L2-Nal	0.20 \pm 0.04 *	3.62 \pm 0.76 *	17576.12 \pm 2537.87 *	0.92 \pm 0.14 *	4.89 \pm 1.83

Statistical differences were determined using one-way ANOVA followed by Tukey's multiple comparison test. For k, $F(2,6) = 136.8$, $P < 0.0001$; for $t_{1/2}$, $F(2,6) = 41.83$, $P = 0.0003$; for AUC_{inf}, $F(2,6) = 98.32$, $P < 0.0001$; for CL/F, $F(2,6) = 75.43$, $P < 0.0001$; for V_{ss}/F, $F(2,6) = 4.915$, $P = .0545$. (* represents $P < 0.05$ compared to naloxone group, a represents $P < 0.05$ of naloxegol compared to AG10-L2-Nal group). All data are presented as mean (\pm s.d.) ($n = 3$ rats per group). (Data generated with Dr. Park and Tuhin)

CHAPTER 7: Evaluation the In Vivo Efficacy of AG10-L2-Nal

7.1 Evaluation of The Hot Plate Latency

To confirm the naloxone conjugates were not able to cross the BBB and interfere with the analgesic effects, hot plate latency study was conducted.

7.1.1 Method of Hot Plate Study

Hot plate study of AG10-L2-Nal, Naloxone, Naloxegol, and MNTX. Analyses of hot plate analgesia. The experiment utilized a hot plate analgesia meter from Columbus Instruments, Ohio, United States. The temperature of the hot plate was $55 \pm 0.5^{\circ}\text{C}$. In order to prevent tissue injury, the maximum exposure time to a hot plate was set at 60 seconds. The withdrawal latency to heat exposure (withdrawal or shaking of the hind paw, withdrawal, licking of front or hind paw, or attempting to escape by jumping) was recorded, and the animal was removed from the hot plate swiftly and carefully. The timer was controlled by an analgesia meter-connected footswitch. The treatment groups were concealed from the experimenters. Before dosing, pre-dose control response was evaluated to establish withdrawal latencies as a baseline. After ranking predose baseline latencies and allocating animals to treatment groups, the mean predose baseline latencies were comparable between groups. The day before the experiment, the rats were placed on the hot plate for a half-hour at room temperature to acclimate them to the device. The temperature in the laboratory was 22 ± 2 degrees Celsius. During the experiment, relative humidity was not controlled in the experiment room. In order to decrease the stress associated with fasting

during these behavioral trials, the rats underwent a brief fast (8-12 hours) when corticosterone hormone levels do not fluctuate.

The following treatment groups (each with $n = 6$ rats) were randomly selected: vehicle and saline groups (saline group 0.9 percent sterile saline followed by vehicle) which is equivalent to 35 $\mu\text{mol/kg}$, followed by vehicle), naloxone 35, 3.5, and 0.7 $\mu\text{mol/kg}$ groups, naloxegol 35, 3.5, and 0.7 $\mu\text{mol/kg}$ groups, methylnaltrexone 35, 3.5, and 0.7 $\mu\text{mol/kg}$ groups, or AG10-L2-Nal 35 $\mu\text{mol/kg}$ group. At time = 0 minute, each rat received an intravenous injection of 200 μL 0.9 % sterile saline (only for saline group) or morphine 35 $\mu\text{mol/kg}$ dissolved in 0.9% saline followed by an injection of 200 μL of saline to flush the compound remained in jugular vein cannula. All but one group received the morphine dose (35 $\mu\text{mol/kg}$) except for the saline group. At $t = 5$ minutes, all the groups were dosed another intravenous injection 200 μL of vehicle (for saline and control groups) or the different opioid antagonist (naloxone, naloxegol, methylnaltrexone, and AG10-L2-Nal) formulated by 10% DMSO, 20% PEG400, and 70% sterile deionized water. After that, each rat received an infusion of 200 μL sterile saline to flush the jugular vein cannula. Prior to the start of the main trial, a dose range-finding test was carried out to evaluate the dose at which morphine consistently displayed powerful analgesia and naloxone influenced the antinociceptive qualities of morphine (data not shown).

7.1.2 Results Of Hot Plate Study

In rats, intravenous injection of AG10-L2-Nal does not counteract morphine-induced analgesia. According to the findings on pharmacokinetics and BBB penetration, AG10-L2-

Nal has a lower BBB penetration than naloxone and the naloxegol, respectively. It will be exciting to see whether the AG10-L2-Nal data might be translated into less reversal of morphine-induced analgesia before looking into the effectiveness of AG10-L2-Nal in reversing OIC. At 55 degrees Celsius, an animal's tolerance for heat is measured by the amount of time it can remain on a hot plate, and this model was utilized in this study. AG10-L2-Nal was evaluated against two FDA-approved PAMORAs for the treatment of OIC (i.e., MNTX and naloxegol). A CNS and PNS opioid antagonist, naloxone, were also included in the list.

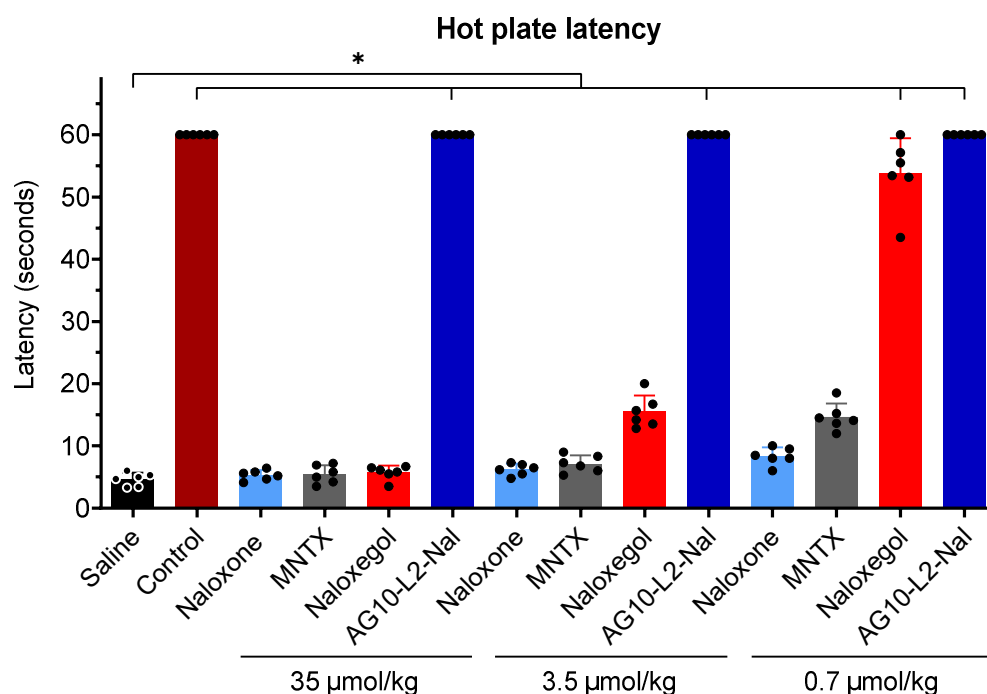


Figure 39 Hot plate study of opioid antagonists in male Sprague-Dawley rats. Hot plate latency test to measure analgesia. Male Sprague-Dawley rats were first administered with saline or a single intravenous (IV) dose of morphine (35 µmol/kg; equivalent to 10 mg/kg). After 5 minutes, the morphine treated animals were administered with a single intravenous dose of vehicle or the opioid antagonists. Saline group: saline + vehicle.; control group: 35 µmol/kg morphine + vehicle; all other groups: 35 µmol/kg

(Figure 39 Continued)

morphine + specified dose of antagonists. The 35 $\mu\text{mol/kg}$ dose of antagonists represent 11.5 mg/kg, 23 mg/kg, 12.5 mg/kg, and 30 mg/kg for naloxone, naloxegol, methylnaltrexone (MNTX), and AG10-L2-Nal, respectively. The hot plate withdrawal latency to heat exposure (withdrawal or shaking of the hind paw, sharp withdrawal, licking of fore or hind paw, or attempting to escape by jumping) was recorded 1 hour after the morphine dose before the rats were removed from the hot plate. Statistical differences were determined using Kruskal–Wallis test followed by Dunn's multiple comparisons test, $H = 77.02$, $P < 0.0001$. All data are presented as mean (\pm s.d.) ($n = 6$ rats per group, $*P < 0.05$). (Data generated with Fang and Tuhin)

Five minutes after receiving a single dosage of opioid antagonists, rats were administered either saline or a single dose of morphine. Compared to saline group (latency = 4.6 ± 1.0 seconds), morphine group (a single dose of 10 mg/kg or 35 $\mu\text{mol/kg}$) were insensitive to heat 1 hour after dosing (latency = 60 seconds), which is the maximum cutoff (Figure 39). According to the scientific literature, a dose of 35 $\mu\text{mol/kg}$ of morphine produces complete analgesia. The antagonists were next evaluated at levels comparable to concurrently delivered morphine (single doses of 35 $\mu\text{mol/kg}$). As anticipated, naloxone was quite effective at reversing morphine-induced analgesia (latency = 5.30 ± 0.80 seconds). Surprisingly, both MNTX and naloxegol were able to completely reverse morphine-induced analgesia (latency = $5.4 \pm 1.5\%$ and $5.7 \pm 1.2\%$, respectively) (Figure 39).

At a 10-fold lower dose (3.5 $\mu\text{mol/kg}$) than morphine, the potential of antagonists to counteract morphine-induced analgesia was evaluated. Naloxone and MNTX were both effective at totally reversing analgesia (latency = 6.2 ± 0.9 seconds and 7.1 ± 1.4 seconds, respectively), although naloxegol significantly reduced latency (latency = 15.5 ± 2.6 seconds) (Figure 39). The BBB measurements (Figure 37) indicated that 30% of naloxegol

in plasma crosses the BBB at a similar dose of 4.8 $\mu\text{mol/kg}$, which is consistent with these latency results. Subsequently, the antagonists were evaluated at a 50-fold lower dose (0.7 $\mu\text{mol/kg}$) than morphine. Naloxone produced a strong analgesia reversal (latency = $8.3 \pm 1.4\%$ seconds). At this lower dose, there was a partial reversal of morphine-induced analgesia by MNTX (latency = 14.7 ± 2.2 seconds), but no reverse by naloxegol (delay = 53.8 ± 5.6 seconds) (Figure 39). The dramatic reversal of analgesia brought about by MNTX has consequences for patients who are suffering from advanced diseases.

7.2 Evaluation of Opioid-induced Constipation

To evaluate the efficacy of the conjugates and to verify the hypothesis, the peripheral opioid induced activity was need to tested.

7.2.1 Method of Gastrointestinal (GI) Transit

Measurement of the distance a charcoal traveled in the GI tract of fasted male SD rats was used to test the effectiveness of opioid antagonists to antagonize morphine-induced constipation. Fasting was restricted to 8-12 hours in order to keep the rats as comfortable as possible for the duration of the study. The charcoal meal was created by adding 10% by weight of charcoal and 10% by weight of gum Arabic to tap water.

For the first 30 minutes, the procedure is the same as hot plate study. At $t = 30$ minutes, 1 mL of a charcoal suspension was administered to each animal by oral gavage. At $t = 60$ minnues, each rat was humanely euthanized by decapitation, and the intestine was exposed. The distance the charcoal had traveled along the intestine from the pyloric

sphincter and the total intestinal length were measured. The distance travelled by the charcoal meal in millimeters was calculated as a percentage of the total length of the intestine

7.2.2 Results of Gastrointestinal (GI) transit

Using the GI transit model, researchers were able to determine the effectiveness of opioid antagonists in reversing the OIC that morphine causes in rats by tracking the distance travelled by an oral dose of charcoal in the GI tract. Morphine were dose at $t = 0$ minutes and antagonists were administered at $t = 5$ minutes (a single intravenous dose of $35 \mu\text{mol/kg}$). In the absence of antagonists, morphine decreased the amount of gastric emptying caused by a charcoal meal to less than 15.5% of the drug-free control (Figure 40). At all studied doses, Naloxone was highly successful at restoring complete GI transit and reversing OIC (96% charcoal GI transit vs to the saline group). MNTX efficiently recovered entire GI transit to 100% at $35 \mu\text{mol/kg}$ (equimolar dose of morphine). A 10-fold reduction in MNTX dosages ($3.5 \mu\text{mol/kg}$) resulted in a considerable reversal of OIC (GI transit= $61.6 \pm 4.4\%$). A 50-fold reduction of MNTX ($0.7 \mu\text{mol/kg}$) (the only dose that demonstrated partial hot plate analgesia, Figure 39), MNTX exhibited little reversal of charcoal movement (GI transit= $29.0 \pm 6.5\%$) in comparison to the saline group (Figure 40). While naloxegol reversed OIC effectively at dosages of $35 \mu\text{mol/kg}$ and $3.5 \mu\text{mol/kg}$ (GI transit = 100 % and $54.6 \pm 6.5 \%$, respectively), there was no substantial reversal of OIC at the $0.7 \mu\text{mol/kg}$ dose (a dose that resulted in no reversal of morphine-induced analgesia, Figure 39 and Figure 40). Intriguingly, the same amounts of naloxegol that reversed OIC also reversed analgesia

(Figure 39). These doses have been shown to penetrate the CNS significantly (Figure 37). Antagonists with more BBB penetration (Figure 37) exhibited more effective reversal of OIC, showing that the CNS plays a significant role in the onset of OIC. There is a direct correlation between the degree of analgesia reversal (with a confirmed CNS site of action for opioids) and the reversal of OIC, according to the results for the test substances (Figure 39 and Figure 40). Our AG10-L2-Nal results also indicate that we have created what we think to be the most peripherally selective PAMORA that does not exhibit considerable BBB penetration, as demonstrated here in rats.

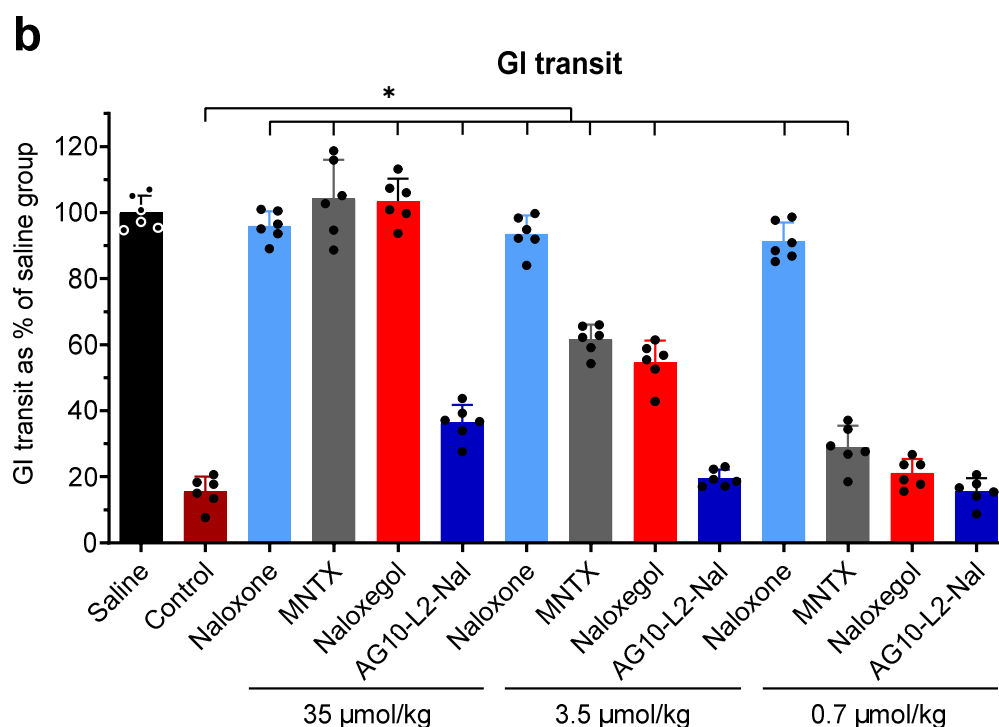


Figure 40 GI transit study of opioid antagonists.

Gastrointestinal (GI) transit assay at 1 hour after different IV bolus doses of the test compounds. The dosing schedule is similar to the hot plate assay with an additional oral gavage of charcoal meal 30 minutes after the saline or morphine dose. The significance of

(Figure 40 Continued)

differences was measured by two-way ANOVA followed by Tukey's post hoc test ($n = 6$ rats per group, $*P < 0.05$), dose $F(2,90) = 262.3$, $P < 0.0001$, compound $F(5,90) = 670.8$, $P < 0.0001$. (Data generated with Fang and Tuhin)

CHAPTER 8: EXPLORING THE MISTS BEHIND THE LOW EFFICIENCY

The in vitro binding affinity of AG10-L2-Nal and the drug exposure (AUC) were much superior to other PAMORAs. However, in contrast, AG10-L2-Nal exhibited a much lower reversal of opioid-induced constipation. After double-checking the characterization, nothing went wrong with the molecule. The animal study protocols and the procedures from other works of literature were fully investigated to make sure nothing wrong with the operation. Then the hot plate study and GI transit study were repeated carefully but the data were consistent with the previous data.

8.1 TTR Did Not Limit The Binding of AG10-L2-Nal To Opioid Receptor

Even though AG10-L2-Nal shows a great binding affinity to opioid receptor in vitro, it does not show good efficacy in vivo. Observing that AG10-L2-Nal was only partially successful in reversing OIC at the highest dose of 35 $\mu\text{mol/kg}$ (GI transit = $36.4 \pm 5.4\%$) was quite surprising. This could be the TTR holds the compound and limits its binding to opioid receptor. In order to prove this, excess of AG10 was predosed to occupied the TTR binding pockets so that AG10-L2-Nal gets free to bind to opioid receptor. However, data was showed no improvement in OIC when AG10 was present (Figure 41). The binding affinity of AG10-L2-Nal to the mu-opioid receptor is comparable in the absence and presence of TTR (0.35 nM vs. 1.3 nM). In addition, the plasma concentration of AG10-L2-Nal was analyzed by LCMS. Result showed that the concentration of AG10-L2-Nal is 7.6 ± 0.5 μM greater than the plasma concentration of TTR (5 μM). Unbound AG10-L2-Nal is not

the limitation of the low efficacy. These suggested that the low efficacy of reversal of opioid-induced constipation is not because of the influence of TTR. To figure out the problem, we need to explore other possibilities.

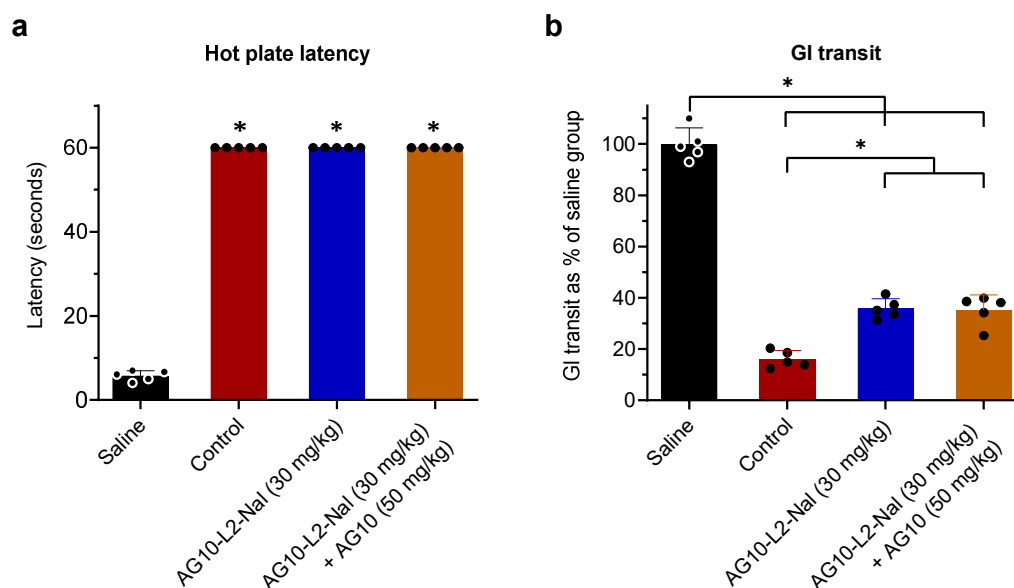


Figure 41 Hot plate and gastrointestinal (GI) transit efficacy studies of AG10-L2-Nal (in the presence and absence of AG10) against morphine.

(a) Hot plate latency test to measure analgesia. Male Sprague-Dawley rats were first administered with a single subcutaneous (SC) dose of vehicle or the 50 mg/kg AG10. After 10 minutes, animals were administered with a single subcutaneous dose of saline or 10 mg/kg morphine (35 μ mol/kg). After another 5 minutes, animals were administered with AG10-L2-Nal or vehicle. Saline group: vehicle + saline + vehicle; control group: vehicle + 10 mg/kg morphine + vehicle; AG10-L2-Nal group: vehicle + 10 mg/kg morphine (35 μ mol/kg) + 30 mg/kg AG10-L2-Nal (35 μ mol/kg); AG10-L2-Nal + AG10 group: AG10 50 mg/kg + 10 mg/kg morphine (35 μ mol/kg) + 30 mg/kg AG10-L2-Nal (35 μ mol/kg). The hot plate withdrawal latency to heat exposure (withdrawal or shaking of the hind paw, sharp withdrawal, licking of fore or hind paw, or attempting to escape by jumping) was recorded 1 hour after the morphine dose before the rats were removed from the hot plate. Statistical differences were determined using Kruskal–Wallis test followed by Dunn's multiple comparisons test, $H = 18.53$, $P = 0.0003$.

(b) Gastrointestinal (GI) transit assay at 1 hour after different SC doses of the test compounds. The dosing schedule is similar to the hot plate assay with an additional oral gavage of charcoal meal 30 minutes after the saline or morphine dose. Statistical differences were determined

(Figure 41 Continued)

using one-way ANOVA followed by Tukey's post hoc test, $F(3,16) = 297.5$, $P < 0.0001$. All data are presented as mean (\pm s.d.) ($*P < 0.05$, $n = 5$ rats per group). Source data are provided as a Source Data file. (Data generated with Tuhin)

8.2 AG10-L2-Nal Did Not Act As A Partial Agonist in Vivo

The antagonists' binding affinities were determined for human mu-opioid receptors, while the in vivo efficacy studies were conducted in rats. However, the human and rat mu-opioid receptors share 94 percent amino acid sequence similarity (Mestek et al., 1995). Therefore, interspecific differences were not expected to be a major factor in the lower in vivo efficacy of AG10-L2-Nal. However, even though the functional assay illustrated that AG10-L2-Nal is an opioid antagonist, it might change into a partial agonist or agonist due to the biotransformation in vivo. In order to verify this hypothesis, AG10-L2-Nal by itself was evaluated in the hot plate and the GI transit study.

Method: Rats were randomly assigned to one of three treatment groups ($n = 5$). At time = 0 minute, each rat received one 500 μ L/250g body weight subcutaneous dose of vehicle, morphine 35 μ mol/kg, or AG10-L2-Nal 35 μ mol/kg dissolved in vehicle. At $t = 1$ h, hot plate latency was measured. The formulation and the experiment procedure were similar as described before.

Results: AG10-L2-Nal was tested on its own in the hot plate and GI transit tests to ensure that the 40% reversal of GI transit caused by AG10-L2-Nal was not related to partial agonistic activity. It was hoped that AG10-L2-Nal would exhibit any partial agonistic properties as a result of naloxone's structural alteration through the use of hot plate analgesia

and GI transit assays. AG10-L2-Nal had no analgesic (latency = 6.3 ± 1.3 seconds) or OIC effects as compared to morphine or OIC effects (GI transit = $98.7 \pm 7.2\%$) (Figure 42).

These results translated well with the mu-opioid receptor functional assay data (Figure 33 and Figure 34) and excluded the hypothesis that AG10-L2-Nal was bio transformed into partial/full agonist.

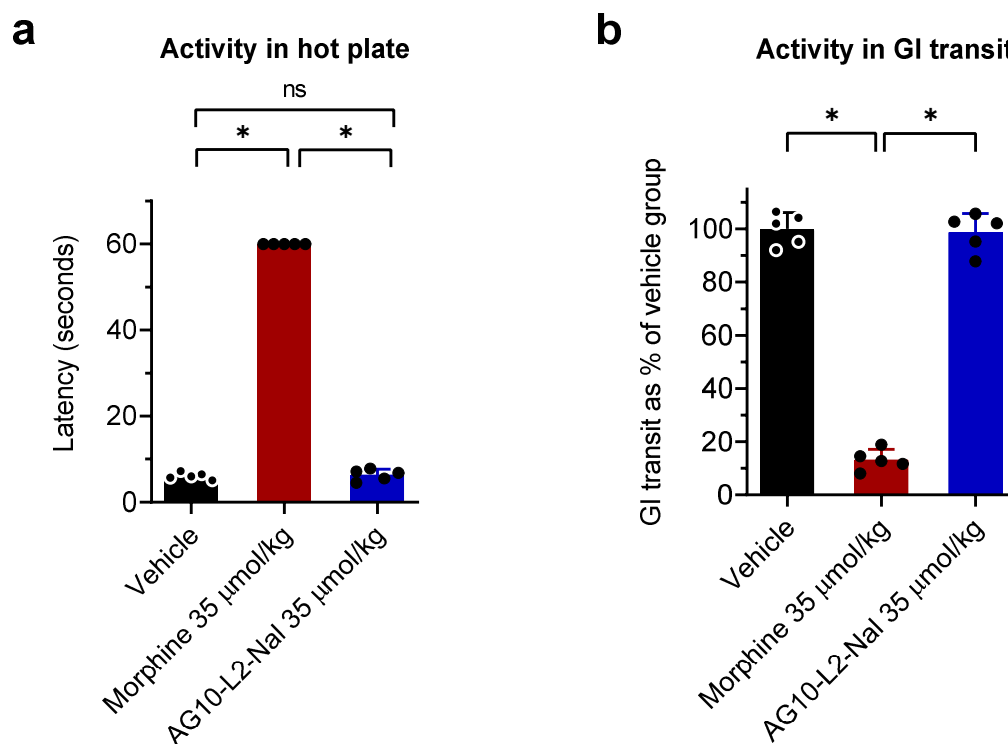


Figure 42 Evaluating the potential partial agonistic behavior of AG10-L2-Nal

a Hot plate latency, statistical differences were determined using Kruskal–Wallis test followed by Dunn's multiple comparisons test, $H = 9.769$, $P = 0.0021$. **b** and gastrointestinal (GI) transit assays to evaluate potential partial agonistic behavior of AG10-L2-Nal. Hot plate latency or GI transit were checked 1 hour after the subcutaneous dose of vehicle, morphine (35 µmol/kg), and AG10-L2-Nal (35 µmol/kg) in male Sprague-Dawley rats. Statistical differences were determined using one-way ANOVA followed by Tukey's post hoc test, $F(2,12)=354.4$, $P < 0.0001$. (Data generated with Tuhin)

8.3 AG10-L2-Nal Provides New Insights Mu-opioid Receptors In The CNS Play

Important Role In OIC

The role of the CNS in OIC precipitation is confused. Mainstream theory in the most studies suggested that the mechanism of opioid-induced constipation is predominantly contributed by the mu opioid receptors in the gastrointestinal tract. In fact, this is the theory basis for development of the current PAMORAs. Considering a substantial naloxegol and MNTX crossing the blood-brain barrier. Also, GI transit studies in rats (Figure 40) indicated a significant role for the central nervous system (CNS) in the OIC. It was hard not to suspect whether mainstream theory was wrong at this point. Probability, CNS, instead of peripheral play a even important role in OIC.

However, the existing data cannot prove whether CNS impact in the OIC, let alone to what extent. Thus, injecting the AG10-L2-Nal directly into brain was very necessary to verify the hypothesis.

8.3.1 Method

Intracerebroventricular (ICV) cannula implantation was performed by Charles River Laboratories Inc, Hollister, CA. The dummy cannula's metal wire stylet was put into the guiding cannula for the ICV injection. The following treatment groups were randomly assigned to the rats (n = 5): saline group (ICV vehicle + SC vehicle dose and + SC saline), control group (ICV vehicle + SC vehicle + SC morphine), AG10-L2-Nal SC group (ICV vehicle + SC AG10-L2-Nal + SC morphine), AG10-L2-Nal ICV group (ICV AG10-L2-Nal +

SC vehicle + SC morphine), and AG10-L2-Nal ICV+SC group (ICV AG10-L2-Nal + a SC AG10-L2-Nal + SC morphine).

At $t = 0$ minute, rats were dosed 10 μ L ICV of vehicle or AG10-L2-Nal (0.35 mol/kg, or 88 nmol in per rat), followed by a subcutaneous (SC) dose of vehicle or AG10-L2-Nal (35 μ mol/kg).

8.3.2 Results

To prove the hypothesis that CNS plays an important role in OIC, an ICV experiment was performed. There, at $t = 0$ minutes, rats were SC administered morphine, distributing in the periphery and CNS, at $t = 10$ minutes, AG10-L2-Nal was either injected in periphery by SC administration, or directly injected into brain by ICV administration, or both ICV + SC.

Due to the high hydrophilicity and the protection of TTR, AG10-L2-Nal was unable to cross the BBB and thus, SC administration will only target the peripheral mu-opioid receptors, whereas, ICV administration should restrict the effect of AG10-L2-Nal to the central nervous system (CNS), and ICV + SC administration will target mu-opioid receptors in both the CNS and the periphery. The data obtained from SC study were in agreement with the results obtained from IV study; AG10-L2-Nal resulted in no analgesia reversal (latency = 60 seconds; Figure 43) and the OIC were partially reversed (GI transit = $36.0 \pm 2.5\%$ compared to morphine control $17.8 \pm 2.6\%$) (Figure 43)

Interestingly, ICV administration of AG10-L2-Nal was effective in analgesia reversal (latency = 11.1 ± 1.7 seconds) and OIC reversal ($50.1 \pm 4.2\%$), which is higher than that in

SC study. It was expected that AG10-L2-Nal would have an ICV effect on reversing analgesia (since mu-opioid receptors in the CNS are known to cause analgesia), but the OIC results were unexpected.

More surprisingly, concomitant administration of AG10-L2-Nal via both ICV and SC resulted in complete reversal of analgesia (latency = 3.6 ± 0.9 seconds) and OIC (GI transit = 100%) (Figure 43). These data strongly suggested analgesic and OIC effects are enhanced when mu-opioid receptors in both the peripheral and central nervous system are targeted simultaneously. Although synergy was described for the analgesic impact of opioids (Pasternak & Pan, 2013), to the best of knowledge, these are the evidence that also imply the occurrence of synergy or an additive effect for OIC.

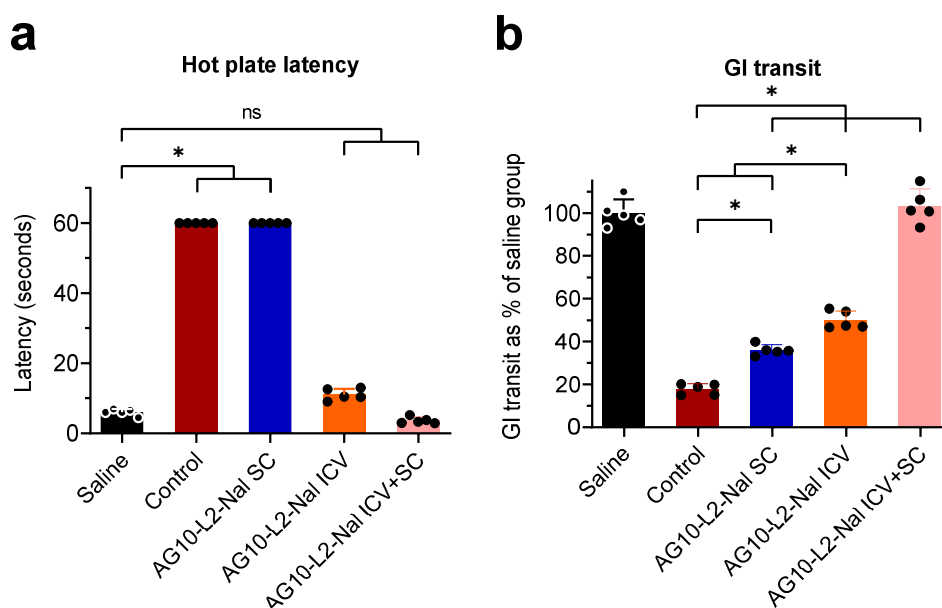


Figure 43 Evaluating the contribution of mu-opioid receptors in the CNS to analgesia and OIC.

a Hot plate latency, the significance of differences was measured by Kruskal–Wallis test followed by Dunn's multiple comparisons test, $H = 23.23$, $P = 0.0001$ and **b** GI transit assays to evaluate the contribution of central and peripheral mu-opioid receptors to OIC. AG10-L2-Nal (35 $\mu\text{mol/kg}$; subcutaneous route, SC) and/or (0.35 $\mu\text{mol/kg}$ equivalent to 88 nmol per rat; intracerebroventricular route, ICV) or vehicle (control group) was administered at $t=0$ minutes. Morphine (35 $\mu\text{mol/kg}$ SC) or saline (saline group) was administered at 10 minutes. The antagonists were administered 10 minutes before morphine to allow enough time to handle the animals during the ICV and SC dosing. Charcoal was given at 40 minutes. Hot plate latency and GI transit were measured at 70 minutes. Statistical differences were determined using one-way ANOVA followed by Tukey's post hoc test $F(4,20)=274.7$, $P < 0.0001$. All data are presented as mean (\pm s.d.) (* $P < 0.05$, $n = 5$ rats per group). (Data generated with Tuhin)

8.4 Proof From The Opposite Direction – Peripheral Concentrated Opioid Agonist

To prove from other direction, a peripheral agonist need to be used to evaluated.

Before using our novel technology platform to design and synthesize a truly peripheral

restricted opioid agonist, a small trial using a peripheral selective opioid agonist, Loperamide

was conducted. Loperamide enters the brain readily but also get effluxed by P-glycoprotein (P-gp). At therapeutic doses, loperamide mostly distributes in peripheral. However, when taken at larger amounts, loperamide can overcome the efflux transporter, accumulate in the brain, and have adverse effects in CNS, such as overdose and even death(Bishop-Freeman et al., 2016). Fentanyl, on the other hand, is a lipophilic medication that may easily enter the central nervous system. It has a 2-fold predilection for the brain over plasma(Hug Jr & Murphy, 1981). Similar to fentanyl, loperamide is a potent agonist to the mu-opioid receptors ($K_i = 0.53$ nM vs. $K_i = 0.39$ nM for fentanyl)(NCATS, 2022). It has been observed that the ED50 for producing constipation with subcutaneous loperamide is 1 mg/kg (GI transit = 50 percent).(Tan-No et al., 2003). Therefore, 1 mg/kg of loperamide vs. fentanyl in inducing OIC were evaluated. The experiment procedure was similar to the section before. Results demonstrated the inhibition of GI transit by loperamide (GI transit = $54.5 \pm 4.9\%$, which was consistent with literature) was 25-fold lower than that of fentanyl (GI transit = $2.3 \pm 1.8\%$) (Figure 44). These data suggested that the distribution of opioid agonists with similar affinity influenced the OIC a lot, and the CNS might play a more important role. However, Pgp has a limit to efflux the compound out from brain, and the best capacity is restricting the brain concentration 3% of plasma(Ferrier, 2014; Tamai & Tsuji, 2000). The remaining compound acting in the brain would messy the results. In order to obtain a clean data for the conclusion, a truly peripheral opioid agonist was needed for the further confirmation.

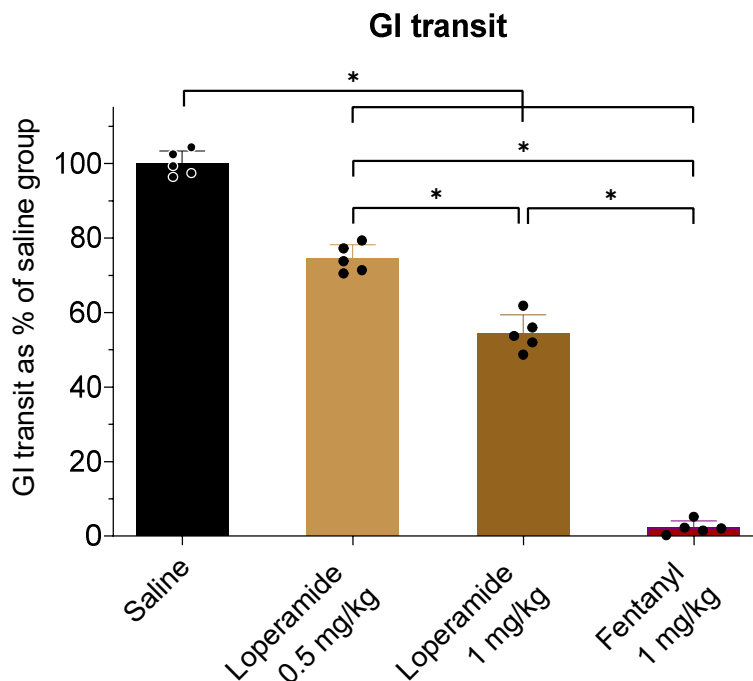


Figure 44 Gastrointestinal (GI) transit assay of loperamide and Fentanyl.

Gastrointestinal (GI) transit assay at 1 hour after SC doses of the test compounds. Male Sprague-Dawley rats were first administered with a single subcutaneous (SC) dose of saline or loperamide 0.5 or loperamide 1 mg/kg doses. The animals received an oral gavage of charcoal meal 30 minutes after the saline or loperamide doses. At 1 hour the rats were euthanized and the GI transit was measured. Statistical differences were determined using one-way ANOVA followed by Tukey's post hoc test $F(3,16) = 649.9$, $P < 0.0001$. All data are presented as mean (\pm s.d.) (* $P < 0.05$, $n = 5$ rats per group). Source data are provided as a Source Data file. (Data generated with Tuhin)

8.5 Confirmed From The Opposite Direction –Peripherally Restricted Opioid Agonist

Probe

To further prove our hypothesis, a BBB restricted agonist probe is needed for the study. Therefore, we designed a new AG10 conjugate.

8.5.1 Synthesis of the agonist probe

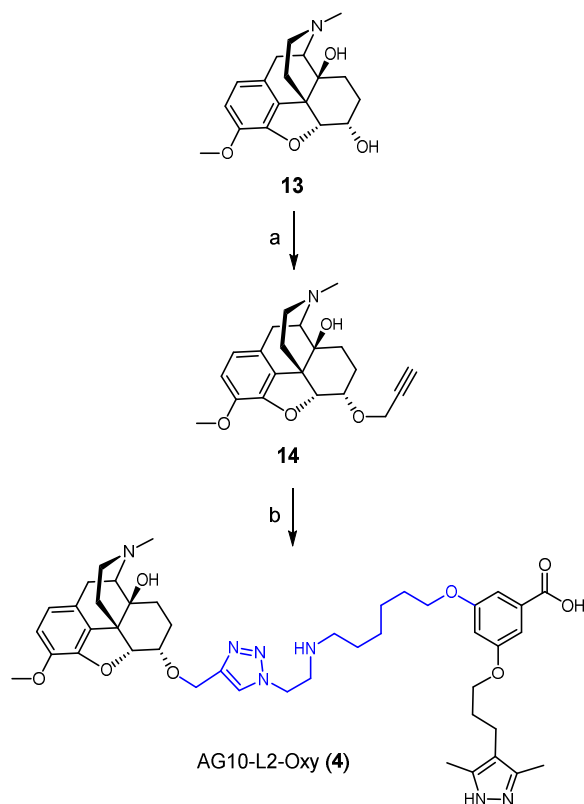
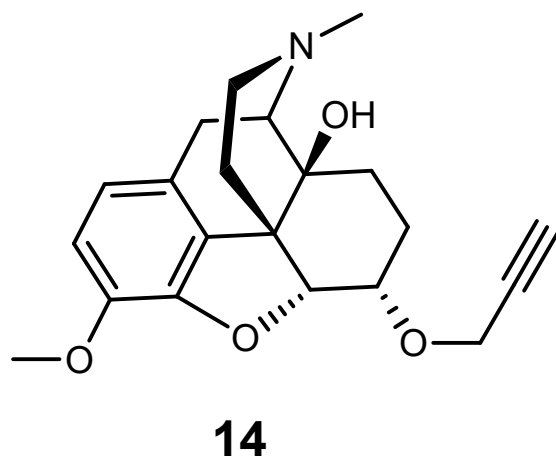


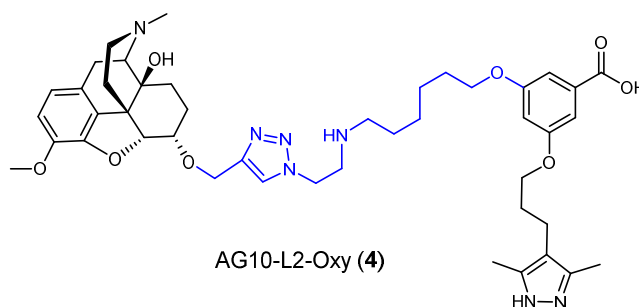
Figure 45 Synthesis of AG10-L2-Oxy (**4**).

Sodium hydride, DMF, propargyl bromide, 4 hours; **(b)** (i) Compound **11**, CuSO₄, sodium ascorbate, THF/H₂O (4:1), room temperature, overnight; (ii) CH₂Cl₂/TFA (4:1), room temperature, 2 hours. (Data generated with Tuhin)



(4R,4aS,7S,7aR,12bS)-9-methoxy-3-methyl-7-(prop-2-yn-1-yloxy)-1,2,3,4,5,6,7,7a-octahydro-4aH-4,12-methanobenzofuro[3,2-e]isoquinolin-4a-ol (**14**).

The synthesis procedure is similar to compound **7**. (4R,4aS,7S,7aR,12bS)-9-methoxy-3-methyl-1,2,3,4,5,6,7,7a-octahydro-4aH-4,12-methanobenzofuro[3,2-e]isoquinoline-4a,7-diol (**13**) (synthesized as reported Patent US 8,575,196 B2) (400.0 mg, 1.26 mmol, 1 equiv) dissolved in anhydrous dimethylformamide (15 mL) under an inert atmosphere at 0 °C (via an ice bath), was added sodium hydride (60% in oil) (201.6 mg, 5.04 mmol, 4 equiv) dropwise. The solution was stirred for one hour in an environment of nitrogen. Then propargyl bromide (80 % w/v) (243.6 μ L, 1.64 mmol, 1.3 equiv) was added dropwise to the solution. And the reaction mixture was stirred at 60 °C overnight. After that, 5 mL deionized water was added to the reaction mixture to quench the reaction. The compound was extracted by brain/ethyl acetate. The organic fractions were dried and purified by flash column chromatography (silica gel, 0-10% dichloromethane/methanol) to afford compound **14** (259.7 mg, 0.73 mmol, 58% yield). ESI-MS: m/z calcd for C₂₁H₂₅NO₄ [M+H]⁺ 356.2; found: 356.1.



3-(3-(3,5-dimethyl-1H-pyrazol-4-yl)propoxy)-5-(((6-((2-(4-(((4R,4aS,7S,7aR,12bS)-4a-hydroxy-9-methoxy-3-methyl-2,3,4,4a,5,6,7,7a-octahydro-1H-4,12-methanobenzofuro[3,2-e]isoquinolin-7-yl)oxy)methyl)-1H-1,2,3-triazol-1-yl)ethyl)amino)hexyl)oxy)benzoic acid (**4**).

Compound **13** (118 mg, 0.332 mmol, 1 equiv), compound **11** (185.5 mg, 0.332 mmol, 1 equiv), CuSO₄·5H₂O (20.74 mg, 0.083 mmol, 0.25 equiv), and sodium ascorbate (32.9 mg, 0.166 mmol, 0.5 equiv) in a 5 mL mixture of THF/H₂O (4:1) to perform the click (CuAAC) coupling reaction. The reaction mixture was stirred at room temperature overnight. After that was dried under reduced pressure and the residue was extracted by hexane:ethyl acetate to yield the intermediate which was used for the next step directly. Then intermediate was added a mixture containing TFA and CH₂Cl₂, (1:4 ratio) (5 mL) and the reaction mixture was stirred at room temperature for 2 hours. The solution was dried and purified by preparative HPLC to afford compound AG10-L2-Oxy (**4**) (229.8 mg, 0.283 mmol, 85% yield over two steps) (98% purity by HPLC); *t_R* (C4 column) = 8.2 minutes; *t_R* (C18 column) = 15.0 minutes.

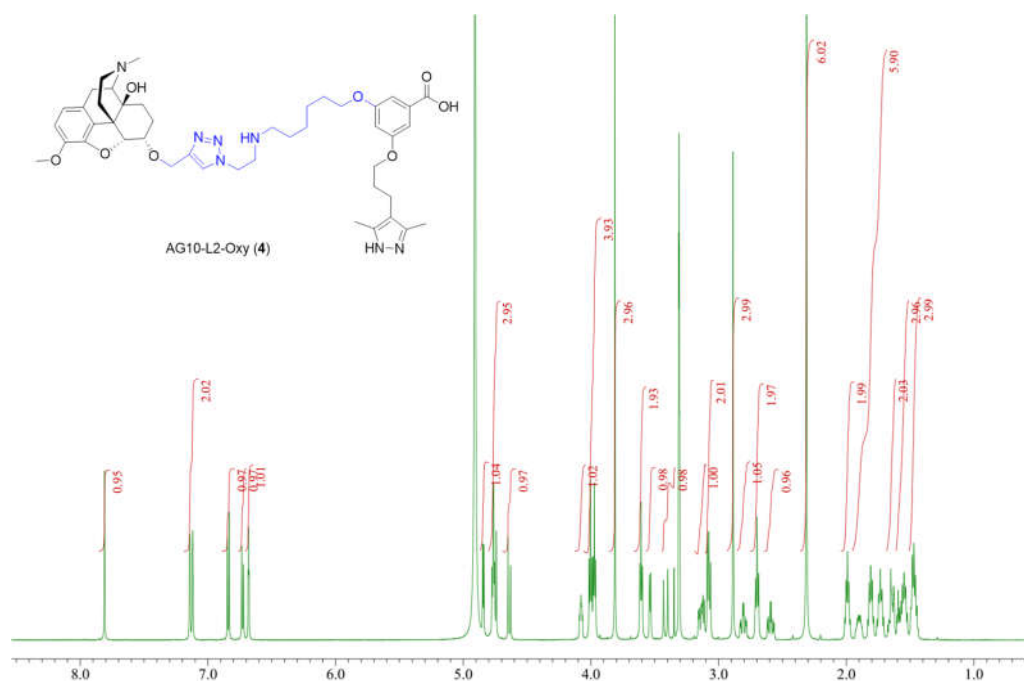


Figure 46 ^1H NMR Spectrum for AG10-L2-Oxy (4).

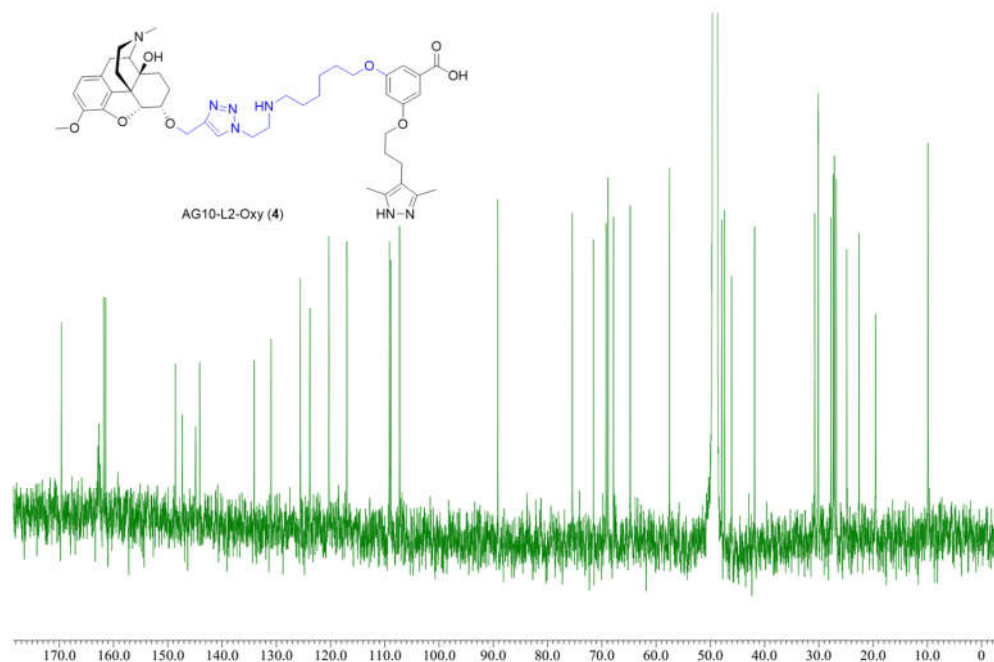


Figure 47 ^{13}C NMR Spectrum for AG10-L2-Oxy (4).

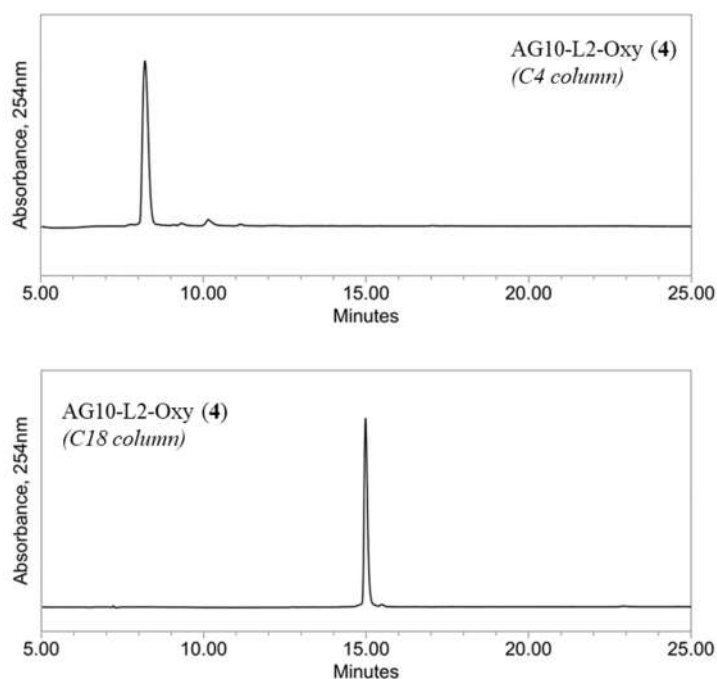


Figure 48 HPLC traces of AG10-L2-Oxy (4).

8.5.2 Evaluation of the agonist probe

Further study with AG10-Oxycodone conjugate (AG10-L2-Oxy, Figure 5) as an agonist probe was carried out to support the previous findings about the relative importance of the central nervous system (CNS) for analgesic and OIC. As with the AG10-L2-Nal experiment. The selection of oxycodone as the probe's opioid agonist was based on the two following considerations. First, an opioid other than morphine, should allow us to determine whether the data observed is not restricted to be applied in morphine. Second, the very high brain to plasma ratio of oxycodone (~3-fold) compared to morphine(Boström, Simonsson, & Hammarlund-Udenaes, 2006; Stain-Textier, Boschi, Sandouk, & Scherrmann, 1999)

would allow it to evaluate the applicability of our approach to limit the BBB penetration of molecules other than naloxone.

AG10-L2-Oxy demonstrated potent binding and selectivity to TTR in buffer and human serum (Figure 28 and Figure 29). Besides, AG10-L2-Oxy displayed potent and selective binding to the mu-opioid receptor ($K_i = 13$ nM vs. oxycodone 3.1 nM) compared to the delta-opioid receptor ($K_i = 410$ nM vs. oxycodone 958 nM) and kappa-opioid receptor ($K_i = 120$ nM vs. oxycodone 677 nM)(Monory et al., 1999).

Pharmacokinetic profile of AG10-L2-Oxy was then evaluated (Figure 50) by the similar procedure of AG10-L2-Nal PK study. Even though there was no detectable oxycodone 6 hours after dosing, on the contrary, AG10-L2-Oxy was still present after 24 hours (detailed PK parameters are shown in Figure 50 and Table 1 and Table 4). Next, Using the same procedure as the AG10-L2-Nal PK study, the BBB penetration of AG10-L2-Oxy in rats was next assessed (Figure 50). These results showed that the brain to plasma ratio was 276 %, and the CSF to plasma ratio was 80 %, which were in line with data on oxycodone by other groups(Boström et al., 2006; Mikus & Klimas, 2014). In contrast, there was no measurable quantities of AG10-L2-Oxy in either brain or CSF, even at a dosage 4-fold higher than that of oxycodone (Figure 50). These data further confirmed our novel technology platform can restrict the biodistribution in peripheral.

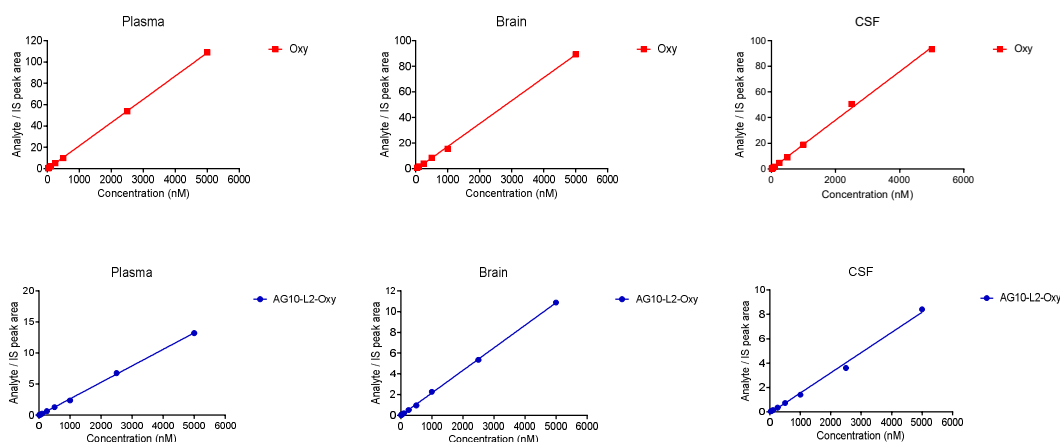


Figure 49 LC-MS/MS calibration curves used to quantitate oxycodone and AG10-L2-Oxy in rat plasma, brain, and CSF.

The calibration curves were for the BBB and subcutaneous pharmacokinetic studies. The identities of the compounds were determined using the following Q1/Q3 transition masses for oxycodone (316.4/241.1), IS reference oxycodone-D6 (322.4/304.5), and AG10-L2-Oxy (814.6/469.1). See Supplementary Table 1 for the detailed multiple reaction monitoring (MRM) parameters. Source data are provided as a Source Data file. (Data generated with Tuhin)

Table 4

Pharmacokinetic Parameters of Oxycodone And AG10-L2-Oxy Determined From The Plasma Concentrations After The Subcutaneous Dosing.

	k	t _{1/2}	AUC _{inf}	CL/F	V _{ss} /F
	(1/h)	(h)	(nM*h)	(L/h/kg)	(L/kg)
Oxycodone	0.9 ± 0.12	0.78 ± 0.09	4852.00 ± 676.31	3.32 ± 0.47	3.76 ± 0.85
AG10-L2-Oxy	0.15 ± 0.02 *	4.68 ± 0.52 *	25755.00 ± 3090.4 *	0.62 ± 0.07 *	4.22 ± 0.86

Statistical differences were determined using two tailed unpaired t-test with equal variance. For k, T(6) = 12.33, $P < 0.0001$; for t_{1/2}, T(6) = 14.78, $P < 0.0001$; for AUC_{inf}, T(6) = 13.21, $P < 0.0001$; for CL/F, T(6) = 11.36, $P < 0.0001$; for V_{ss}/F, T(6) = 0.7609, $P = 0.4756$ (* represents $P < 0.05$ compared to oxycodone group). All data are presented as mean (± s.d.) (n = 4 rats per group). Source data are provided as a Source Data file in Figure 8a source data. (Data generated with Tuhin)

8.5.3 AG10-L2-Oxy confirms CNS play more important role in analgesia and OIC

To directly prove the site of action and the importance of the role, ICV study was

performed. The experimental settings of this hot plate and GI transit were similar as the ICV AG10-L2-Nal study in the preceding section except the dosing schedule and experimental groups. It is reported that the analgesic effect of oxycodone in rats reduced fast 30 minutes after ICV dosage (The analgesic effect after 1 hour was less than 10 % of the maximum at 15 minutes)(Kuo, Wyse, Meutermans, & Smith, 2015). Also, the priori study showed the analgesia effect only at high dose of oxycodone. Therefore, rats were randomly distributed into the following groups (n = 5): ICV vehicle, SC oxycodone (16 $\mu\text{mol/kg}$), ICV oxycodone (640 and 1280 nmol per rat), SC AG10-L2-Oxy (64 $\mu\text{mol/kg}$), or ICV AG10-L2-Oxy (160 nmol). At t = 0 minute, each rat received ICV (10 μL) or SC (500 μL) doses of vehicle or opioid agonists per 250 g body weight. Hot plate latency or GI transit were assessed at t = 40 minutes.

A complete analgesic effect (latency = 56.8 ± 3.8 seconds vs 6.0 ± 0.8 seconds for vehicle) and inhibition of GI transit ($8.0 \pm 2.7\%$ compared to $100 \pm 5.1\%$ for vehicle) were observed as predicted following subcutaneous oxycodone injection (Figure 50). GI transit ($89.5 \pm 3.0\%$) and analgesia (latency = 9.5 ± 0.8 seconds) were only little affected by AG10-L2-Oxy administered subcutaneously. The ~10% OIC generated by the peripheral effect of AG10-L2-Oxy (Figure 50) is equivalent to ~18% the reversal of morphine-induced constipation for AG10-L2-Nal (Figure 43). Oxycodone by ICV administration did not induce significant analgesia or constipation even at a 4-fold greater dosage than AG10-L2-Oxy.

Interestingly, there was a significant analgesic effect (41.6 ± 4.6 seconds) and the

inhibition of GI transit ($18.7 \pm 3.0\%$) at a 8-fold greater dosage than AG10-L2-Oxy. This may be due to the increased clearance rate of oxycodone from the brain (15-fold faster than morphine)(Boström et al., 2006; Syvänen, Xie, Sahin, & Hammarlund-Udenaes, 2006) and this is consistent with reports indicating less than 2% of oxycodone persists in the brain 10 minutes after ICV administration(Yang et al., 2016). In contrast, ICV administration of an 8-fold lower dosage of AG10-L2-Oxy produced excellent analgesia (latency = 54.2 ± 4.8 seconds) and significant inhibition of GI transit ($9.5 \pm 2.8\%$). These data confirmed the important role of CNS in analgesia and OIC, and also highlighted how critical was the longer duration of compound in efficacy.

These results (Figure 39, Figure 40, Figure 42, and Figure 43) provide new insights that underscore the important function that mu-opioid receptors play in inducing OIC in both the central nervous system and the peripheral nervous system. These findings challenged the mainstream theory that OIC is predominantly controlled by the peripheral mu-opioid receptor.

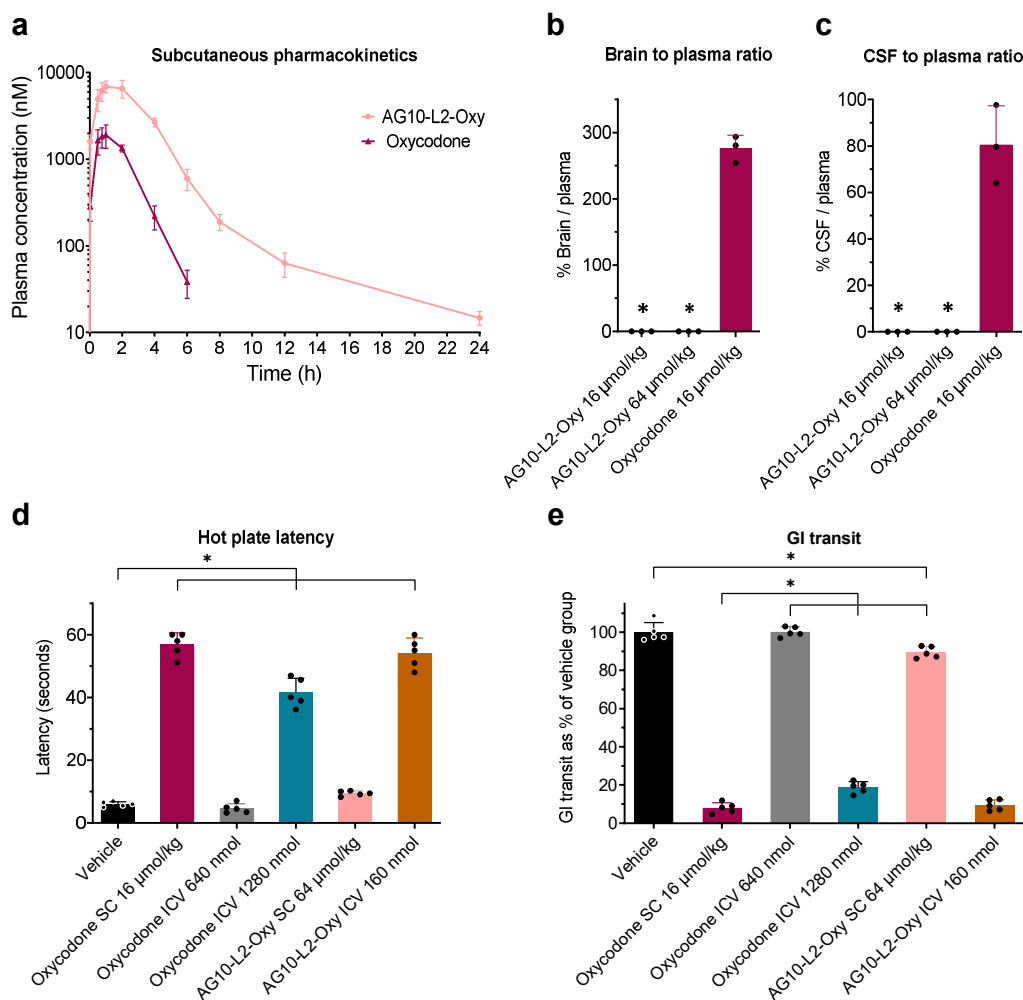


Figure 50 Pharmacokinetic and pharmacodynamic evaluation of AG10-Oxycodone conjugate (AG10-L2-Oxy).

a Pharmacokinetic profile of AG10-L2-Oxy and oxycodone after a single subcutaneous dose of 16 $\mu\text{mol/kg}$ to rats ($n = 4$ per group). Plasma concentration of test compounds at different time points is expressed as means \pm s.d. of three biological replicates. **b** Brain to plasma ratios and **c** cerebrospinal fluid (CSF) to plasma ratios of AG10-L2-Oxy and oxycodone ($n = 3$ per group). Male Sprague Dawley rats were dosed subcutaneously with 16 $\mu\text{mol/kg}$ (equivalent to 5 mg/kg) oxycodone and both 16 and 64 $\mu\text{mol/kg}$ AG10-L2-Oxy (equivalent to 13 mg/kg and 52 mg/kg, respectively). The plasma, brain tissue, and CSF were collected at 60 minutes after dosing. The ratio of the brain (ng/g) versus plasma concentration (ng/mL) is expressed as the percentage brain to plasma ratio. The ratio of the CSF (ng/mL) versus plasma concentration (ng/mL) is expressed as the percentage CSF to plasma ratio. Bar graphs show the respective mean (\pm s.d.) ($n = 3$ per group). Statistical differences were determined using One Way ANOVA followed by Tukey's post-hoc test ($*P < 0.05$ compared to oxycodone 16 $\mu\text{mol/kg}$ group). For the brain to plasma ratio experiment $F(2,6) = 577.6$, $P < 0.0001$ and for the CSF to plasma ratio experiment $F(2,6) = 68.84$, $P < 0.0001$. **d** Hot plate

(Figure 50 Continued)

latency and e GI transit assays to evaluate the contribution of opioid agonists on central and peripheral mu-opioid receptors in OIC. Oxycodone (16 $\mu\text{mol/kg}$; subcutaneous route, SC), Oxycodone (640 and 1280 nmol per rat; intracerebroventricular route, ICV), AG10-L2-Oxy (64 $\mu\text{mol/kg}$; subcutaneous route, SC), AG10-L2-Oxy (160 nmol per rat; intracerebroventricular route, ICV), or vehicle was administered at $t = 0$ minutes. Charcoal was given at 10 minutes. Hot plate latency and GI transit were measured at 40 minutes. Bar graph showing the respective mean (\pm s.d.) ($n = 5$ rats per group). Statistical differences were determined using one-way ANOVA followed by Tukey's post-hoc test ($*P < 0.05$). $F(5,24) = 300.5$, $P < 0.0001$ for the hot plate assay and $F(5,24) = 983.3$, $P < 0.0001$ for the GI transit assay. (Data generated with Tuhin)

CHAPTER 9: DISCUSSION

Over the past almost half a century, a lot of efforts have been made to revealing the site of action for opioid-induced constipation. Previous research has established a theory that opioid-induced constipation is predominantly controlled by peripheral, while the CNS effects is minor(Gao et al., 2021; Manara et al., 1986; Mori et al., 2013; Moss, 2019; Reimer et al., 2009; Stein, 2018; Thomas et al., 2008). Even though some data indicated the CNS contributed a decent amount of constipation, scientists did not raise the concern about the old theory but still define a more important role in peripheral(Mori et al., 2013).

This wrong statement was attributed to two main reasons. The first one was the variance of experiment design. For example, the cutoff of hot plate study was set as 10 seconds in the study of Naloxegol. It reported not reverse the analgesia effects(Costanzini et al., 2021). However, we repeated the experiment found that the analgesia decreased sharply from 60 seconds to 17 seconds while AG10-L2-Nal maintained the full analgesial effect even at 10-fold higher dose than Naloxegol (Figure 39). The second reason was there were lacking a truly peripheral restricted opioid agonist/antagonist probe for investigation in depth. Besides, there were other factors other than science involved.

At the same time, a lot of money and resources have been applied to the discover PAMORAs for the treatment of OIC which was based on the theory above. However, there are a lot of challenge in developing the technology preventing drug crossing the BBB. For example, PEGlation results in compromising the potency (Figure 30 and Figure 33) while it

still penetrates to the BBB (Figure 37). Patients need to take a more pills if the potency becomes lower, consequently, the lower BBB penetration rate gets compensated by the large dose. For another example, quaternary amine modification increases the polarity and thus reduce the amount penetrating the BBB. However, similar to PEGlation, the polarity of the quaternary amine moiety has interaction with the receptors, reduce the binding affinity by 100-fold (Greenwood-Van Meerveld & Standifer, 2008). Even worse, it has been reported that N-demethylation (Walentiny et al., 2021) forming the metabolite tertiary amine analogue can readily cross BBB. These were supported by our data that MNTX and Naloxegol reversed the analgesia even at a low dose (Figure 39). Nonetheless, the brain penetration and the analgesia reversal were underemphasized, and the drugs were claimed to be safe. For example, even though there were a descent amount of patients suffer from the opioid withdrawal symptoms, it was blamed on the disruption of BBB of the patients while the drug was efficient and safe ("Relistor (methylnaltrexone bromide) [package insert]. Bridgewater, NJ: Salix Pharmaceuticals, Inc. (2020),").

A considerable percentage of the amount of PAMORAs, which are being used therapeutically to treat OIC, penetrating the BBB was a surprise to observe in our study. This might explain why some individuals may have opioid withdrawal symptoms and start suffering from pain again. And these results translated into losing the analgesic effects when co-administration of naloxegol/MNTX and morphine. Only at some certain sweet point of dosage, naloxegol or MNTX can retain a little analgesic effect (latency ~ 15 seconds) while increasing the GI movement a bit (GI transit = 30% to 50%). A higher dose resulted

in complete anagesic reversal while a lower dose did not help GI movement. Due to the individual differences, these data could explain why some patients did not respond to the current PAMORAs while some patients faced serious opioid withdrawal symptoms.

To the best of my knowledge, AG10-L2-Nal/AG10-L2-Oxy were the first truly peripheral selective without compromising potency opioid probes have discovered (Figure 30). In addition, the stability (Figure 35) of the compounds ensures no metabolites cross the brain and interfere the results. Besides, the half-life of these conjugates was long enough to access the opioid effects before eliminating them from the body (Figure 38).

By systemic administration, AG10-L2-Nal did not reverse the analgesia of morphine, at the same time relived the OIC around 40% (Figure 40). Increasing dose of AG10-L2-Nal did not further mitigate the OIC (data not showed). Considering AG10-L2-Nal did not cross the BBB, therefore only peripheral mu-opioid receptors got antagonist and the central mu-opioid receptors were still activated. This suggested the relief from peripheral reach a plateau. And the ICV study confirmed this hypothesis, showing fully reversal of OIC by SC (peripheral distribution) plus ICV (CNS distribution) administration of AG10-L2-Nal (Figure 43). These data were further supported by the AG10-L2-Oxy agonist, where ICV administration induced substantial constipation while SC administration induced limited constipation (Figure 50). Besides, other factors such as TTR influence or forming a partial agonist metabolite were excluded by experiments. Overall, our results revealed the crucial role of mu-opioid receptors in the CNS in producing OIC challenging the mainstream theory that opioid agonists impair GI motility predominantly controlled by peripheral while the

contribution of CNS is minor (Gao et al., 2021; Manara et al., 1986; Mori et al., 2013; Moss, 2019; Reimer et al., 2009; Stein, 2018; Thomas et al., 2008). This information provides new insight that explain deficiencies of current PAMORAs whose theoretical cornerstone is unreliable.

Even though AG10-L2-Nal only partially relived the OIC, it is stable in long term study (PBS stability data no showed) and safe without withdrawal symptoms and toxicity (MTT data not showed).

Furthermore, it is crucial to note that the dose of AG10-L2-Nal is 7-fold larger than the amount used in the BBB testing (Figure 37), demonstrating that this novel technology platform is highly effective at preventing the BBB penetration. Indicating that the high polarity of our conjugates (contributed by the zwitterion in AG10) is the important for preventing the conjugates from crossing the BBB. These results are similarly comparable with those for compound **1**, where there was no substantial BBB penetration even at a higher dose (50 $\mu\text{mol/kg}$; Figure 3). As many drug candidates have central adverse effects so that clinical outcomes are unsatisfactory or even fail, the truly peripheral restricted delivery system is very needed and has a very wide range of applications such as ciprofloxacin, methotrexate, and indomethacin.

Another application is developing a truly peripheral opioid which is supposed to be efficient in analgesia without causing tolerance, respiratory depression, euphoria, and addiction.

The preliminary study of opioid agonist AG10-L2-Oxy indicated this potential (Figure 50).

And it will be an excellent probe to investigate the mechanism of peripheral analgesia.

REFERENCES

- (NCATS), T. N. C. f. A. T. S. (2022). Loperamide. Retrieved from
- Alhamadsheh, M. M., Connelly, S., Cho, A., Reixach, N., Powers, E. T., Pan, D. W., . . .
- Graef, I. A. (2011). Potent kinetic stabilizers that prevent transthyretin-mediated cardiomyocyte proteotoxicity. *Sci Transl Med*, 3(97), 97ra81.
- doi:10.1126/scitranslmed.3002473
- Alt, A., Mansour, A., Akil, H., Medzihradsky, F., Traynor, J., & Woods, J. (1998). Stimulation of Guanosine-5'-O-(3-[35S] Thio) Triphosphate Binding by Endogenous Opioids Acting at a Cloned MuReceptor. *Journal of Pharmacology and Experimental Therapeutics*, 286(1), 282-288.
- Ballabh, P., Braun, A., & Nedergaard, M. (2004). The blood-brain barrier: an overview: structure, regulation, and clinical implications. *Neurobiol Dis*, 16(1), 1-13.
- doi:10.1016/j.nbd.2003.12.016
- Banks, W. A. (2016). From blood-brain barrier to blood-brain interface: new opportunities for CNS drug delivery. *Nat Rev Drug Discov*, 15(4), 275-292. doi:10.1038/nrd.2015.21
- Bell, T. J., Panchal, S. J., Miaskowski, C., Bolge, S. C., Milanova, T., & Williamson, R. (2009). The prevalence, severity, and impact of opioid-induced bowel dysfunction: results of a US and European Patient Survey (PROBE 1). *Pain Med*, 10(1), 35-42.
- doi:10.1111/j.1526-4637.2008.00495.x

- Bishop-Freeman, S. C., Feaster, M. S., Beal, J., Miller, A., Hargrove, R. L., Brower, J. O., & Winecker, R. E. (2016). Loperamide-related deaths in North Carolina. *Journal of analytical toxicology*, 40(8), 677-686.
- Blake, C. C., Geisow, M. J., Oatley, S. J., Rerat, B., & Rerat, C. (1978). Structure of prealbumin: secondary, tertiary and quaternary interactions determined by Fourier refinement at 1.8 Å. *J Mol Biol*, 121(3), 339-356. doi:10.1016/0022-2836(78)90368-6
- Boström, E., Simonsson, U. S., & Hammarlund-Udenaes, M. (2006). In vivo blood-brain barrier transport of oxycodone in the rat: indications for active influx and implications for pharmacokinetics/pharmacodynamics. *Drug Metab Dispos*, 34(9), 1624-1631. doi:10.1124/dmd.106.009746
- Bulawa, C. E., Connelly, S., Devit, M., Wang, L., Weigel, C., Fleming, J. A., . . . Labaudinière, R. (2012). Tafamidis, a potent and selective transthyretin kinetic stabilizer that inhibits the amyloid cascade. *Proc Natl Acad Sci U S A*, 109(24), 9629-9634. doi:10.1073/pnas.1121005109
- Chamberlain, B. H., Rhiner, M., Slatkin, N. E., Stambler, N., & Israel, R. J. (2020). Subcutaneous methylnaltrexone for opioid-induced constipation in advanced-illness patients with or without active cancer. *Pain Manag*, 10(2), 73-84. doi:10.2217/pmt-2019-0045
- Choi, S., Connelly, S., Reixach, N., Wilson, I. A., & Kelly, J. W. (2010). Chemoselective small molecules that covalently modify one lysine in a non-enzyme protein in plasma. *Nat Chem Biol*, 6(2), 133-139. doi:10.1038/nchembio.281

- Choi, S., & Kelly, J. W. (2011). A competition assay to identify amyloidogenesis inhibitors by monitoring the fluorescence emitted by the covalent attachment of a stilbene derivative to transthyretin. *Bioorg Med Chem*, 19(4), 1505-1514.
doi:10.1016/j.bmc.2010.12.050
- Cody, V., & Wojtczak, A. (2009). Mechanisms of molecular recognition: structural characteristics of transthyretin ligand interactions. In *Recent Advances in Transthyretin Evolution, Structure and Biological Functions* (pp. 1-21): Springer.
- Costanzini, A., Ruzza, C., Neto, J. A., Sturaro, C., Malfacini, D., Sternini, C., . . . Calò, G. (2021). Pharmacological characterization of naloxegol: In vitro and in vivo studies. *European Journal of Pharmacology*, 903, 174132.
- Daneman, R., & Prat, A. (2015). The blood-brain barrier. *Cold Spring Harb Perspect Biol*, 7(1), a020412. doi:10.1101/cshperspect.a020412
- Ferrier, J. (2014). Domperidone as an unintended antipsychotic. *Can Pharm J (Ott)*, 147(2), 76-77. doi:10.1177/1715163514521969
- Floettmann, E., Bui, K., Sostek, M., Payza, K., & Eldon, M. (2017). Pharmacologic Profile of Naloxegol, a Peripherally Acting. *J Pharmacol Exp Ther*, 361(2), 280-291.
doi:10.1124/jpet.116.239061
- Foss, T. R., Wiseman, R. L., & Kelly, J. W. (2005). The pathway by which the tetrameric protein transthyretin dissociates. *Biochemistry*, 44(47), 15525-15533.
doi:10.1021/bi051608t

- Gao, H., Zhang, Y., Li, Y., Chang, H., Cheng, B., Li, N., . . . Wang, Q. (2021). μ -Opioid Receptor-Mediated Enteric Glial Activation Is Involved in Morphine-Induced Constipation. *Mol Neurobiol*, 58(7), 3061-3070. doi:10.1007/s12035-021-02286-0
- Greenwood-Van Meerveld, B., & Standifer, K. M. (2008). Methylnaltrexone in the treatment of opioid-induced constipation. *Clin Exp Gastroenterol*, 1, 49-58. doi:10.2147/ceg.s3889
- Hug Jr, C. C., & Murphy, M. R. (1981). Tissue redistribution of fentanyl and termination of its effects in rats. *Anesthesiology*, 55(4), 369-375.
- Kumar, L., Barker, C., & Emmanuel, A. (2014). Opioid-induced constipation: pathophysiology, clinical consequences, and management. *Gastroenterol Res Pract*, 2014, 141737. doi:10.1155/2014/141737
- Kuo, A., Wyse, B., Meutermans, W., & Smith, M. (2015). In vivo profiling of seven common opioids for antinociception, constipation and respiratory depression: no two opioids have the same profile. *British Journal of Pharmacology*, 172(2), 532-548.
- Liu, F., Ul Amin, T., Liang, D., Park, M. S., & Alhamadsheh, M. M. (2021). Enhancing the Pharmacokinetic Profile of Interleukin 2 through Site-Specific Conjugation to a Selective Small-Molecule Transthyretin Ligand. *J Med Chem*, 64(19), 14876-14886. doi:10.1021/acs.jmedchem.1c01426
- Manara, L., Bianchi, G., Ferretti, P., & Tavani, A. (1986). Inhibition of gastrointestinal transit by morphine in rats results primarily from direct drug action on gut opioid sites. *J Pharmacol Exp Ther*, 237(3), 945-949.

Manglik, A., Kruse, A. C., Kobilka, T. S., Thian, F. S., Mathiesen, J. M., Sunahara, R. K., . . .

Granier, S. (2012). Crystal structure of the μ -opioid receptor bound to a morphinan antagonist. *Nature*, 485(7398), 321-326. doi:10.1038/nature10954

Mestek, A., Hurley, J. H., Bye, L. S., Campbell, A. D., Chen, Y., Tian, M., . . . Yu, L. (1995).

The human mu opioid receptor: modulation of functional desensitization by calcium/calmodulin-dependent protein kinase and protein kinase C. *Journal of Neuroscience*, 15(3), 2396-2406.

Mikus, G., & Klimas, R. (2014). Contribution of oxycodone and its metabolites to the analgesic effect. *British Journal of Anaesthesia*, 112(5), 944-945.

doi:10.1093/bja/aeu123

Miller, M., Pal, A., Albusairi, W., Joo, H., Pappas, B., Haque Tuhin, M. T., . . . Alhamadsheh,

M. (2018). Enthalpy-Driven Stabilization of Transthyretin by AG10 Mimics a Naturally Occurring Genetic Variant That Protects from Transthyretin Amyloidosis. *J Med Chem*, 61(17), 7862-7876. doi:10.1021/acs.jmedchem.8b00817

Monaco, H. L., Rizzi, M., & Coda, A. (1995). Structure of a complex of two plasma proteins: transthyretin and retinol-binding protein. *Science*, 268(5213), 1039-1041.

doi:10.1126/science.7754382

Monory, K., Greiner, E., Sartania, N., Sallai, L., Pouille, Y., Schmidhammer, H., . . . Borsodi,

A. (1999). Opioid binding profiles of new hydrazone, oxime, carbazone and semicarbazone derivatives of 14-alkoxymorphinans. *Life Sci*, 64(22), 2011-2020.

doi:10.1016/s0024-3205(99)00148-4

- Mori, T., Shibasaki, Y., Matsumoto, K., Shibasaki, M., Hasegawa, M., Wang, E., . . . Suzuki, T. (2013). Mechanisms that underlie μ -opioid receptor agonist-induced constipation: differential involvement of μ -opioid receptor sites and responsible regions. *J Pharmacol Exp Ther*, 347(1), 91-99. doi:10.1124/jpet.113.204313
- Moss, J. (2019). Identifying and Treating Opioid Side Effects: The Development of Methylnaltrexone. *Anesthesiology*, 130(1), 142-148.
doi:10.1097/ALN.0000000000002428
- Moss, J., & Rosow, C. E. (2008). Development of peripheral opioid antagonists' new insights into opioid effects. *Mayo Clin Proc*, 83(10), 1116-1130. doi:10.4065/83.10.1116
- Müller, C., Farkas, R., Borgna, F., Schmid, R. M., Benešová, M., & Schibli, R. (2017). Synthesis, Radiolabeling, and Characterization of Plasma Protein-Binding Ligands: Potential Tools for Modulation of the Pharmacokinetic Properties of (Radio)Pharmaceuticals. *Bioconjug Chem*, 28(9), 2372-2383.
doi:10.1021/acs.bioconjchem.7b00378
- Nalamachu, S. R., Pergolizzi, J., Taylor, R., Slatkin, N. E., Barrett, A. C., Yu, J., . . . Forbes, W. P. (2015). Efficacy and Tolerability of Subcutaneous Methylnaltrexone in Patients with Advanced Illness and Opioid-Induced Constipation: A Responder Analysis of 2 Randomized, Placebo-Controlled Trials. *Pain Pract*, 15(6), 564-571.
doi:10.1111/papr.12218
- Ngai, S. H., Berkowitz, B. A., Yang, J. C., Hempstead, J., & Spector, S. (1976). Pharmacokinetics of naloxone in rats and in man: basis for its potency and short

duration of action. *Anesthesiology*, 44(5), 398-401. doi:10.1097/00000542-

197605000-00008

Pal, A., Albusairi, W., Liu, F., Tuhin, M. T. H., Miller, M., Liang, D., . . . Alhamadsheh, M.

M. (2019). Hydrophilic Small Molecules That Harness Transthyretin To Enhance the

Safety and Efficacy of Targeted Chemotherapeutic Agents. *Mol Pharm*, 16(7), 3237-

3252. doi:10.1021/acs.molpharmaceut.9b00432

Pasternak, G. W., & Pan, Y. X. (2013). Mu opioids and their receptors: evolution of a

concept. *Pharmacol Rev*, 65(4), 1257-1317. doi:10.1124/pr.112.007138

Penchala, S. C., Connelly, S., Wang, Y., Park, M. S., Zhao, L., Baranczak, A., . . .

Alhamadsheh, M. M. (2013). AG10 inhibits amyloidogenesis and cellular toxicity of

the familial amyloid cardiomyopathy-associated V122I transthyretin. *Proc Natl Acad*

Sci U S A, 110(24), 9992-9997. doi:10.1073/pnas.1300761110

Penchala, S. C., Miller, M. R., Pal, A., Dong, J., Madadi, N. R., Xie, J., . . . Alhamadsheh, M.

M. (2015). A biomimetic approach for enhancing the in vivo half-life of peptides. *Nat*

Chem Biol, 11(10), 793-798. doi:10.1038/nchembio.1907

Reimer, K., Hopp, M., Zenz, M., Maier, C., Holzer, P., Mikus, G., . . . Leyendecker, P. (2009).

Meeting the challenges of opioid-induced constipation in chronic pain management -

a novel approach. *Pharmacology*, 83(1), 10-17. doi:10.1159/000165778

Relistor (methylnaltrexone bromide) [package insert]. Bridgewater, NJ: Salix

Pharmaceuticals, Inc. (2020).

- Richardson, S. J., & Cody, V. (2009). *Recent advances in transthyretin evolution, structure and biological functions*: Springer.
- Shaffer, C. L. (2010). *Chapter 4 - Defining Neuropharmacokinetic Parameters in CNS Drug Discovery to Determine Cross-Species Pharmacologic Exposure–Response Relationships* (Vol. 45): Annual Reports in Medicinal Chemistry.
- Sobczak, M., Salaga, M., Storr, M. A., & Fichna, J. (2014). Physiology, signaling, and pharmacology of opioid receptors and their ligands in the gastrointestinal tract: current concepts and future perspectives. *J Gastroenterol*, 49(1), 24-45.
doi:10.1007/s00535-013-0753-x
- Stabilini, R., Vergani, C., Agostoni, A., & Agostoni, R. P. (1968). Influence of age and sex on prealbumin levels. *Clin Chim Acta*, 20(2), 358-359. doi:10.1016/0009-8981(68)90173-3
- Stain-Textier, F., Boschi, G., Sandouk, P., & Scherrmann, J. M. T. (1999). Elevated concentrations of morphine 6-beta-D-glucuronide in brain extracellular fluid despite low blood-brain barrier permeability. *British Journal of Pharmacology*, 128(4), 917–924.
- Stein, C. (2018). New concepts in opioid analgesia. *Expert Opin Investig Drugs*, 27(10), 765-775. doi:10.1080/13543784.2018.1516204
- Stein, C., Clark, J. D., Oh, U., Vasko, M. R., Wilcox, G. L., Overland, A. C., . . . Spencer, R. H. (2009). Peripheral mechanisms of pain and analgesia. *Brain Res Rev*, 60(1), 90-113. doi:10.1016/j.brainresrev.2008.12.017

- Syvänen, S., Xie, R., Sahin, S., & Hammarlund-Udenaes, M. (2006). Pharmacokinetic consequences of active drug efflux at the blood-brain barrier. *Pharm Res*, 23(4), 705-717. doi:10.1007/s11095-006-9780-0
- Tamai, I., & Tsuji, A. (2000). Transporter-mediated permeation of drugs across the blood-brain barrier. *J Pharm Sci*, 89(11), 1371-1388. doi:10.1002/1520-6017(200011)89:11<1371::aid-jps1>3.0.co;2-d
- Tan-No, K., Nijima, F., Nakagawasai, O., Sato, T., Satoh, S., & Tadano, T. (2003). Development of tolerance to the inhibitory effect of loperamide on gastrointestinal transit in mice. *European journal of pharmaceutical sciences*, 20(3), 357-363.
- Thomas, J., Karver, S., Cooney, G. A., Chamberlain, B. H., Watt, C. K., Slatkin, N. E., . . . Israel, R. J. (2008). Methylnaltrexone for opioid-induced constipation in advanced illness. *N Engl J Med*, 358(22), 2332-2343. doi:10.1056/NEJMoa0707377
- Tuhin, M. T. H., Liang, D., Liu, F., Aldawod, H., Amin, T. U., Ho, J. S., . . . Alhamadsheh, M. M. (2022). Peripherally restricted transthyretin-based delivery system for probes and therapeutics avoiding opioid-related side effects. *Nature Communications*, 13(1), 3590. doi:10.1038/s41467-022-31342-z
- Walentiny, D. M., Komla, E., Moisa, L. T., Mustafa, M. A., Poklis, J. L., Akbarali, H. I., & Beardsley, P. M. (2021). Methylnaltrexone crosses the blood-brain barrier and attenuates centrally-mediated behavioral effects of morphine and oxycodone in mice. *Neuropharmacology*, 185, 108437. doi:10.1016/j.neuropharm.2020.108437

Yang, P. P., Yeh, G. C., Yeh, T. K., Xi, J., Loh, H. H., Law, P. Y., & Tao, P. L. (2016).

Activation of delta-opioid receptor contributes to the antinociceptive effect of